AFCRL-72-0180

F61 (052)-69-C-0016 February 1972

1st Rep - AD722538

FINAL SCIENTIFIC REPORT

Research on Atmospheric Optical Radiation Transmission

1 Jan 1971 - 31 Dec 1971

E de Bary, K. Bullrich, R. Eiden, G. Eschelbach, G. Hänel

Institut für Meteorologie
der
Johannes Gutenberg-Universität
Mainz, Germany

This research has been sponsored in part by the AIR FORCE CAMBRIDGE RESEARCH LABORATORIES, through the European Office of Aerospace Research, OAR, US Air Force under Contract

F61 (052)-69-C-0016

78

14 KEY WORDS	LINK A		LINK B		LINK C	
	ROLE	WT	ROLE	WT	ROLE	WT
Atmospheric aerosol particles and relative humidity of air complex refractive index of aerosol particles						
Density of aerosol particles						
Light scattering and absorption						
Stokes parameters of mixed aerosols						
Aerosol size distributions						
Atmospheric aerosols and energy balance						
Radiant divergence						

UNCLASSIFIED
Security Classification

DOCUMENT CONTROL DATA - R & D

Security classification of title, body of abstract and indexing annotation must be entered when the overall report is classified

1 ORIGINATING ACTIVITY (Corporate author)	2a. REPORT SECURITY CLASSIFICATION
Meteorologisch-Geophysikalisches Institut Johannes Gutenberg Universitat Mainz, Germany	Unclassified
	2b. GROUP

3 REPORT TITLE

4 DESCRIPTIVE NOTES (*Type of report and inclusive dates*)
Scientific ~~Interim~~ (or Final in the case of the Final Report)

5 AUTHOR(S) (*First name, middle initial, last name*)
Elisabeth de Bary, Kurt Bullrich, Reiner Liden, Günter Eschelbach, Gottfried Hänel

6 REPORT DATE	7a. TOTAL NO OF PAGES	7b. NO OF REFS
February 1972	23 Text, 25 Fig.	23

CONTRACT OR GRANT NO	9a. ORIGINATOR'S REPORT NUMBER(S)
F61052-69-C-0016	
b. PROJECT NO 7621-03	
c. 62101F	9b. OTHER REPORT NO(S) (*Any other numbers that may be assigned this report*)
d. 681000	

10. DISTRIBUTION STATEMENT

This document has been approved for public release and sale; its distribution is unlimited.

11 SUPPLEMENTARY NOTES	12 SPONSORING MILITARY ACTIVITY
	Air Force Cambridge Research Laboratories (CROA), L. G. Hanscom Field, Bedford, Mass. 01730

13 ABSTRACT

Two chapters (II, III) describe our knowledge of the number and the size of the atmospheric aerosol particles and the possibilities to evaluate them by optical methods. There are used the parameters: extinction coefficient, scattering function, degree of polarization and the ellipticity of polarization.

Chapter IV contains theoretical results of the influence of absorbent aerosol particles on the energy balance of the atmosphere in the visible wavelength range. The absorption of light by aerosols has an influence on the heating rate in the atmosphere which is of similar importance as that of the water vapor absorption.

Chapter V represents some measurement results of spectral solar extinction and sky radiances performed at the Hohenpeissenberg Observatory. They have been done to compare experimental and theoretical work.

Chapter VI gives a survey of new experimental results of some fundamental parameters of the atmospheric aerosol particles, as there are: density, refractive index, extinction coefficient, volume- and masschange as a function of the relative humidity of the air.

DD FORM 1 NOV 68 1473

F61 (052)-69-C-0016

February 1972

FINAL SCIENTIFIC REPORT

Research on Atmospheric Optical Radiation Transmission

1 Jan 1971 - 31 Dec 1971

E. de Bary, K. Bullrich, R Eiden, G. Eschelbach, G. Hänel

Institut für Meteorologie
der
Johannes Gutenberg-Universität
Mainz, Germany

This research has been sponsored in part by the AIR FORCE CAMBRIDGE RESEARCH LABORATORIES, through the European Office of Aerospace Research, OAR, US Air Force under Contract

F61 (052)-69-C-0016

Table of Contents **Page**

Abstract

Two chapters (II, III) describe our knowledge of the number and the size of the atmospheric aerosol particles and the possibilities to evaluate them by optical methods. There are used the parameters: extinction coefficient, scattering function, degree of polarization and the ellipticity of polarization.
Chapter IV contains theoretical results of the influence of absorbent aerosol particles on the energy balance of the atmosphere in the visible wave length range. The absorption of light by aerosols has an influence on the heating rate in the atmosphere which is of similar importance as that of the water vapor absorption.
Chapter V represents some measurement results of spectral solar extinction and sky radiances performed at the Hohenpeissenberg Observatory. They have been done to compare experimental and theoretical work.
Chapter VI gives a survey of new experimental results of some fundamental parameters of the atmospheric aerosol particles, as there are: density, refractive index, extinction coefficient, volume- and masschange as a function of the relative humidity of the air.

List of Illustrations

abscissa scattering angle. Left side: scattering only, right side: including absorption, refractive index m = 1.5 - o.o2 i.

Fig. 6 Computed degree of polarization P (ordinate) of an air volume containing only aerosol particles as a function of the scattering angly φ (abscissa) wavelengths λ = o.4 μ and λ = 1.2 μ. Curves 1 and 2 are valid for ν^* = 4.o, 3 and 4 for ν^* = 2.5 (Junge distribution). The light source is neutral.

Fig. 7 Same as Fig. 6. The light source is linearpolarized Left side: scattering only, Gaussian aerosol particle size distribution following the curve 1o on Fig. 1. Collective radius r_o = o.1o μ. Right side: including absorption, Junge aerosol distribution. Refractive index m = 1.5 - o.o2 i.

Fig. 8 Aerosol particle size distribution composed of 6 Gaussian distributions $dN_L = n_{r_o} \exp A (\log r/r_o)^2 dr$; A = 8o

Fig. 9 same as Fig. 8, model changed

Fig. 1o Aerosol particle size distribution model 1

a) Degree of polarization P as a function of the scattering angle φ

b) Ellipticity $\tan\beta$ as a function of the scattering angle φ

c) Position of the plane of polarization χ of the scattering light as a function of the scattering angle φ

Fig. 11 Same as Fig. 1o, but model III

Fig. 12 Percentage ratio $R = \frac{S_\lambda^\uparrow}{S_{o\lambda}}$ of the radiant flux density $S_\lambda^\uparrow$ which at the upper edge of the atmosphere is reflected into space, to the solar flux density $S_{o\lambda}$. Abscissa turbidity factor T.
_____ refractive index m = 1.5 (scattering only)
----- m = 1.5 - 0.02 i (absorption included).
Zenith distance of the sun Z = 37°, surface albedo A = 0.0 (above) and A = 0.25 (below).
λ Wavelength.

Fig. 13 Same as Fig. 12, but total absorption of the atmosphere in case of absorbent aerosol particles.

Fig. 14 Spectral divergences of radiant fluxes (abscissa) at different heights (ordinate) in percent of the downwards radiant fluxes.

Fig. 15 -----measured and _____ calculated results of sky radiance performed at the Observatory Hohenpeissenberg, Southern Bavaria, alt 980 m, June 1971, including scattering of higher order. Solar elevation 30°. Measured turbidity faktor T = 3.9. Aerosol size distribution model after Junge, $\nu^* = 3.5$ ordinate sky radiance, abscissa scattering angle (solar almucantar).

Fig. 16 Measurement results of haze extinction a_D of the solar radiation (Observatory Hohenpeissenberg) for two wavelengths at different solar elevations. (Ordinate a_D, abscissa solar elevation, a.m. and p.m.). Hatching indicates anomalous extinction a) oct 2, b) oct 3. 1971.

Fig. 17 - 19 Measurement results of sky radiance (ordinate) in the solar almucantar (abscissa scattering angle) at different solar elevations. (Observatory Hohenpeissenberg). O wavelength λ = o.4o5 μ, 1 λ = o.443 μ, 2 λ = o.548 μ, 3 λ = o.639 μ, 4 λ = o.7o8 μ. No 1 - 7 october 2 p.m., 8 - 13: oct 3 a.m., 14 - 21: oct 3 p.m.

Fig. 2o - 25 Measurement results of the parameters: the mean density ρ (f), the real part of refractive index n (f), the volume ratio V (f)/V_o, the mass ratio $m_w(f)/m_o$, The extinction coefficients of the air born particles $\sigma_K(f)/\sigma_{K_o}$ - as a function of the relative humidity of the air, f resp. 1 - f. Decreasing resp. increasing relative humidities are indicated by arrows. Fig. 2o summer 1966, Mainz. Fig. 21 January 197o, Mainz. Fig. 22 summer 197o, Observatory Hohenpeissenberg (98o m alt). Fig. 23 ocean sea spray. Fig. 24 April 13 - 16, 1969, "Meteor" North Atlantic. Fig. 25 April 16 - 25, 1969, "Meteor" Atlantic, the air contains Sahara dust.

Table I Radius r_o and the number particle density per radius interval n_{r_o} of the maximum of the log normal size distributions and the refractive indices M of the different combinations of the log normal size distributions

	r_o μ	0.100	0.180	0.320	0.550	1.00	1.80
Model I	n_{r_o} cm^{-4}	5.0	5.0	5.0 w^{-1}	5.95 w^{-2}	5.5 w^{-3}	5.0 w^{-4}
Model III	n_{r_o} cm^{-4}	5.0	5.0	3.0	5.0	5.0 w^{-1}	4.5 w^{-2}
	a) M	1.5	1.5	1.5	1.5	1.5	1.5
	b) M	1.95-io.66	1.5	1.5	1.5	1.5	1.5
	c) M	1.5	1.95-io.66	1.5	1.5	1.5	1.5
	d) M	1.5	1.5	1.95-io.66	1.5	1.5	1.5
	e) M	1.5	1.5	1.5	1.95-io.66	1.5	1.5
	f) M	1.5	1.5	1.5	1.5	1.95-io.66	1.5
	g) M	1.5	1.5	1.5	1.5	1.5	1.95-io.66

List of Abbreviations and Symbols

a_D	extinction coefficient, molecular scattering subtracted
f	relative humidity of the air
k	imaginary part of the complex refractive index
m	refractive index; mass of aerosol particles
n	real part of the complex refractive index
r	radius of the aerosol particles
r_o	collective radius (most frequent particle radius in a Gaussian size distribution)
A	Albedo of the earth surface
D	radiant divergence
H_D	height of the homogenious turbid atmosphere
M	complex refractive index
N	number of aerosol particles per cm^3
P	degree of polarization
R	reflection
S	radiant flux
T	turbidity factor
V	volume
Z	zenith distance
β	ellipticity of the polarized radiaiton
λ	wavelength
μ	$1o^{-4}$ cm
ν	exponent in the power law size distribution
ϱ	density
σ	extinction coefficient of the airborne aerosol particles
φ	scattering angle; volume growth coefficient
ψ	angle between the main axis of the ellipse and the plane of polarization

I. Introduction

Studies are needed to determine scattering, reflection, absorption and emission by particles which are suspended in the atmosphere. The role of atmospheric aerosols in the heat balance, radiaiton net fluxes and radiation divergences remains one of the great importances - and uncertainties - of the explanation of how the atmosphere behavees. To assess the contribution of particulate pollutants to radiative processes and radiative transfer, it is necessary to know the radiation characteristics of natural and anthropogenious particles. Also effects such as the influence of water vapor and relative humidity on the extinguishing properties of aerosol particles are still not well known. The same is true on the double role which aerosol plays in scattering and absorbing radiation.

This study should be a contribution to claryfy some of the problems which concern the atmospheric radiation transmission, radiant fluxes through the atmosphere for clean and polluted atmospheres and its modification with increasing pollution.

II. The Evaluation of Atmospheric Aerosol Particles by Means of Optical Radiation Measurements

1. Aerosol Particle Size Distributions

Various types of aerosol size distribution have been plotted in the Fig. 1. They have been selected for three aspects:

a) The curves 3, 4, 5 and 6 are valid for size distributions which have been measured in a clean atmosphere, R. Jaenicke, C. Junge, H.J.Kanter 1970 (1).

b) The continental atmosphere is represented by the size distributions of the curves 1 and 2, C. Junge 1963 (2) and (1).

c) The size distributions which are characterized by the curves 7, 8, 9 and 10 are those which the optical radiation computations have been based upon. They enable one to show the influence of the aerosol particle size distribution on the radiational properties of the atmosphere which are manifested by optical means. Vice versa, if this connexion is known, optical measurements of radiational parameters give hints to the atmospheric aerosol.

2. Extinction of Radiation

The attenuation of radiation in the atmosphere is due to scattering and absorption of radiation. The scattering takes place on air molecules and aerosol particles, the absorption takes place also on aerosol particles, however, on gaseous suspensoids as well. This report deals only with the influence of the aerosol particles. The extinction of the radiation in the atmosphere depends on the wavelength because of the scattering of the radiation on aerosol particles, whereas the absorption of radiation by aerosol particles is assumed to be independent of the wavelength.

The extinction in case of a continental aerosol particle size distribution which corresponds to the model represented by the curve 7 in Fig. 1, has been plotted in the Fig. 2 as a function of the wavelength in double logarithmic scale. The numerical values have been taken from tabulations compiled by E. de Bary, B. Braun, K. Bullrich 1965 [3] for a turbidity factor T = 2, refractive index m = 1.5, height of the homogenous turbid atmosphere H_D = 1.25 km, imaginary part of the complex index of refraction k = o and for 3 exponents of aerosol particle size distributions ν^* = 2.5, ν^* = 3 and ν^* = 4. (The curve 7 in the Fig. 1 refers to ν^* = 3).

The assumption of an aerosol particle size distribution following a power law implies the relation: The turbid extinction coefficient $a_D(\lambda) \sim \lambda^{2-\nu^*}$.
The aforementioned tabulations reveal the following:

The variation of the boundary radii, i.e. r_1 the lower and r_2 the upper radius, shows that the significant radius range falls in between $0.1\ \mu < r < 10\ \mu$. Thus, the extinction only slightly changes due to a change of the particle number within the radius ranges $r < 0.1\ \mu$ or $r > 10\ \mu$ resp. Quite another relation between the extinction and the wavelength results from an aerosol particle size distribution other than following a power law. Aerosol particle size distributions corresponding to the curves 8, 9 and 10 in the Fig. 1 yield wavelength dependences which have been labeled Ns 8 and 9 in the Fig. 2 b); the values have been taken from a publication by K. H. Danzer and K. Bullrich 1966 [4].

R. Eiden 1971[5] has applied similar models, an example of which with the collective radius $r_o = 0.18\ \mu$ is represented by the curve 10 in the Fig. 1. Such an aerosol particle size distribution yields a wavelength dependent extinction corresponding to the curve 10 in the Fig. 2 b). It is obvious that the decrease of extinction with increasing wavelength as obtained due to a power law distribution of the aerosol over the continent, does not

show in case of a Gaussian distribution of the aerosol particle size. The absence of aerosol particles with $r < 0.18\ \mu$ results in shifting the maximum of extinction into the green or red portion of the visible radiation. Measurements of the spectral extinction coefficient have verified this relation: K. Bullrich, R. Eiden, R. Jaenicke and W. Nowak 1968 (6) in Hawaii; K. Bullrich and R. Eiden 1969 (7) in New Mexico; H. Quenzel on the Atlantic 1968 (8). Anomalous extinction, i.e. increase of the extinction with decreasing wavelength except for decreasing extinction in the blue portion of the visible radiation, has been found by U. Kurtz and D. Silz in a few measurements taken at Mainz 1970 (9); Silz has observed this phenomenon especially on the Atlantic coast (Bretagne) during the sea breeze regime. Biased results are yielded if the interpretation of the measurements is based upon a constant index of refraction. It is known that the real and the imaginary parts of the complex index of refraction vary with the relative humidity. This has been discussed by G. Hänel and K. Bullrich 1970 (10) and G. Hänel 1971 (11); see also Chapter VI of this report.

3. The Scattering Function

In analogy to the extinction, the computation of the scattering function has been based upon the aerosol particle size distribution represented by the curve 7 in the Fig. 1. The scattering functions for the wavelengths o.4 μ and 1.2 μ have been plotted in the Fig. 3, the abscissa shows the scattering angle φ in linear scale, the ordinate shows the scattering function for an air volume containing only aerosol particles, in logarithmic scale. The numerical values have been taken from tabulations compiled by E. de Bary, B. Braun and K. Bullrich 1965 [3] for T = 2 and ν^* = 3. It is to be seen that all the values referring to λ = o.4 μ are greater than those referring to λ = 1.2 μ. The integration taken over φ yields the extinction coefficient with the characteristic wavelength dependence, represented in the Fig. 2 b). The significant range of the particle radii as revealed from the tabulations falls in between o.o6 μ < r < 3o μ. The assumption that the aerosol particles are absorbents, K. Fischer 1968 [12], yields decreasing values of the scattering function, especially in the range of backward scattering.

The Fig. 4 shows computations of the sky radiance for the wavelengths o.4 μ, o.65 μ and 1.2 μ, taken from [3] for the almucantar with the zenith distance

$Z = 60^{o}$, $T = 2$, $\nu^{*} = 2.5$ and $\nu^{*} = 4$. The Fig. 4 a) shows that in case of $\nu^{*} = 2.5$, a relatively great number of large particles is characterized by strong foreward scattering (great values at small angles). It can be seen from (3) that the values highly depend on the boundary radius r_2. This is still valid for an aerosol particle size distribution with $\nu^{*} = 3$. This foreward scattering effect is greatly reduced under the assumption of a relatively great number of small particles as it evident from the Fig. 4 b) for $\nu^{*} = 4$. In this case, the upper boundary radius r_2 is insignificant, whereas the sky radiance closely responds to the lower boundary radius r_1; the significant radius range reches as far down as to $r_1 = 0.03\ \mu$.

The Fig. 5 a) presents computations of scattering functions which have been based upon a Gaussian aerosol particle size distribution corresponding to the curve 1o in the Fig. 1 for the collective radius $r_o = 0.18\ \mu$ R. Eiden (5).

Except for the small scattering angle range $\varphi \leq 5^{o}$ and the great scattering angle range $\varphi \geq 158^{o}$, the values in the long wave portion always supersede those in the short wave portion. This result had to be expected from the computations of the extinction coeffi-

cient. The difference in the aerosol particle size distribution as showing in the curves 7 and 10 in the Fig. 1 exerts a strong influence on the spectral behavior of the scattering function and thus on the extinction. Under the additional assumption of absorption as to be seen in the Fig. 5 b), the values of the scattering function in the long wave portion always supersede those in the short wave portion within the range of great scattering angles, too.

4. Degree of Polarization

The Fig. 6 shows the plot of the degree of polarization of an air volume containing only aerosol particles, for two wavelengths as a function of the scattering angle φ from 0° through 180°. The results are valid for a power law size distribution; they have been taken from (3).

The entry parameters for the power law distributions have been chosen in such a way as to manifest the effect of the influence exerted by the small particles. $\nu^* = 2.5$ implies a relatively great number of large particles. The relevant lower boundary radius has been set $r_1 = 0.08\ \mu$, i.e. the distribution has been truncated at this radius. $\nu^* = 4$

implies a relatively great number of small particles. The relevant lower boundary radius has been set $r_1 = 0.04\ \mu$ i.e. the truncation has been shifted towards a smaller particle radius range. The result proves that many small particles cause a high degree of polarization. Only a weakly marked wavelength dependence is observed. The values in the red visible spectrum always supersede those in the blue visible spectrum. In case of only a few small particles, a low degree of polarization and a strong wavelength dependence is to be seen, furthermore, a high degree of negative polarization within the range of scattering angles $\varphi > 120^\circ$. The selection of the upper boundary radius (not demonstrated in the figures) does hardly play any role.

Finally, the aerosol particle size distribution as represented through the curve 7 in the Fig. 1 is considered once more, i.e. a power law distribution with the exponent $\nu^* = 3$. The Fig. 7 a) shows results computed by R. Eiden 1971 [5] which represent the degree of polarization of an air volume as a function of the scattering angle φ. For specific reason - not discussed in detail here - the emitting source effects linear polarization of the incident radiation. It is obvious that within the scattering angle range $60^\circ < \varphi < 160^\circ$ the degree of polarization at the wavelength $\lambda = 0.4\ \mu$ is higher than at $\lambda = 1.2\ \mu$.

If, however, the computation is based upon a Gaussian distribution with the collective radius $r_o = 0.18\ \mu$ corresponding to the curve 10 in the Fig. 1, almost the reverse is true, as it can be seen in the Fig. 7 b). The latter shows that

within the angle range $0^{\circ} < \varphi < 152^{\circ}$ the degree of polarization at $\lambda = 1.2\ \mu$ is higher than that at $\lambda = 0.4\ \mu$, i.e. the absence of small particles has a strong influence.

Summary

The extinction, the scattering function and the degree of polarization as functions of the wavelength and the scattering angle are sensitive indicators for the aerosol particle size distribution. Moreover, there is a marked influence on the scattering function in specific angle ranges due to the absorption which is exerted by the aerosol particles.

The above results show that measurements of the spectral extinction, the scattering function and the degree of polarization as single parameters each can only give hints on the size distribution of the aerosol particles. If, however, all the three parameters are considered together, the variety of interpretation is compatible with that of the direct sampling measuring methods.

III. The Stokes's Parameters of Mixed Aerosol Particle Size Distributions

It is rather difficult to carry out a systematic investigation of the influence exerted by variations of the refractive index within an aerosol particle size distribution.

Thus, only a few papers have been published which deal with tne clarification of this relation.

By way of simplification, it has been tried to investigate the influence of refractive index variations within an aerosol particle size distribution under the assumption of two types of size distribution which are composed each of six narrow Gaussian distributions (Fig. 8, 9).

Thi_ way means an approximation to a power law distribution which, in the range of sm_ll particles, is followed by a section of "constant" particle size. These composite aerosol particle size distributions are called model I and III. In comparison with the model I, the beginning of the "constant" portion of the distribution has been shifted towards larger particles in the model III; this means a greater weighting of large particles within the size distribution.

The straight lines connecting the maximum values of the Gaussian distributions at the radius r_o are expressed in the following way:

Model I

$$\frac{dN}{dr} = n_{r_o} = 0.18\ \mu\ \left(\frac{r}{r_o}\right)^{0} \quad ; \quad 0.1\ \mu \leq r \leq 0.18\ \mu$$

$$\frac{dN}{dr} = n_{r_o} = 0.18\ \mu\ \left(\frac{r}{r_o}\right)^{-4} \quad ; \quad 0.18\ \mu \leq r \leq 1.8\ \mu$$

Modell III

$$\frac{dN}{dr} = n_{r_o} = 0.55\ \mu\ \left(\frac{r}{r_o}\right)^{0} \quad ; \quad 0.1\ \mu \leq r \leq 0.55\ \mu$$

$$\frac{dN}{dr} = n_{r_o} = 0.55\ \mu\ \left(\frac{r}{r_o}\right)^{-4} \quad ; \quad 0.55\ \mu \leq r \leq 1.8\ \mu$$

The Gaussian distributions the model distributions have been based upon are expressed with:

$$dN_L = n_{r_o} \left[\exp A \, (\log r/r_o)^2 \right] dr \quad ; \qquad A = 80$$

The refractive indices $M = m - ik$ of the aerosol particles in each of the model distributions have been varied in the following way:

At the beginning, a uniform refractive index $M = 1.5 - i \cdot 0.0$ has been assumed for the entire size distribution. Then, successively, starting at the small particles, a size range one after another, represented by a separate Gaussian distribution, is substituted by particles with the refractive index $M = 1.95 - i \cdot 0.66$ (coal) (see Table).

Table Radius r_o and the Particle Numbers per Radius Interval n_{r_o} of the Maximum of the Gaussian Distribution, as well as the Refractive Indices of each of the Gaussian Distributions.

For these models and refractive index distributions computations have been carried out for the Stokes's parameters Q, U and V or for their equivalent quantities P, $\tan\beta$ and χ resp. as functions of the scattering angle φ. P is the degree of polarization, $\tan\beta = \pm a/b$ is the ratio of the axes of the ellipse described by the electrical vector of the polarized portion of radiation, ψ is the angle between the main axis of the ellipse, b, and the plane of observation ($0 \leq \psi < \pi$). The first of the Stokes's parameters, I, has not been included in this investigation.

P, tan β and ψ are mere ratios and thus, independent of the absolute number of particles. The incident radiation, which is subject to the scattering effect, is characterized by linear polarization with an angle of 45° between the plane of polarization and the plane of observation.

Discussion of the Computational Results

The computational results for the model I have been plotted in the Fig. 1o. The degree of polarization, which is shown in the Fig. 1o a_1/a_2, undergoes noticeable changes due to the appearance of coal particles in the size distribution, especially within the range of backward scattering. The degree of polarization decreases reaching a minimum value for coal particles in the radius range $r_o = 0.18\ \mu$. If, however, the coal particles are shifted towards larger particles, their influence lessens. This implies that under the assumption of the model I a change of the refractive index has an effect only in the radius range $r < 0.35\ \mu$. The larger particles have an insignificant weighting within the size distribution.

The surves of the ellipticity tan β have been plotted in the Fig. 1o b_1/b_2; they show the same trend as the degree of polarization of the model I.

The inclination of the plane of polarization of the scattered light, ψ, is hardly changed by variations of the refractive index; only within the particle size range $r_o = 0.3\ \mu$ it shows a significant change (Fig. 1o c_1/c_2).

The results for the Model III are markedly distinguished from those for the Model I:

Previously, the main effect due to the change in the refractive index and the section of the size distribution was felt for the model I at about $r \approx 0.35\ \mu$. Now, it can be seen from the Figures 11 a, b and c that the main effect appears in the particle size ranges $0.35\ \mu \leq r \leq 1.0\ \mu$. This implies that the greater weighting of the large particles becomes visible here.

The generalized statement can be made that the influence of changes in the optical properties of the particles in an exponential aerosol particle size distribution is evident in the particle size range $0.1\ \mu \leq r \leq 10\ \mu$. With increasing weighting of the large particles of the size distribution, the maximum change is also shifted towards the larger particles. The influence of the refractive index, however, for particles with radii $r > 1\ \mu$ must be expected to decrease in spite of a great weighting of these particles within a size distribution, because the scattering on these particles becomes more and more independent of their optical properties, i.e. of their refractive index.

IV. The Influence of the Aerosol Particles on the Energy Balance of the Atmosphere in the Visible Range of the Solar Spectrum

This Chapter deals with the influence of the aerosol particles on the energy balance of the atmosphere in the visible

range of the solar spectrum. Computational results including multiple scattering are given for the radiation fluxes and their divergence in a turbid atmosphere. Mention will be made only of those essential parameters which in this context could not be taken into consideration until now:

a) The properties of the atmospheric aerosol particles which effect the attenuation of radiation,
b) the multiple scattering of the radiation of the visible spectrum in the turbid atmosphere.

This paper deals with the application of model computations under consideration of the multiple scattering effect in order to investigate in which way the aerosol particles in the atmosphere influence the solar radiation field.

These computations have been based upon the assumption of the aerosol particles being both either absorbents or non-absorbents, and the absorption has been assumed to be a grey one. Results are given for both the radiation reflected from the planet earth into space and the energy fed into the system surface - atmosphere of the earth, at various turbidity factors and various values of the ground albeo A.

The results have been obtained from the equation of radiational transfer for a plane parallel atmosphere (S. Chandrasekhar 1950 [13]) by means of a numerical computational technique (G. Eschelbach 1971 [14]). All the data presented are based upon the assumption of spherical aerosol particles with specific complex indices of refraction and with a radius size distribution following a power law (C. Junge 1963 [2]) with $\nu^* = 3.0$ and the boundary radii $r_1 = 0.04\ \mu$ and $r_2 = 10\ \mu$.

Furthermore, it has been assumed that the particle number per cm^3 decreases with height exponentially following the factor e^{-h/H_D}, with $H_D = 1.25$ km and h measured in km. Finally, Lambert reflection is assumed to take place at the surface.

1. <u>The Reflection of the Planet Earth</u>

The Fig. 12 shows the percentage ratio $R = \frac{S_\lambda \uparrow}{S_{o\lambda}}$ of the radiant flux density $S_\lambda \uparrow$ (energy per unit of time, wavelength and surface normal to the zenith vector) which at the upper edge of the atmosphere is reflected into space, to the solar flux density $S_{o\lambda}$ which is incident at the upper edge of the atmosphere at the wavelength λ. The calibration of the abscissa represents Linke's turbidity factor T referring to $\lambda = 0.55\ \mu$ (T = 1 corresponds to the Rayleigh atmosphere). The solid curves are based upon a refractive index of the aerosol particles of m = 1.5. The imaginary part of the complex index of refraction, which characterizes the absorption, is zero. The broken curves represent the results for an index of refraction m = 1.5 - 0.02 i; thus, they account for the absorption exerted by the aerosol particles. The measurements, which have been taken during the last years (G. Hänel 1968 [15], K. Fischer 1968 [12]), have proved that the real part being 1.5 is valid for relative humidity values around 70 % and that the imaginary part being -0.02 is a rather realistic characterization of the continental aerosol particles.

All the values of the figure refer to a zenith distance of the sun Z = 36.9°.

If the aerosol particles are non-absorbents, the reflection increases with increasing turbidity in a practically linear way for both A = 0 and A = o.25. This implies that the energy fed into the system surface - atmosphere decreases with increasing particle number at all the three wavelength under consideration.

E.g., at λ = o.45, T = 4 and A = 0 there is a surplus of reflected energy of about 5.5 % and at A = o.25 of about 2.7 % in comparison with that reflected in a Rayleigh atmosphere.

With increasing values of the earth's albedo the energy loss of the planet earth due to the influence of aerosol particles gradually decreases; at A = o.8 it almost vanishes (here not shown). This implies that the interaction of the radiation field with the extinctive medium is compensated by the strong reflection at the surface. The reflection of the planet earth approaches that at the surface, i.e. at A = o.8 it increases up to 8c %.

In case of an absorbent aerosol, the planetary reflection for A = 0 also increases with increasing turbidity, however, at a smaller rate than without absorption. For A = o.25 the reverse becomes true: The reflection decreases with increasing turbidity. The greater number of extinction processes at greater values of A results in a greater energy absorption of the atmosphere so that less energy is left at the upper edge of the atmosphere for going out into space. Thus, the addition of aerosol effects that the system atmosphere - surface gains energy, which e.g. for λ = o.45 μ and T = 4 amounts to about 1.7 % in comparison with the

Rayleigh atmosphere.
For A = o.8, the interaction with the extinctive medium is not compensated by the reflection at the surface any more: The planetary reflection decreases with increasing turbidity factor, e.g. at λ = o.45 μ and T = 4 it decreases by about 11 % in comparison with T = 1.

2. The Total Absorption of the Atmosphere

The Fig. 13 shows the total absorption of the atmosphere in case of an absorbent aerosol, i.e. the percentage ratio of the radiant flux density at a specific wavelength which is absorbed by the entire atmosphere, to the incident spectral solar flux density $S_{o\lambda}$. The abscissa again represents the turbidity factor T. The total absorption shows a practically linear increase with increasing turbidity, while the rate of increase grows with increasing values of the albedo of the earth A.
The consideration of the interaction between the total absorption and the reflection of the planet earth reveals that only the atmosphere takes the benefit of the energy gain of the system atmosphere - surface in comparison with the Rayleigh atmosphere as it is observed with increasing values of the earth's albedo A. In addition to that: The total absorption is partly also due to a reduction of the energy fed to the surface in comparison with a non-absorbent atmosphere.
E.g. at λ = o.45 μ and A = o.25 and T = 1 the surface receives about 69 % of the incident spectral solar flux density; in case of a non-absorbent aerosol with T = 4 this percentage is reduced to 66 % in case of an absorbent aerosol, however, it is as low as 5o %.

The above values of the reflection and total absorption are of the same order of magnitude as those published by G. M. Yamamoto 1971 [16]; for a larger wavelength range and slightly differing parameters though.

3. Radiant Divergence

The energy absorbed by the aerosol results in a heating rate of the atmosphere which depends on the height. This rate is proportional to the divergence of the spectral radiant flux density integrated over the wavelength.

The Fig. 14 shows the plot of the ratio D of the spectral radiant divergence to the incident spectral solar radiant flux density $S_{o\lambda}$, expressed as % per km, as a function of the height h km for T = 4 and the zenith distance of the sun Z = 36.9°.
The striking feature of the run of the curves is the fact that at Z = 66.5° and A = 0 ~~(these not shown)~~ the spectral divergence near the surface is greater for λ = 0.55 μ than for λ = 0.45 μ, though the reverse is true with the relevant volume absorption coefficients. Obviously, the greater volume absorption coefficient related with smaller wavelengths is overcompensated by stronger attenuation of the direct solar radiation because of greater optical thickness due to the great zenith distance of the sun.

The spectral divergences in the figure enable one to read out the energy which is absorbed per unit of time and volume at a specific height in the spectral interval between λ = 0.45 μ and λ = 0.55 μ.

The following table lists the values for $Z = 36.9^{o}$ at the heights of 0 and 1 km, in cal min^{-1o} cm^{-3}:

km	A = 0	A = o.25	A = o.8
0	$o.12 \cdot 1o^{-6}$	$o.17 \cdot 1o^{-6}$	$o.29 \cdot 1o^{-6}$
1	$o.o9 \cdot 1o^{-6}$	$o.12 \cdot 1o^{-6}$	$o.19 \cdot 1o^{-6}$

For reason of comparison, mention is made of the corresponding value for the absorption exerted by water vapor taken over the entire solar spectrum of an atmosphere with 2 g cm^{-2} water vapor at the surface according to W. T. Roach 1961 (17); it amounts to $o.4 \cdot 1o^{-6}$ cal min^{-1} cm^{-3}.

The consideration that the incident radiation between $\lambda = o.45\mu$ and $\lambda = o.55\ \mu$ is only about 15 % of the total solar radiation leads to the estimate that the energy rates due to the aerosol absorption in the total solar spectrum amount to values near the surface which supersede those of the water vapor absorption.

4. Conclusions

The above results prove that the addition of aerosol to the atmosphere yields an influence on the energy balance of the planet earth which is of an order of magnitude that cannot be neglected any more. Especially, the absorption which is exerted by the aerosol, must be taken into account and this results in the necessity of measuring exactly the imaginary part of the complex refractive index of aerosol. The latter

may reach an influence on the heating rate in the atmosphere which is of similar importance as that of the water vapor absorption.

V. Measurements Results of the Spectral Solar Extinction and Sky Radiance Performed at the Hohenpeissenberg Observatory, Southern Bavaria, 980 m alt

Measurements of solar extinction and sky radiance have been done to compare the calculated values of the sky radiance with the measured ones.
On Fig. 15 are plotted the measured (dashed lines) and the calculated results of sky radiance in the solar almucantar. The measurements have been performed in June 1971. The calculated results are based on the new theoretical method by G. Eschelbach 1971 [14] which includes the scattering of higher order in the turbid atmosphere. There have been used the model 7 on Fig. 1, of an aerosol size distribution which has been measured in Middle Europe mostly. The refractive index of the aerosol particles has been measured by G. Hänel.
It is to be seen a rather good agreement between theory and experiment.
On Fig. 16 - 19 are given some more results of the measurements from Hohenpeissenberg performed in October 1971. They show the diurnal variation of the spectral extinction and sky radiances at different scattering angles, different solar elevations and different wavelengths.

VI. Results of Measurements of the Physical Properties of Samples of Atmospheric Aerosol Particles as Functions of the Relative Humidity

Former and recent measurements have been evaluated by means of a computer program. The results are presented in the Figures 2o - 2). The following parameters have been plotted as functions of the relative humidity f: The mean density $\rho(f)$, the real part of the mean complex index of refraction n (f), the volume ratio $V(f)/V_o$, the mass ratio $m_w(f)/m_c$, the extinction coefficients of the air borne aerosol particles $\sigma_K(f)/\sigma_{K_o} = [V(f)/V_o]^{2/3}$, G. Hänel 1971 (11). The ratios $V(f)/V_o$ and the ratio $\sigma_K(f)/\sigma_{K_o}$ have been plotted in double logarithmic scale as functions of (1 - f), the others in linear scale.

For some samples, the Figures also show values for decreasing relative humidities as indicated by arrows. The value of the volume growth coefficient φ close to f = o for increasing relative humidity could not be determined with the equipment at hand; therefore, it has been set: $\varphi(f = o) = o$.

The measurements show that at low relative humidities the mass of water condensed on the aerosol particles is but small. No sooner than from f = o.5 to o.7 on the samples adsorb larger amounts of water. The same feature is valid for the volume of the samples and for the extinction coefficient of the particles. Consequently, the mean density and the real part of the mean complex index of refraction (except for the Fig. 2o a) only slightly decrease at low relative humidities. Whereas at high relative humidities their values gradually come close to those of water.

The volume growth coefficients show particularities in the volume growth as a function of the relative humidity. At f = 1, they have finite values (see G. Hänel 1970 [18], Fig. 1).

Furthermore, it is a striking feature that there are different results obtained at increasing or decreasing relative humidity resp. insofar as the samples contain more water at decreasing relative humidity than at increasing relative humidity. This hysteretic effect has already been described by E. Wall (1942)[19], C. Junge (1952)[20], C. Orr et al. (1958)[21] and P. Winkler (1969)[22]. Special experiments in this institute and computations conducted by R. Defay et al. (1966)[23] indicate that a suitable choice of the pre-condition with regard to the change in humidity, enables one to obtain values which lie inside the hysteresis loop. Thus, it is obvious that range of relative humidity which is subject to hysteretic effects, the physical parameters of the aerosol particles depend on the previous change in humidity, too.

The Figures prove that the hysteretic effect varies from one sample to the other. Its maximum occurs at different values of relative humidity. Thus, it must not be neglected.

Furthermore, it has been found that the values of the parameters presented in the figures also differ from one sample to the other within those ranges of humidity which are not subject to hysteretic effects. E.g. the values of the ratio $\sigma_K(f = 0.9)/\sigma_{K_0}$ fall in between 2 and 5.

This leads to the conclusion that more measurements are needed, a thorough investigation into the hysteretic effect is important, because the relative humidity values related with it do frequently occur under atmospheric conditions.

VII. Conclusions

Since some years research on atmospheric optical radiation transmission, air pollution and radiation fluxes through the atmosphere has been performed at the Institute for Meteorology, University of Mainz. The extinction properties of the atmospheric aerosol particles have been investigated comprehensively. They depend on the material of the aerosol particles (demonstrated by the complex refractive index). It could be shown that the material changes localy and temporally. These changes are dependend on the relative humidity of the air strongly. In spike of the submitted results it is necessary to perform some more research in this field. We need an increased research on the refractive index, including absorption of atmospheric particles in relation to their composition, origin, size and shape and its change with increasing pollution for short- and longwave radiation. Also more data on particle growth and density with humidity are necessary to understand the influence on the refractive index with relative humidity. At suitable time intervalls the refractive index and the detailed size distribution of particles should be determined at selected places in both clean and polluted air. Furthermore more detailed measurements of the 4 Stokes parameters would improve our knowledge of the optical behaviour of our atmosphere.

References

1. Jaenicke, R., Junge, Ch., Kanter, H.J. (1971): Messungen der Aerosolgrössenverteilung über dem Atlantik. Meteor-Forschungsergebnisse Reihe B, Verlag Gornträger, Berlin.

2. Junge, Ch. (1963): Air Chemistry and Radioactivity, Chapter 2, Academic Press, New York and London.

3. de Bary, E., Braun, B., Bullrich, K. (1965): Tables Related to Light Scattering in a Turbid Atmosphere. AF Cambridge Research Lab., 65 - 71o (I - III). Special Reports, No. 33.

4. Danzer, K.H., Bullrich, K. (1965): The Influence of Absorption on the Extinction of Solar and Sky Radiation. Applied Optics, 4, 1500.

5. Eiden, R. (1971): unpublished, see Chapter III in this Report.

6. Bullrich, K., Eiden, R., Jaenicke, R., Nowak, W. (1968): Solar Radiation Extinction, Sky Radiation, Sky Light Polarization and Aerosol Particle Total Number and Size Distribution on the Island Maui (Hawaii). PAGEOPH, 69 - 71, 280.

7. Bullrich, K. and Eiden, R. (1969): Research on Atmospheric Optical Radiation Transmission. Scientific Report No. 6, Contr. F 61052 67 C 0046, Jan 1968, AF Cambridge Research Lab.

8. Quenzel, H. (1968): Optische Bestimmung der Kontinuum-Absorption maritimer Luftmassen im Spektralbereich der Sonnenstrahlung. "Meteor" Forschungsergebnisse, Reihe B, No. 1.

9 a. Silz, D. (1969): Die spektrale Schwächung der Sonnenstrahlung in der Atmosphäre. Master Thesis. Mainz-University.

9 b. Kurz, U. (1969): Extinktionsmessungen mit einem horizontalen Scheinwerferstrahl. Master Thesis, Mainz-University.

10. Hänel, G. and Bullrich, K. (1970): Berechnungen der spektralen Strahlungsextinktion an atmosphärischen Aerosolpartikeln mit verschiedenen komplexen Brechungsindices. Beitr. Phys. Atm., 43, 202.

11. Hänel, G. (1970): New Results Concerning the Dependence of Visibility on Relative Humidity and Their Significance in a Model for Visibility Forecast. Beitr. Phys. Atm. 44, 137.

12. Fischer, K. (1971): Bestimmung der Absorption von sichtbarer Strahlung durch Aerosolpartikeln. Beitr. Phys. Atm. 43, 244.

13. Chandrasekhar, S. (1950): Radiative Transfer. Dover Publ., New York.

14. Eschelbach, G. (1971): A direct Method for the Intergration of the Equation of Radiative Transfer in a turbid atmosphere. J. Quant. Spectrosc. Radiat. Transfer 11, 757.

15. Hänel, G. (1968): The Real Part of the Mean Complex Refractive Index and the Mean Density of Samples of Atmospheric aerosol particles. Tellus XX, 371.

16. Yamamoto, G. and Tanaka, M. (1971): Increase of Global Albedo due to air pollution (to be published) SMIC Conference, July 1971, Stockholm, MIT, Cambridge, Mass.

17. Roach, W. T. (1961): The Absorption of Solar Radiation by Water Vapour and Carbon Dioxyde in a Cloudless Atmosphere. Quat. Journal of the Royal Meteorol. Soc. 87, 364.

18. Hänel, G. (197o): Die Grösse atmosphärischer Aerosolteilchen als Funktion der relativen Luftfeuchtigkeit. Beitr. Phys. Atm. 43, 119

19. Wall, E. (1942): Zur Physik der Wasserdampfkondensation an Kernen. Zeitschr. f. angew. Meteorol. 59, 1o6.

2o. Junge, Ch. (1952): Die Konstitution des atmosphärischen Aerosols. Ann. Meteorol. Suppl. I.

21. Orr, C. et al. (1958): Aerosol size and relative humdity. J. Colloid Sc. 13, 472.

22. Winkler, P. (1969): Untersuchungen über das Grössenwachstum natürlicher Aerosolteilchen mit der relativen Feuchte nach einer Wägemethode. Ann. der Meteorol. N. F. 4, 134

23. Defay, R. et al (1966): Surface Tension and Absorption. Longmans, London.

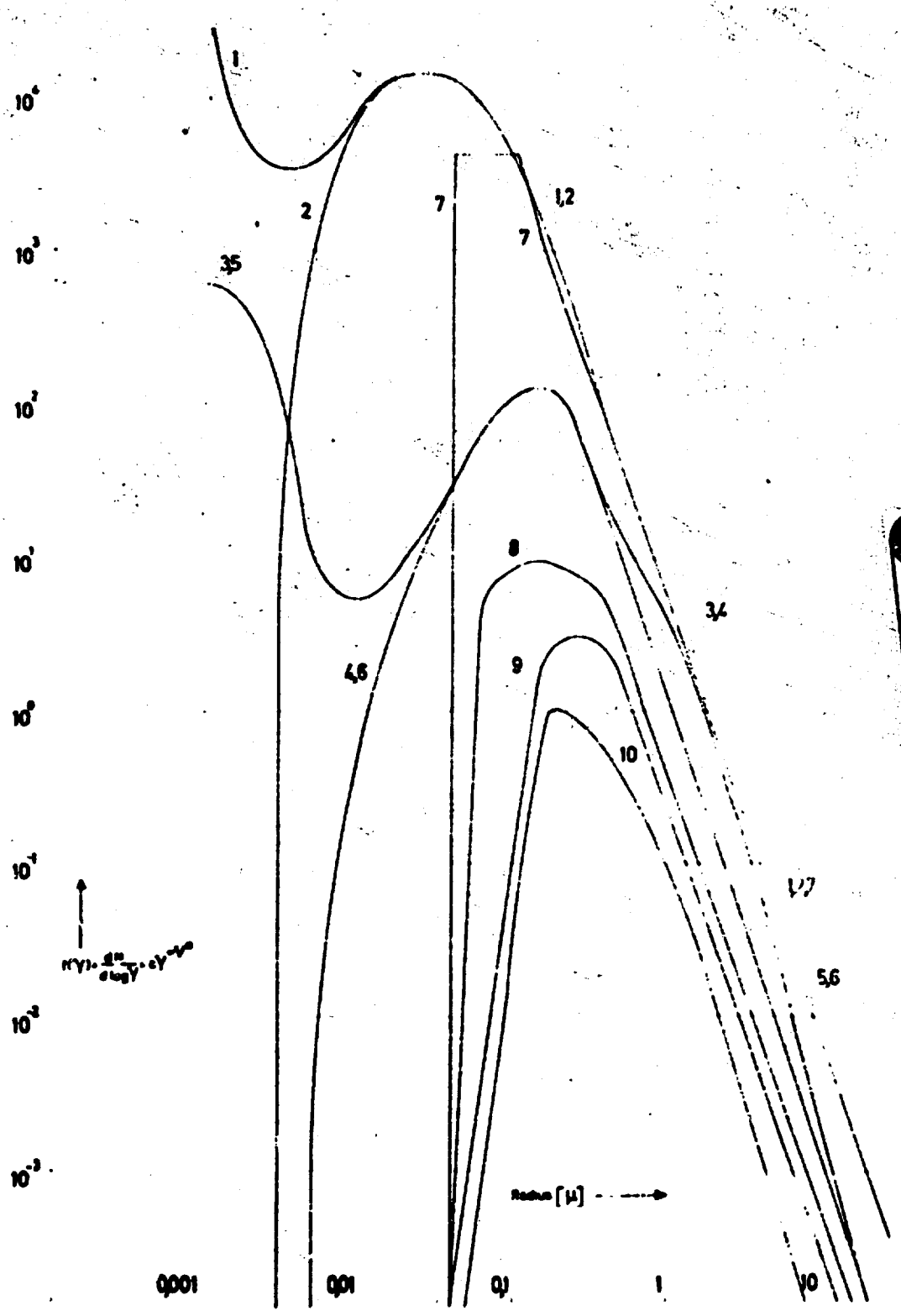

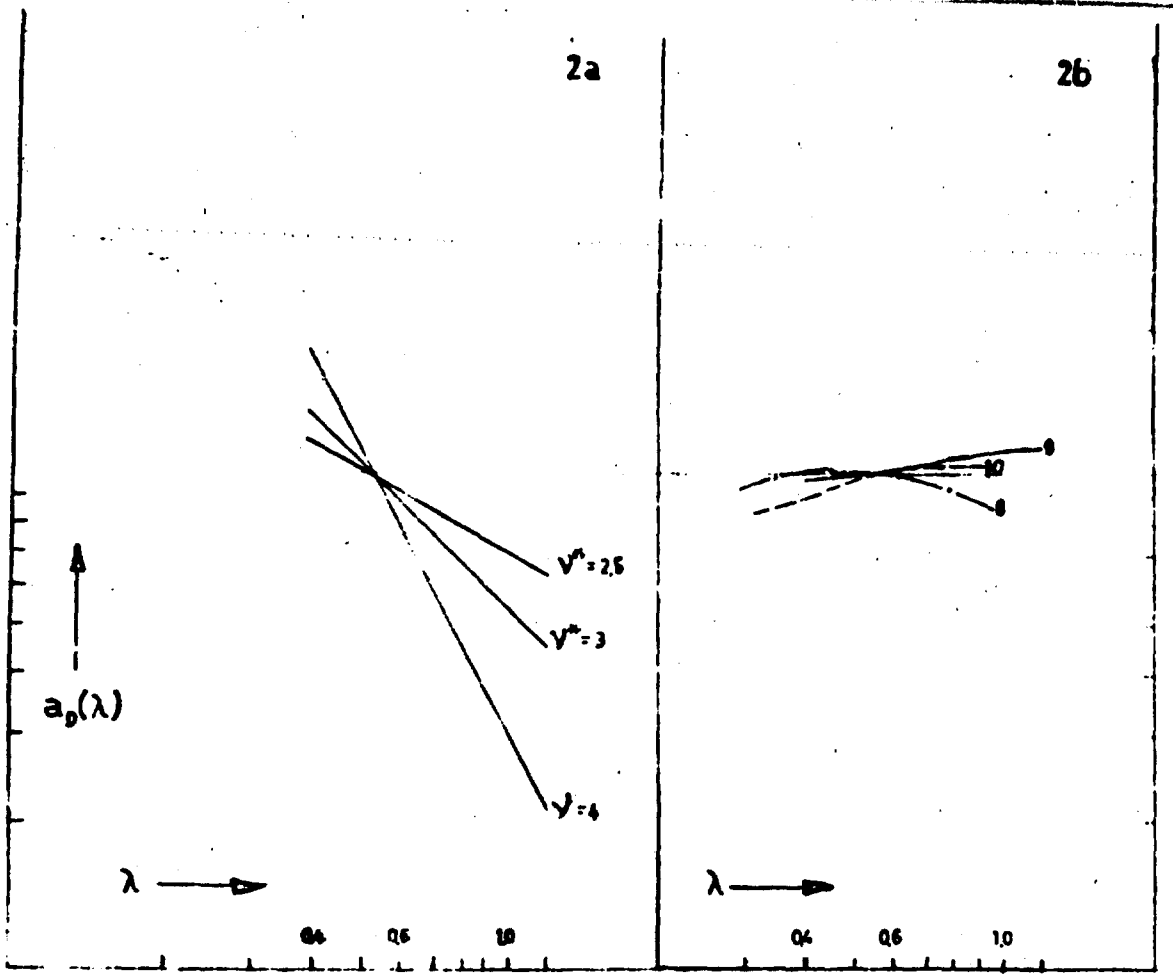
2a
2b
$a_p(\lambda)$
$\nu = 2,5$
$\nu = 3$
$\nu = 4$
λ
λ
0,4
0,6
1,0
0,4
0,6
1,0

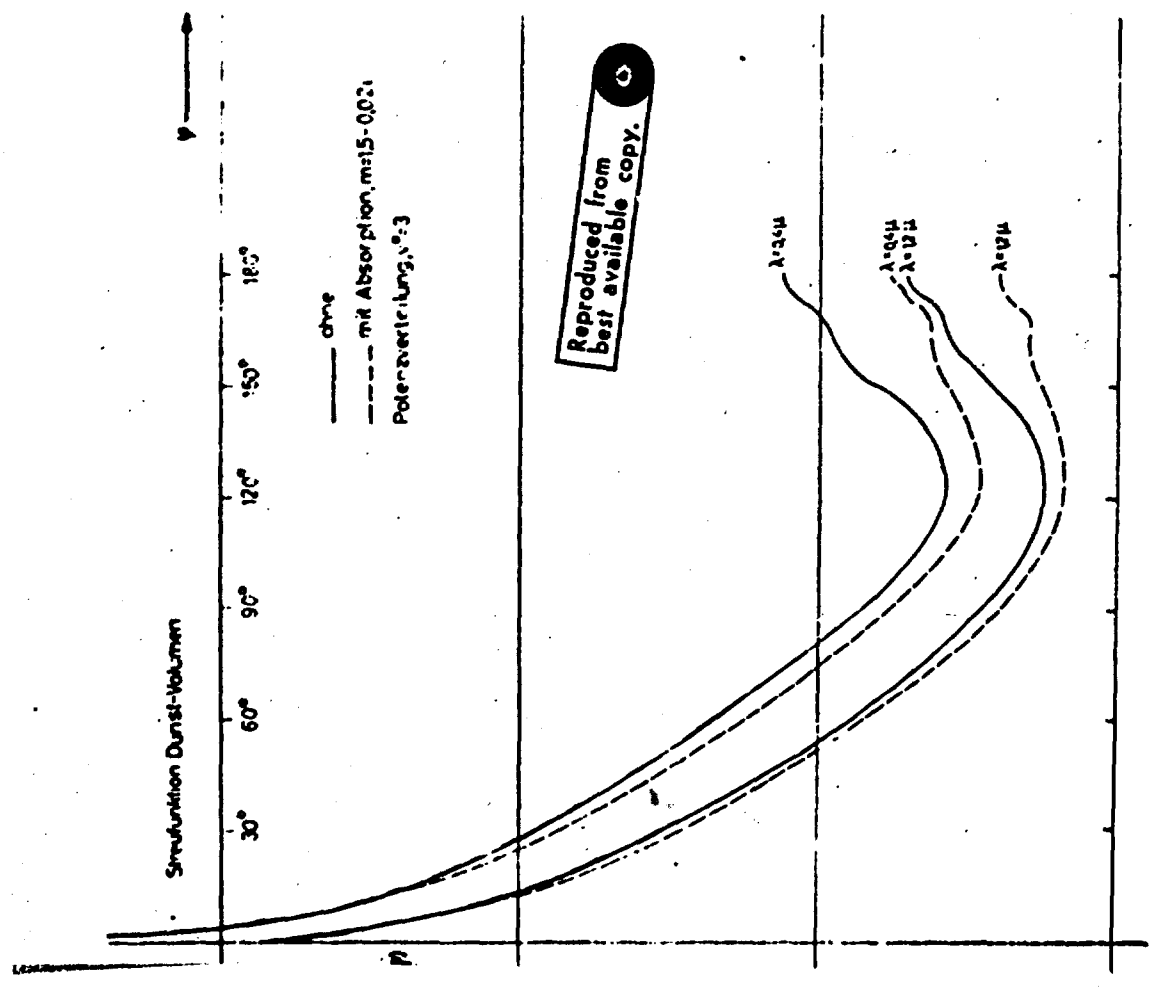
Streufunktion Dunst-Volumen
30°
60°
90°
120°
150°
180°
ohne
mit Absorption, m=1,5-0,02i
Polarisationsrichtung, ν=3
Reproduced from best available copy.

3

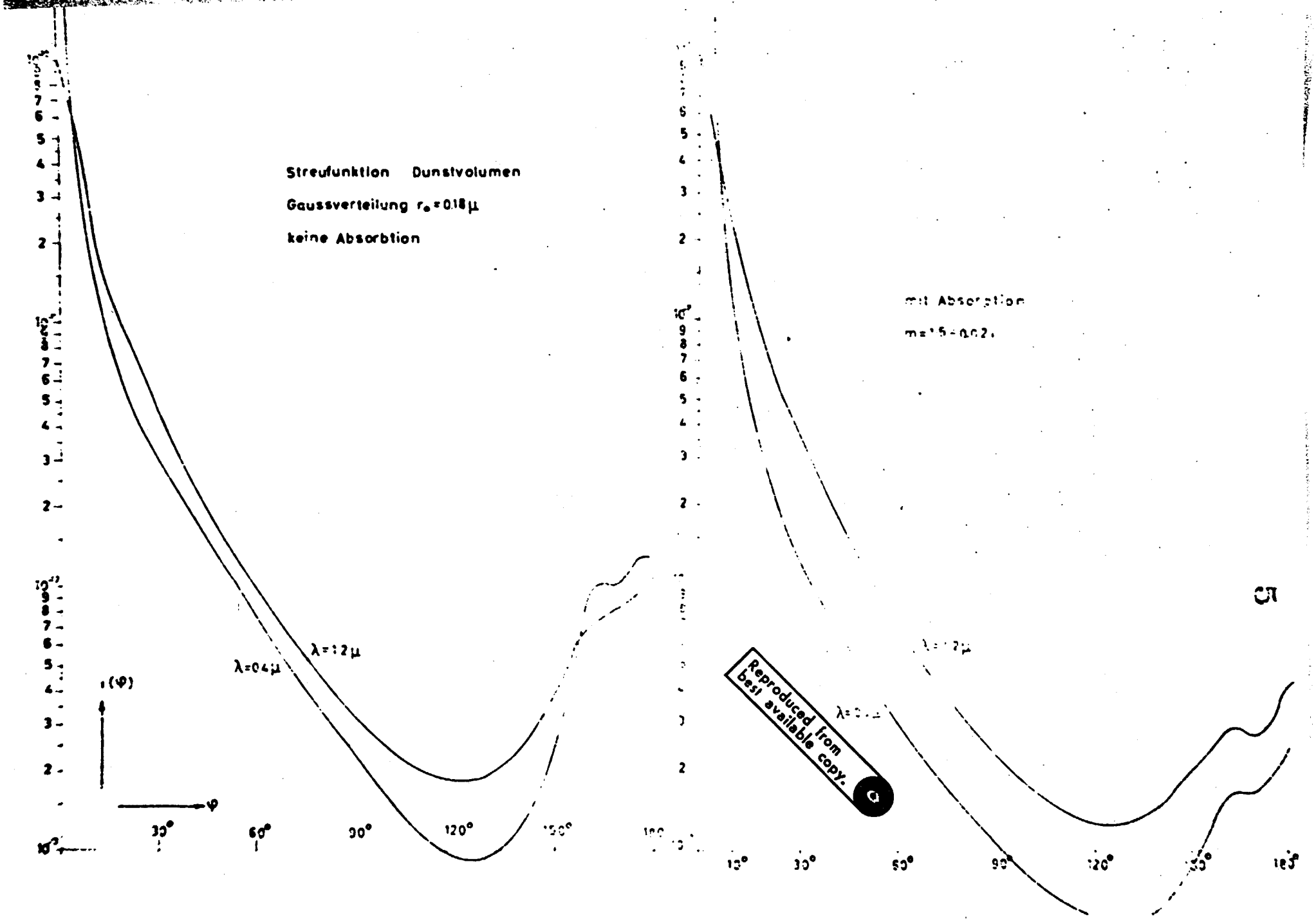
Streufunktion Dunstvolumen
Gaussverteilung $r_e = 0.18\mu$
keine Absorbtion
$\lambda = 0.4\mu$
$\lambda = 1.2\mu$
$i(\varphi)$
φ
30°
60°
90°
120°
150°
180°
mit Absorption
$m = 1.5 - 0.02i$
$\lambda = 1.2\mu$
Reproduced from best available copy.

4a

4b

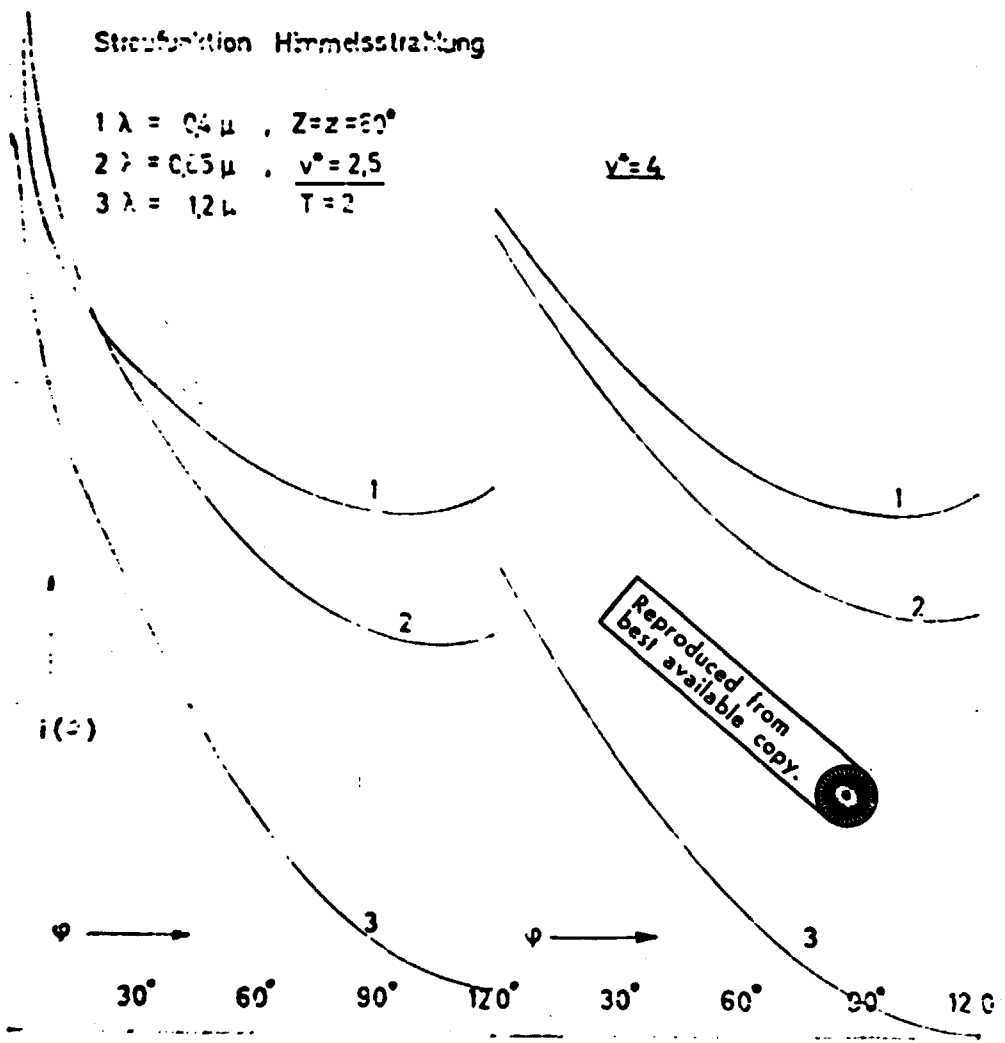

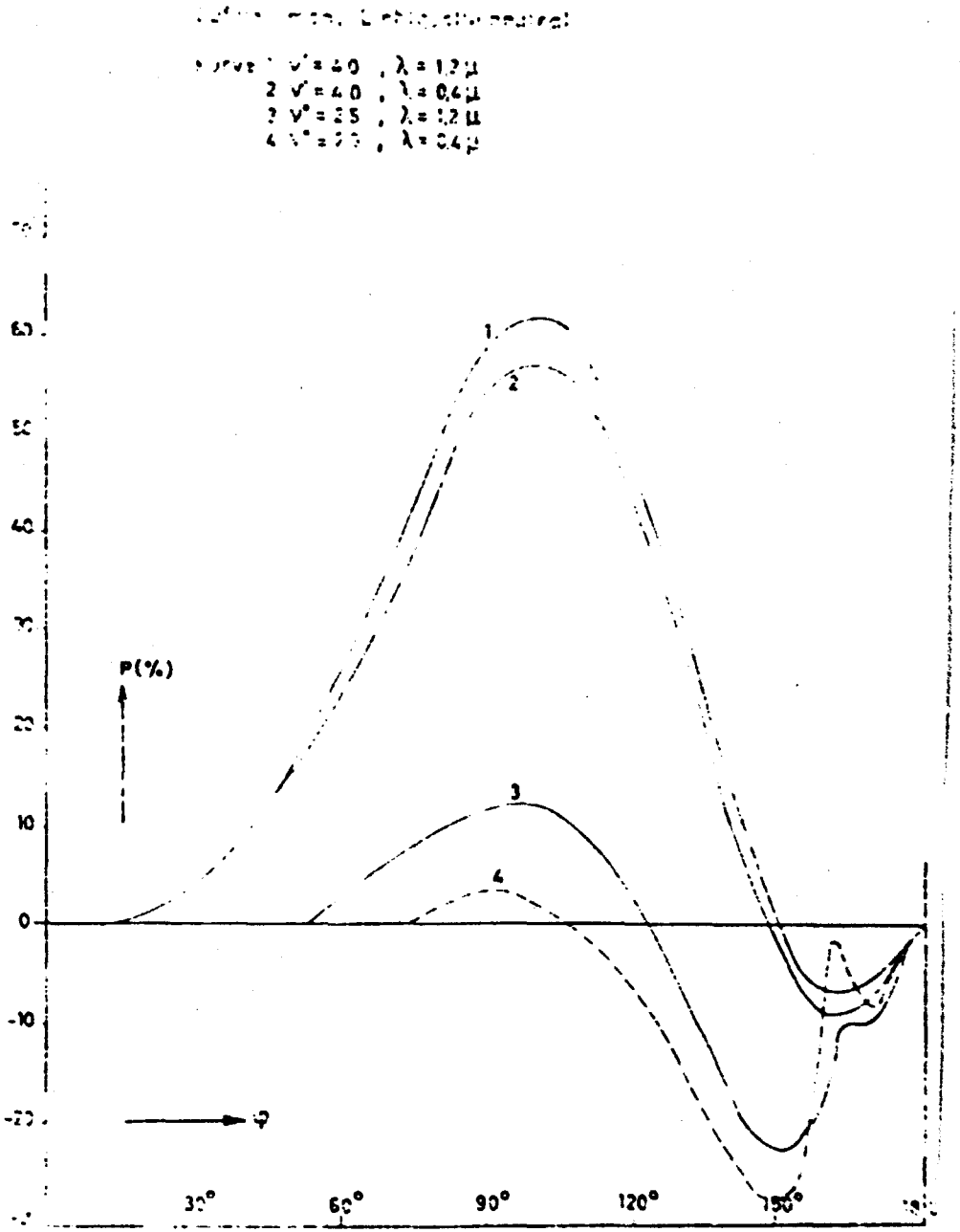

Polarisation Dunstvolumen
Gaussverteilung, $r_e = 0,18\mu$

Lichtquelle linear polarisiert

keine Absorption

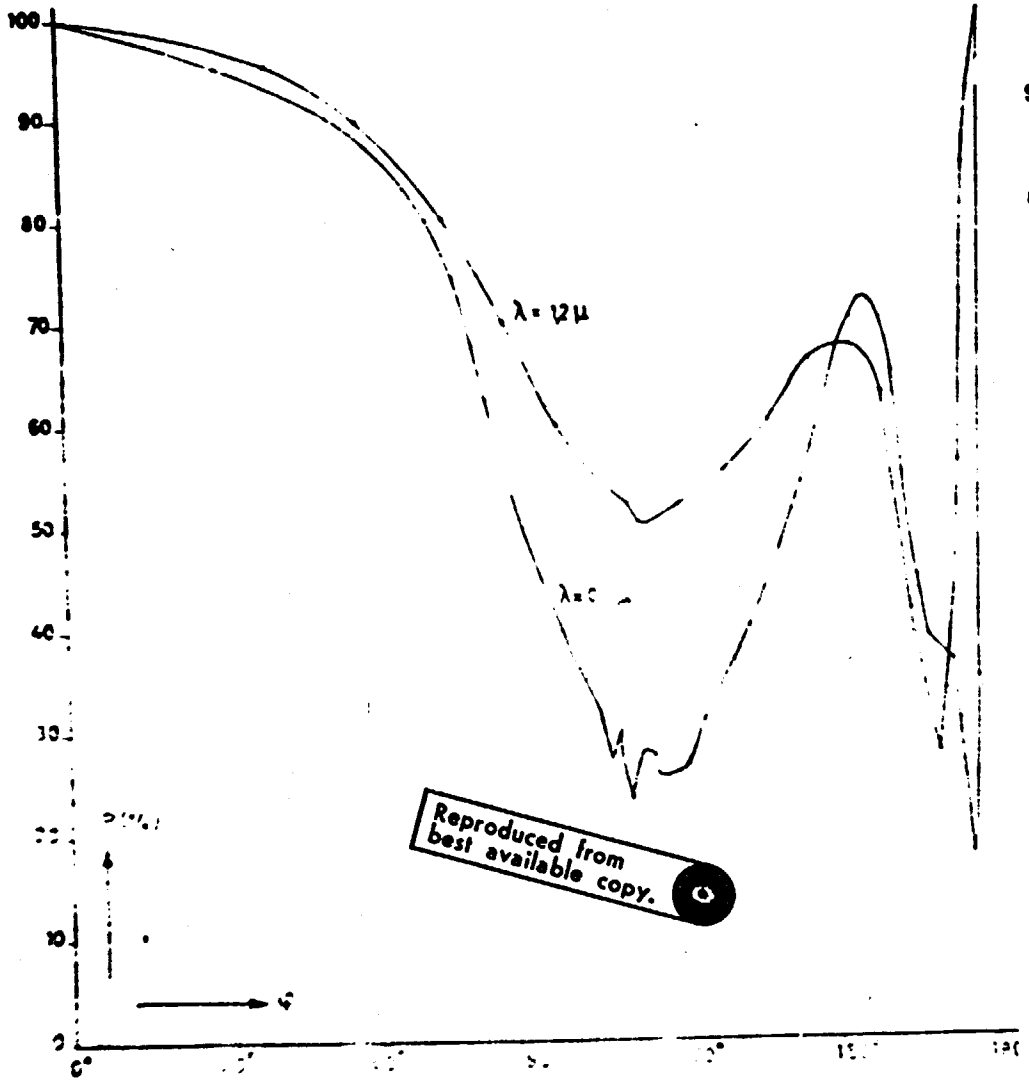

Polarisationsgrad Dunstvolumen

Potenzgrössenverteilung $V^6 = 3,0$

Lichtquelle linear polarisiert

mit Absorbtion, m=1,5 - 0,02 i

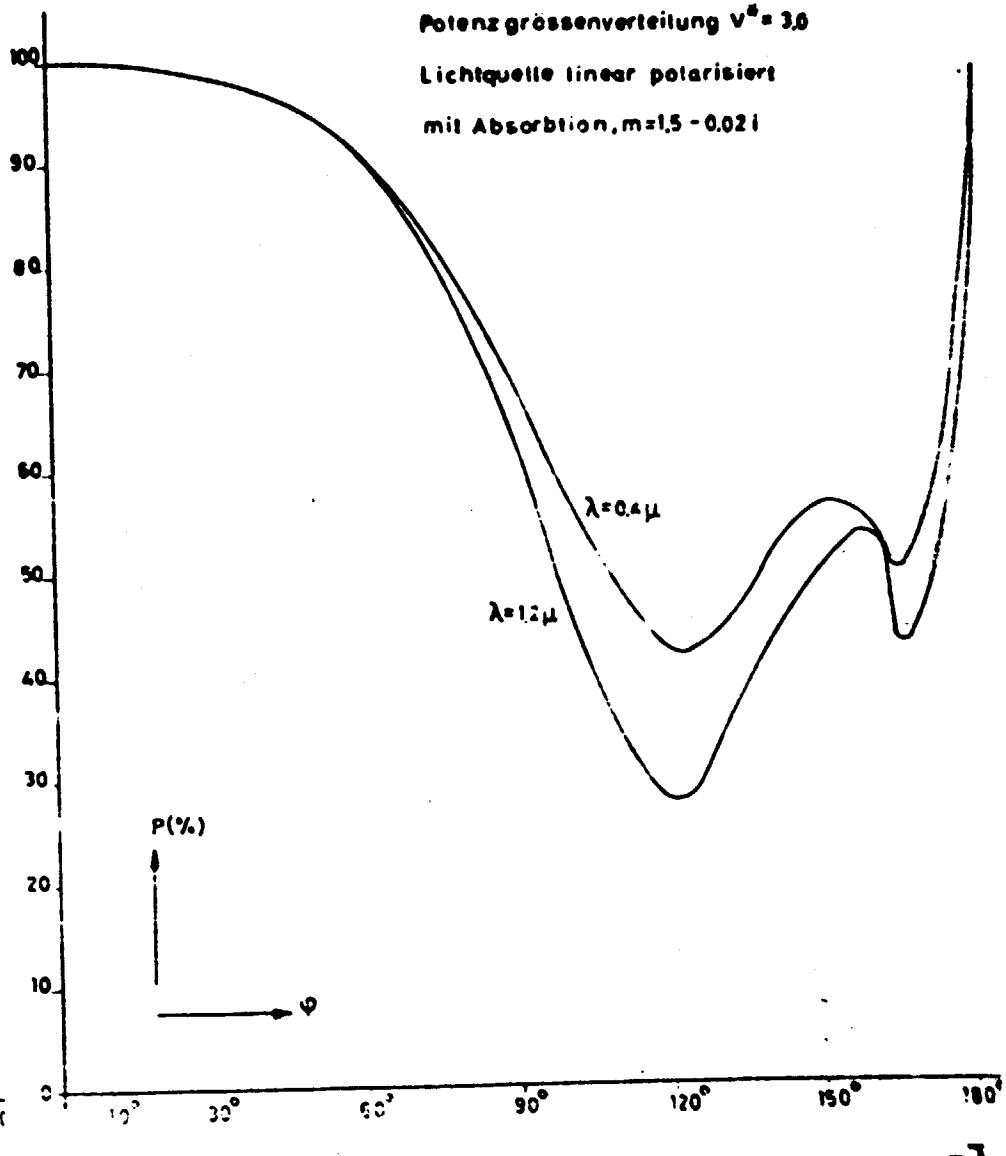

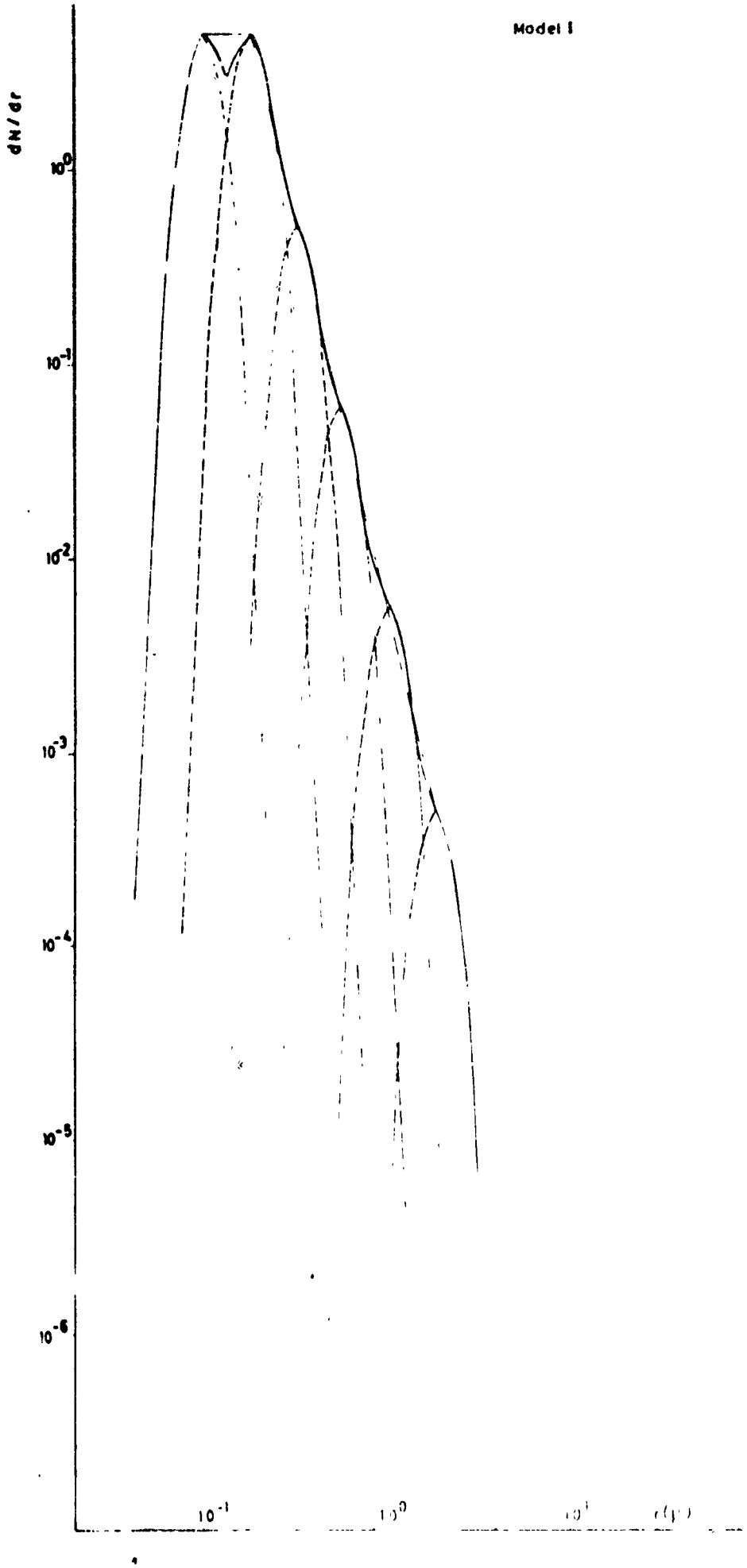
Model I
dN / dr
10^{0}
10^{-1}
10^{-2}
10^{-3}
10^{-4}
10^{-5}
10^{-6}
10^{-1}
10^{0}
10^{1}
r(pc)

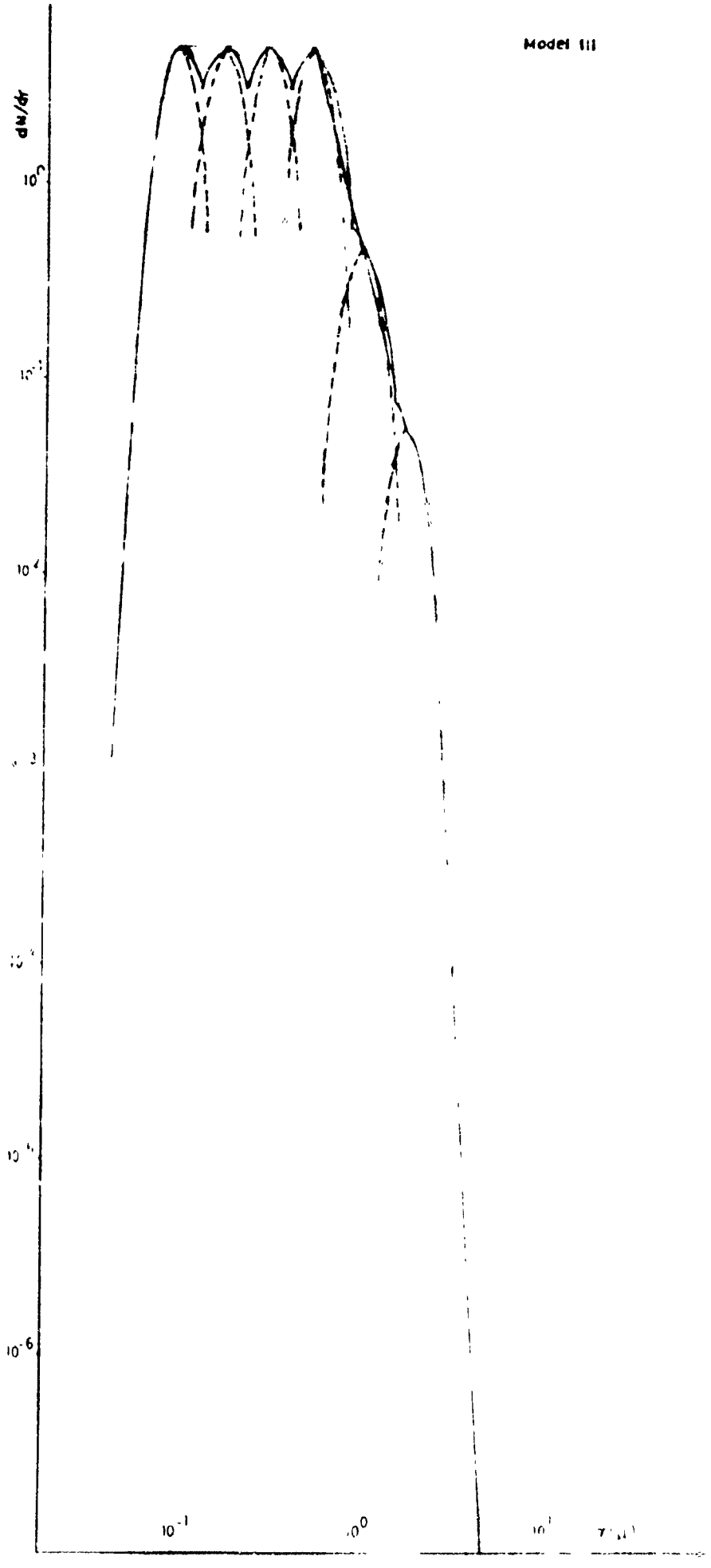
Model III
dN/dr
10^{0}
10^{-4}
10^{-6}
10^{-1}
10^{0}

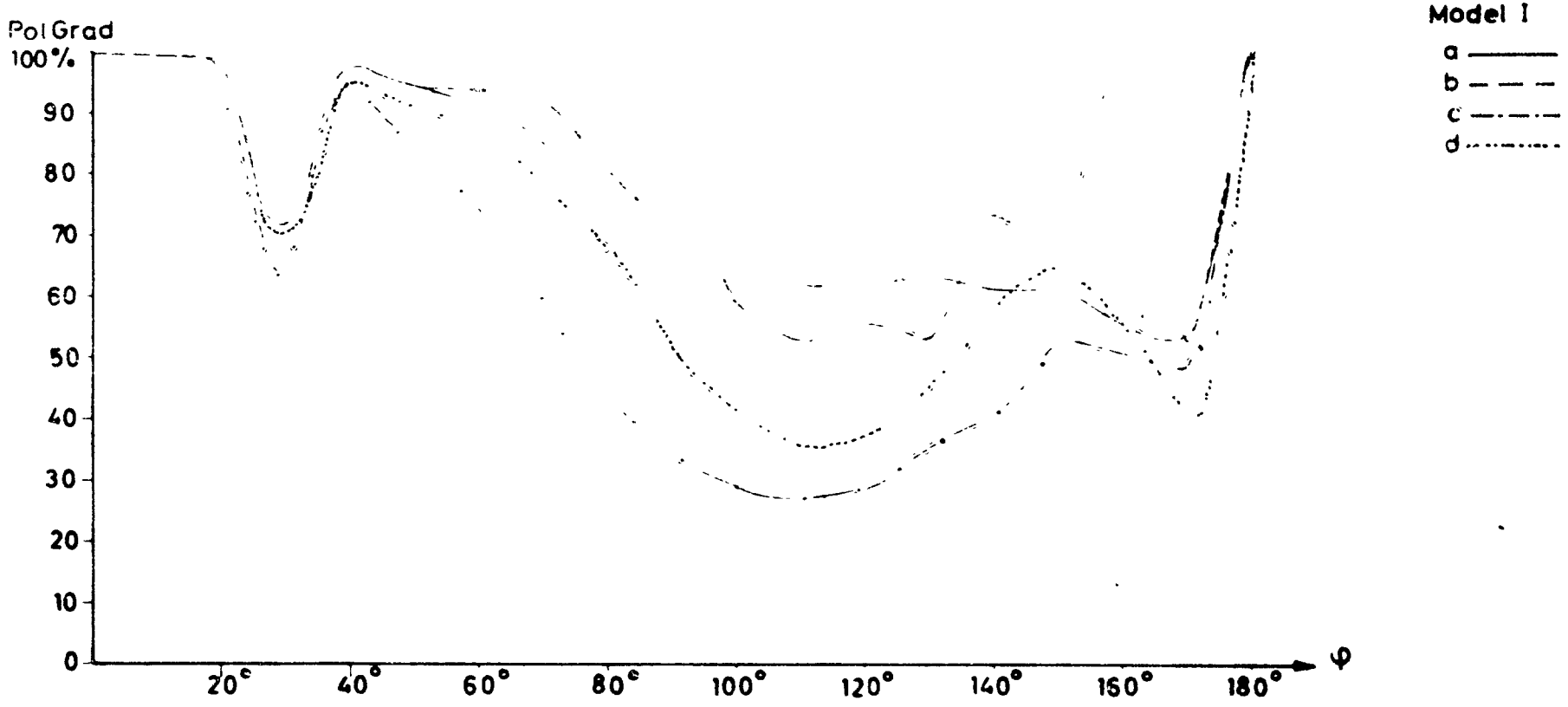
Pol Grad
100%
90
80
70
60
50
40
30
20
10
0
20°
40°
60°
80°
100°
120°
140°
160°
180°
φ
Model I
a
b
c
d

10a1

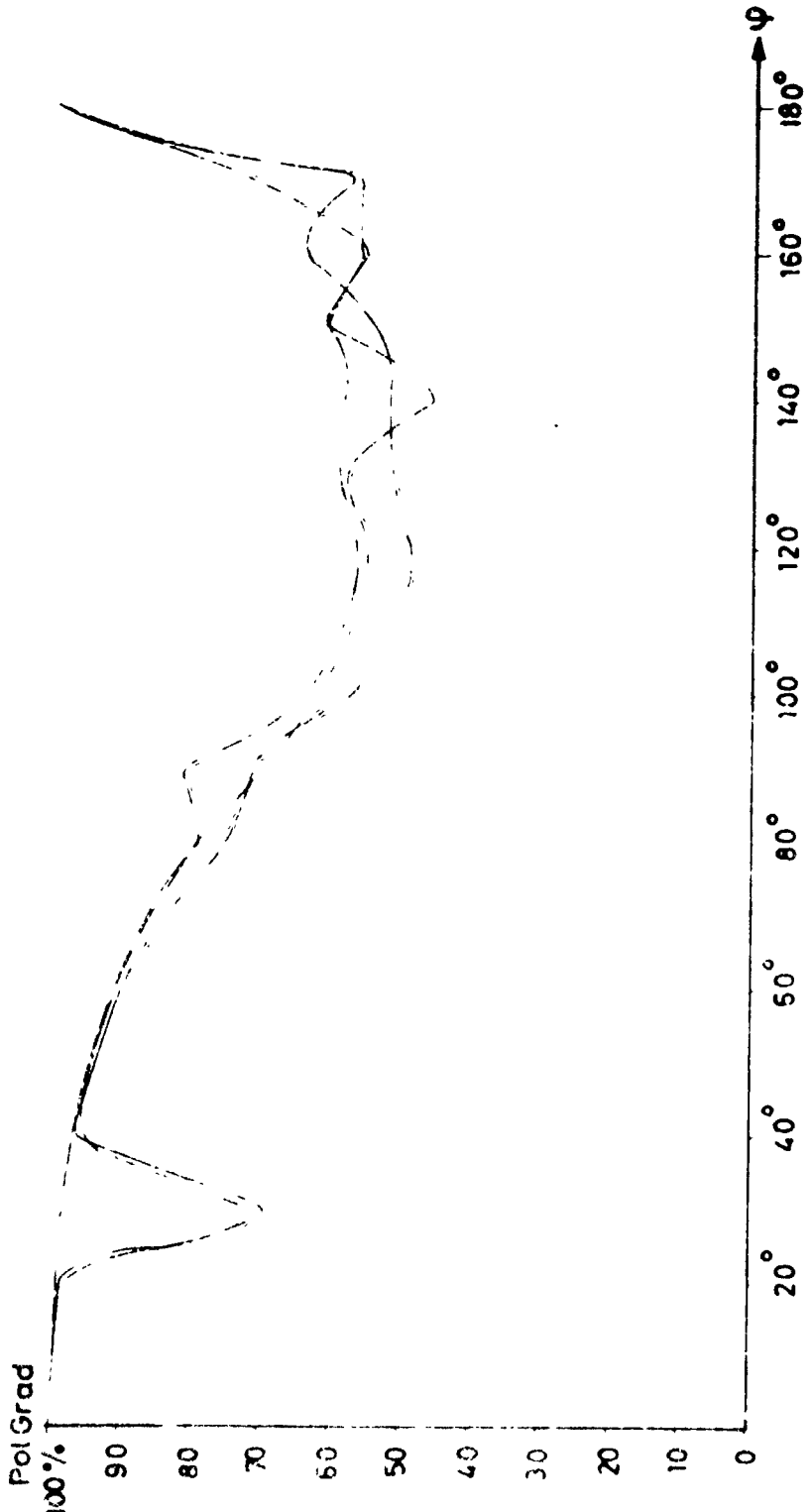
Model I
e
f
g
Pol Grad
100%
90
80
70
60
50
40
30
20
10
0
20°
40°
50°
80°
100°
120°
140°
160°
180°
φ

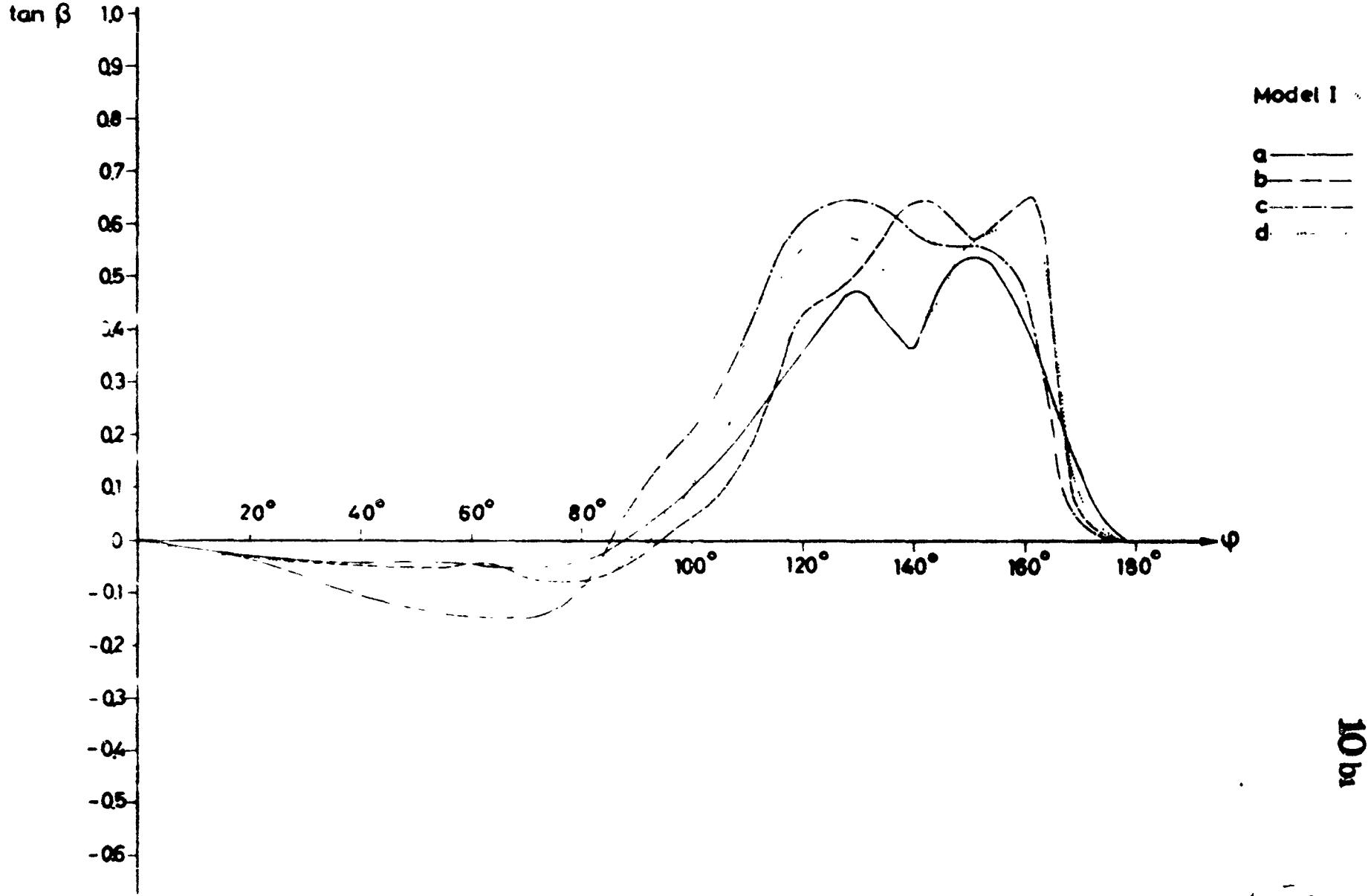
tan β
1.0
0.9
0.8
0.7
0.6
0.5
0.4
0.3
0.2
0.1
0
-0.1
-0.2
-0.3
-0.4
-0.5
-0.6
20°
40°
60°
80°
100°
120°
140°
160°
180°
φ
Model I
a
b
c
d

Abb. 10b

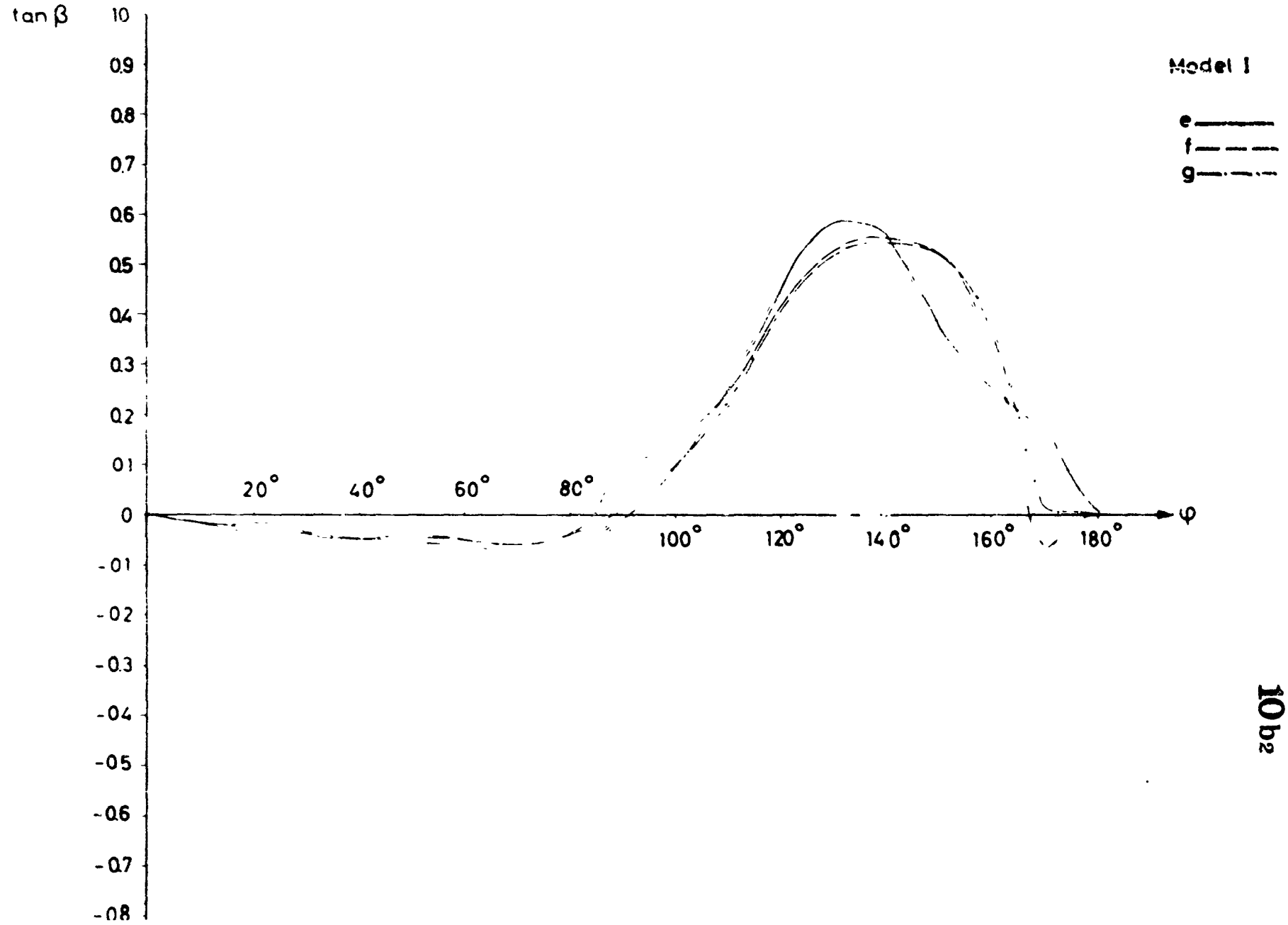
tan β
10
0.9
0.8
0.7
0.6
0.5
0.4
0.3
0.2
0.1
0
-0.1
-0.2
-0.3
-0.4
-0.5
-0.6
-0.7
-0.8
20°
40°
60°
80°
100°
120°
140°
160°
180°
φ
Model I
e
f
g

$10 b_2$

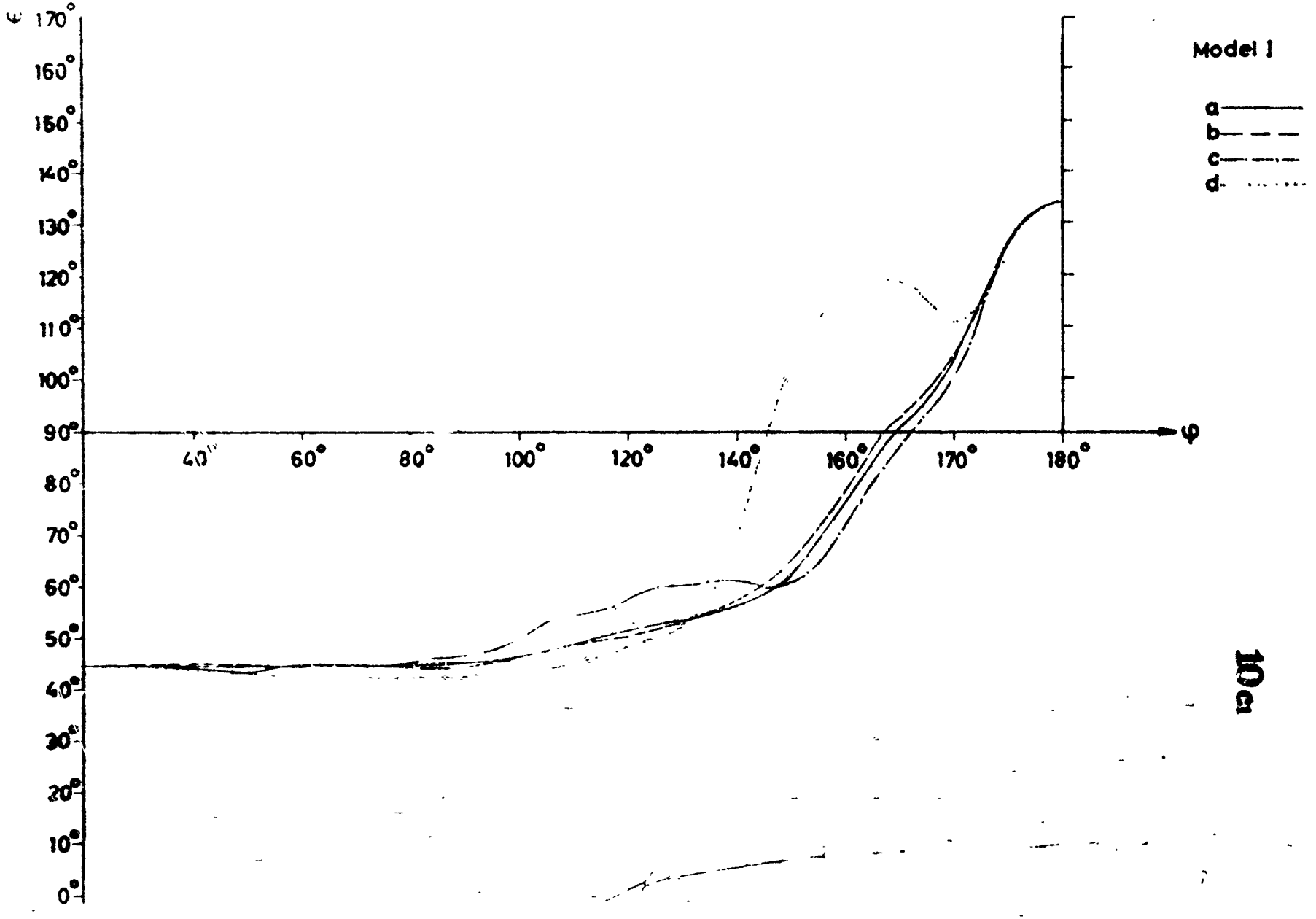
Model I
a
b
c
d
ψ
φ
170°
160°
150°
140°
130°
120°
110°
100°
90°
80°
70°
60°
50°
40°
30°
20°
10°
0°
40°
60°
80°
100°
120°
140°
160°
170°
180°

Fig. 10

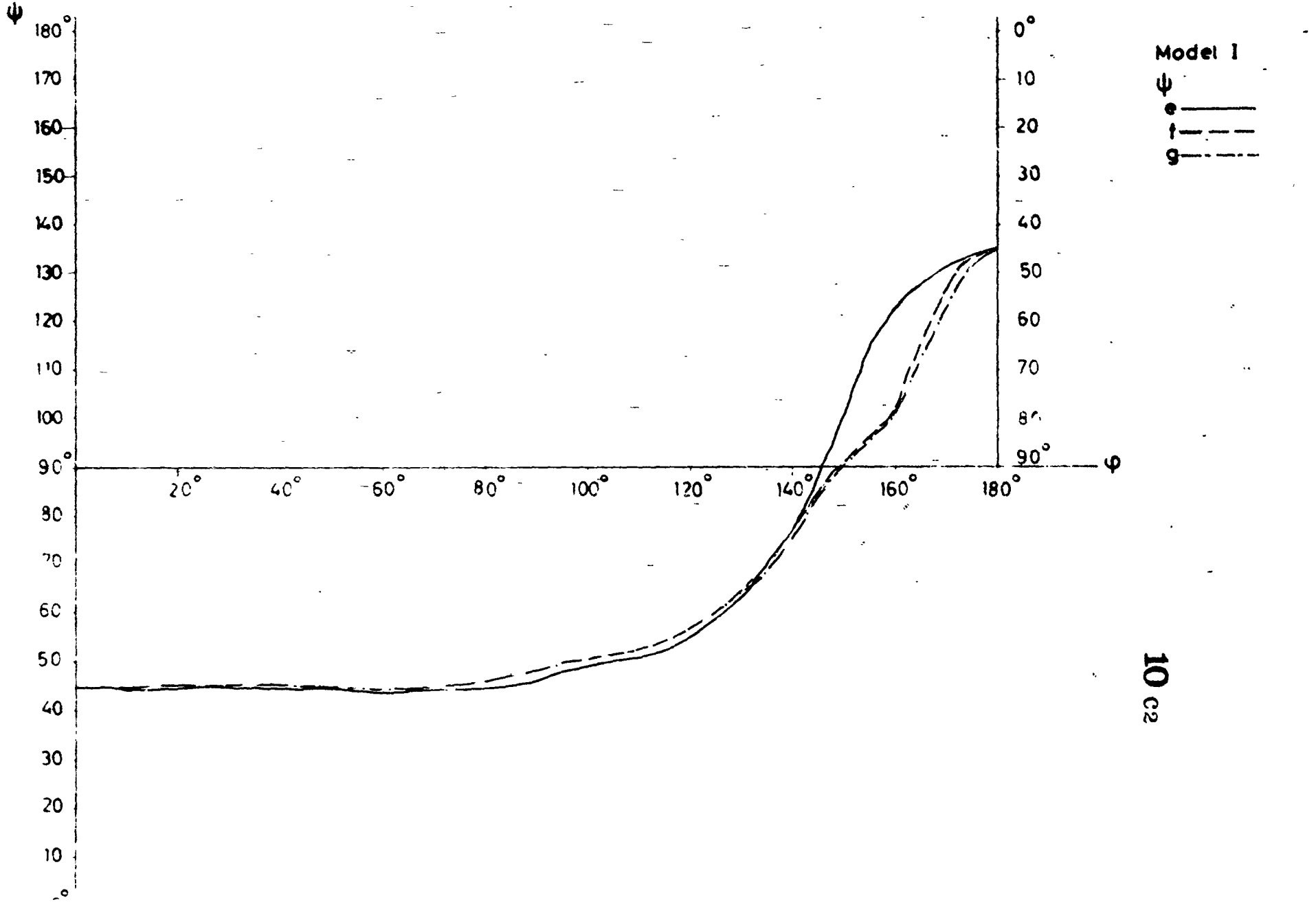
ψ
180°
170
160
150
140
130
120
110
100
90°
80
70
60
50
40
30
20
10
0°
10
20
30
40
50
60
70
80
90°
20°
40°
60°
80°
100°
120°
140°
160°
180°
φ
Model I
ψ
e
f
g

10 C2

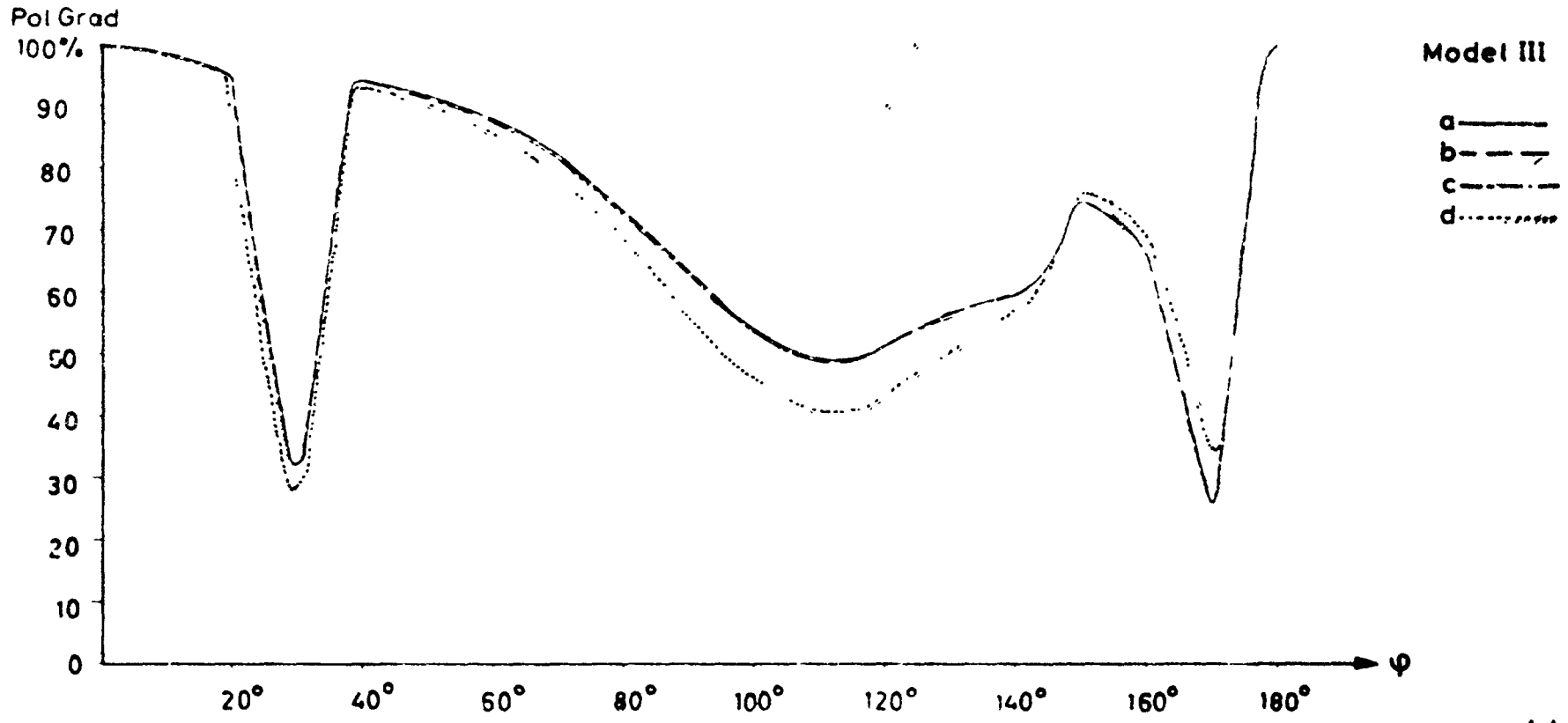
Pol Grad
100%
90
80
70
60
50
40
30
20
10
0
20°
40°
60°
80°
100°
120°
140°
160°
180°
φ
Model III
a
b
c
d

11 a1

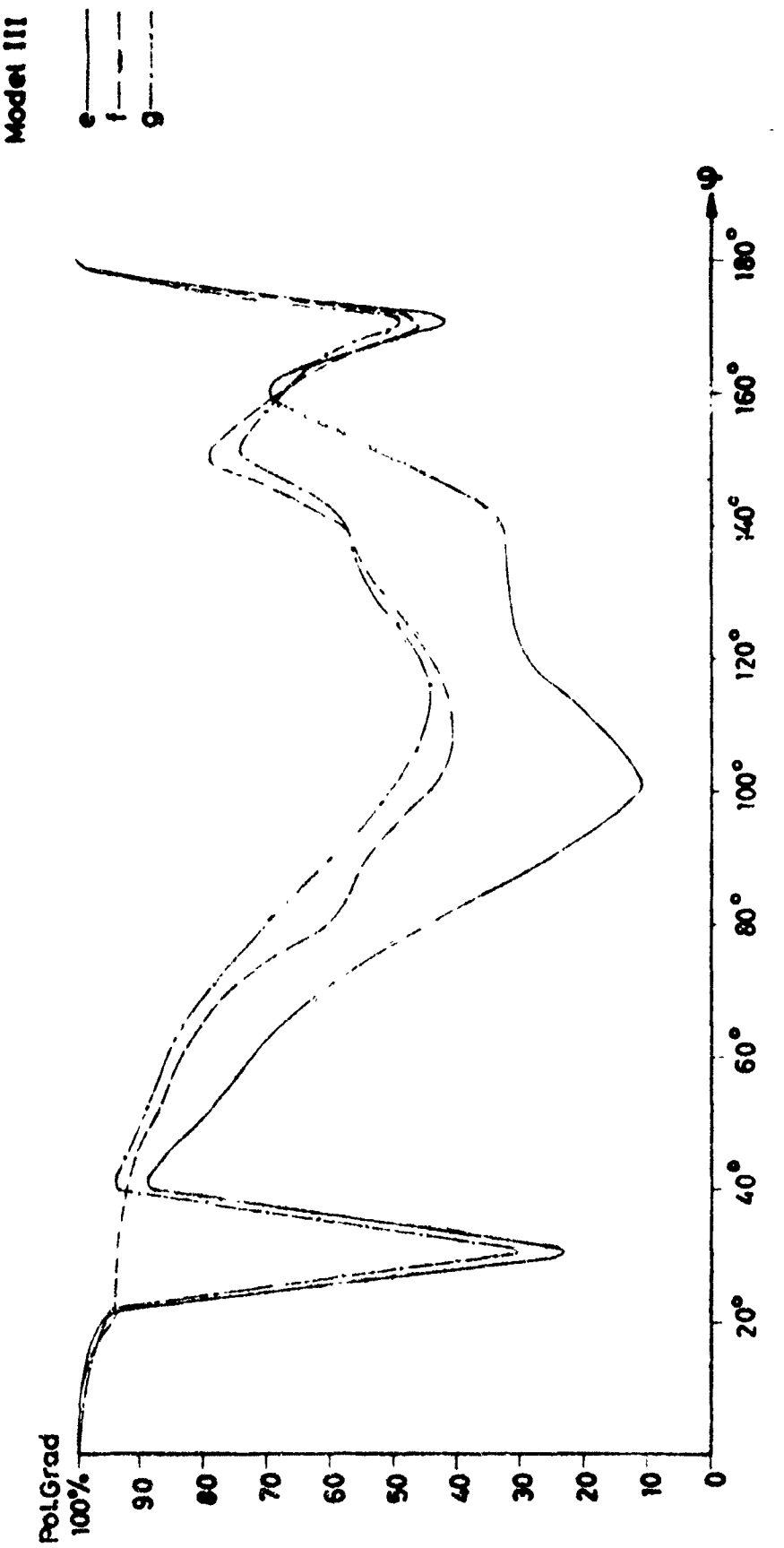
Model III
Pol.Grad
100%
90
80
70
60
50
40
30
20
10
0
20°
40°
60°
80°
100°
120°
140°
160°
180°
ϑ

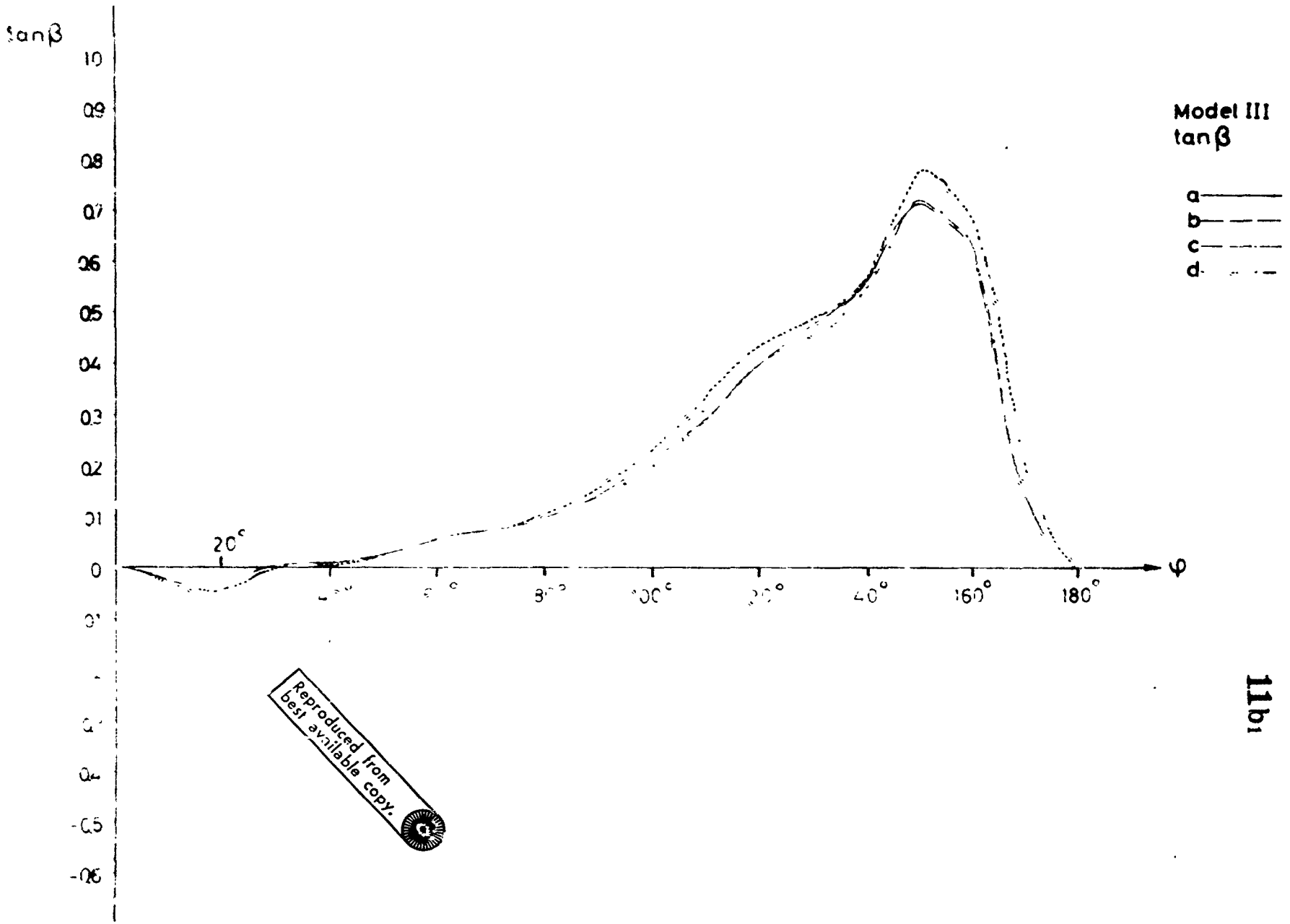

11b1

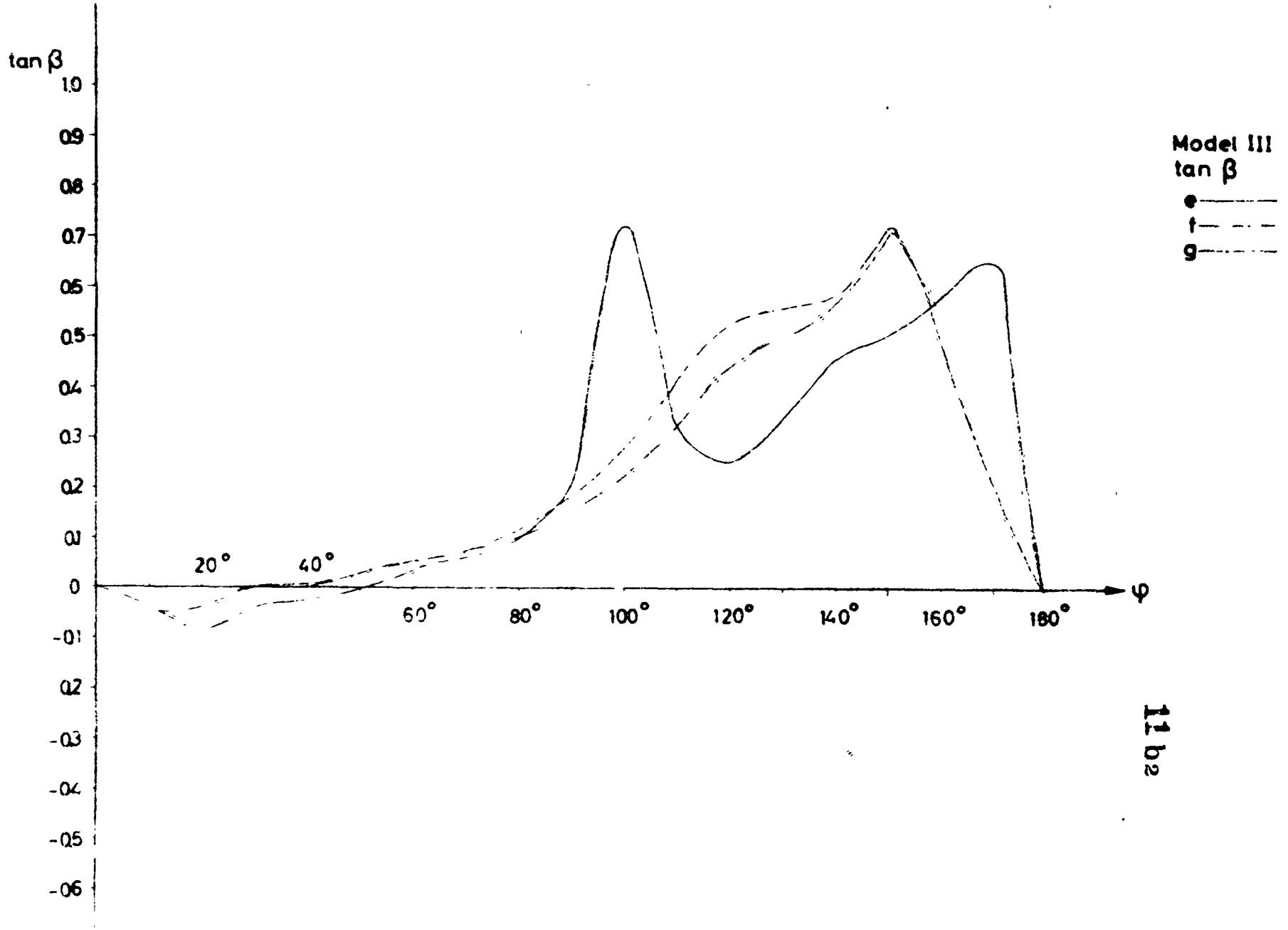
tan β
1.0
0.9
0.8
0.7
0.6
0.5
0.4
0.3
0.2
0.1
0
-0.1
-0.2
-0.3
-0.4
-0.5
-0.6
20°
40°
60°
80°
100°
120°
140°
160°
180°
φ
Model III
tan β
f
g

11 b2

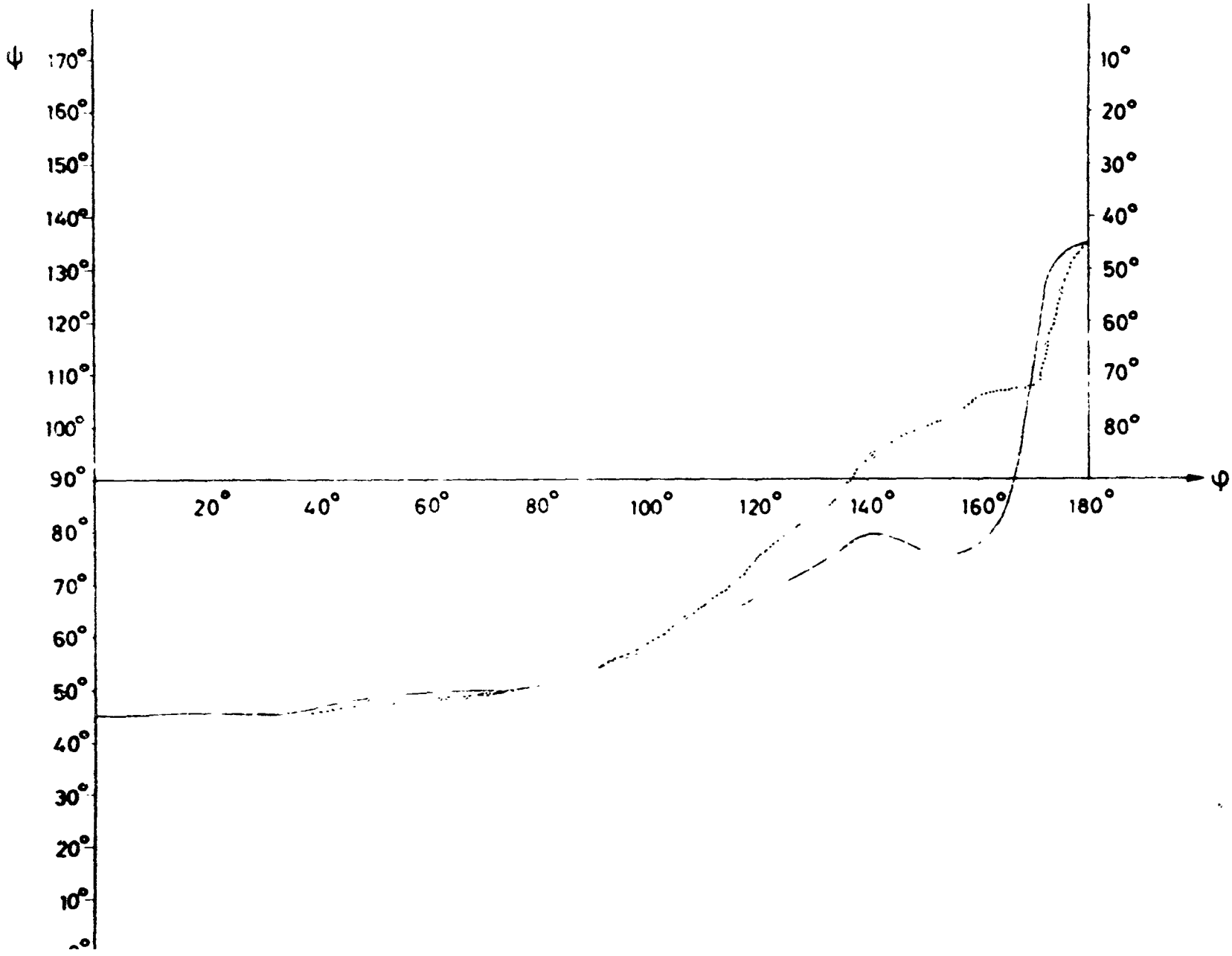
ψ
170°
160°
150°
140°
130°
120°
110°
100°
90°
80°
70°
60°
50°
40°
30°
20°
10°
20°
40°
60°
80°
100°
120°
140°
160°
180°
φ
10°
20°
30°
40°
50°
60°
70°
80°
Model III
ψ
a
b
c
d

11c1

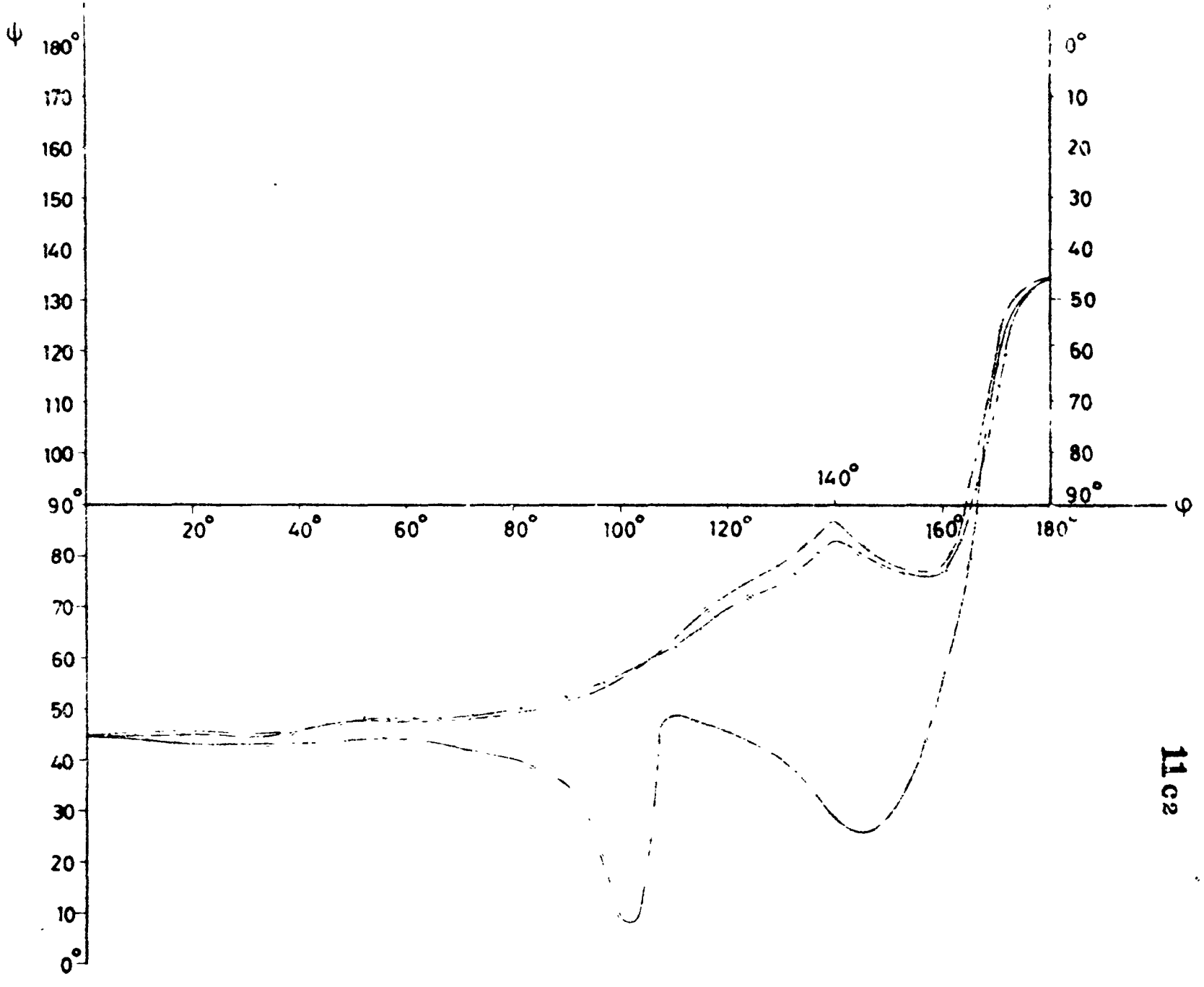
ψ
180°
170
160
150
140
130
120
110
100
90°
80
70
60
50
40
30
20
10
0°
20°
40°
60°
80°
100°
120°
140°
160°
180°
φ
0°
10
20
30
40
50
60
70
80
90°
Model III
ψ
e
f
g

11 c2

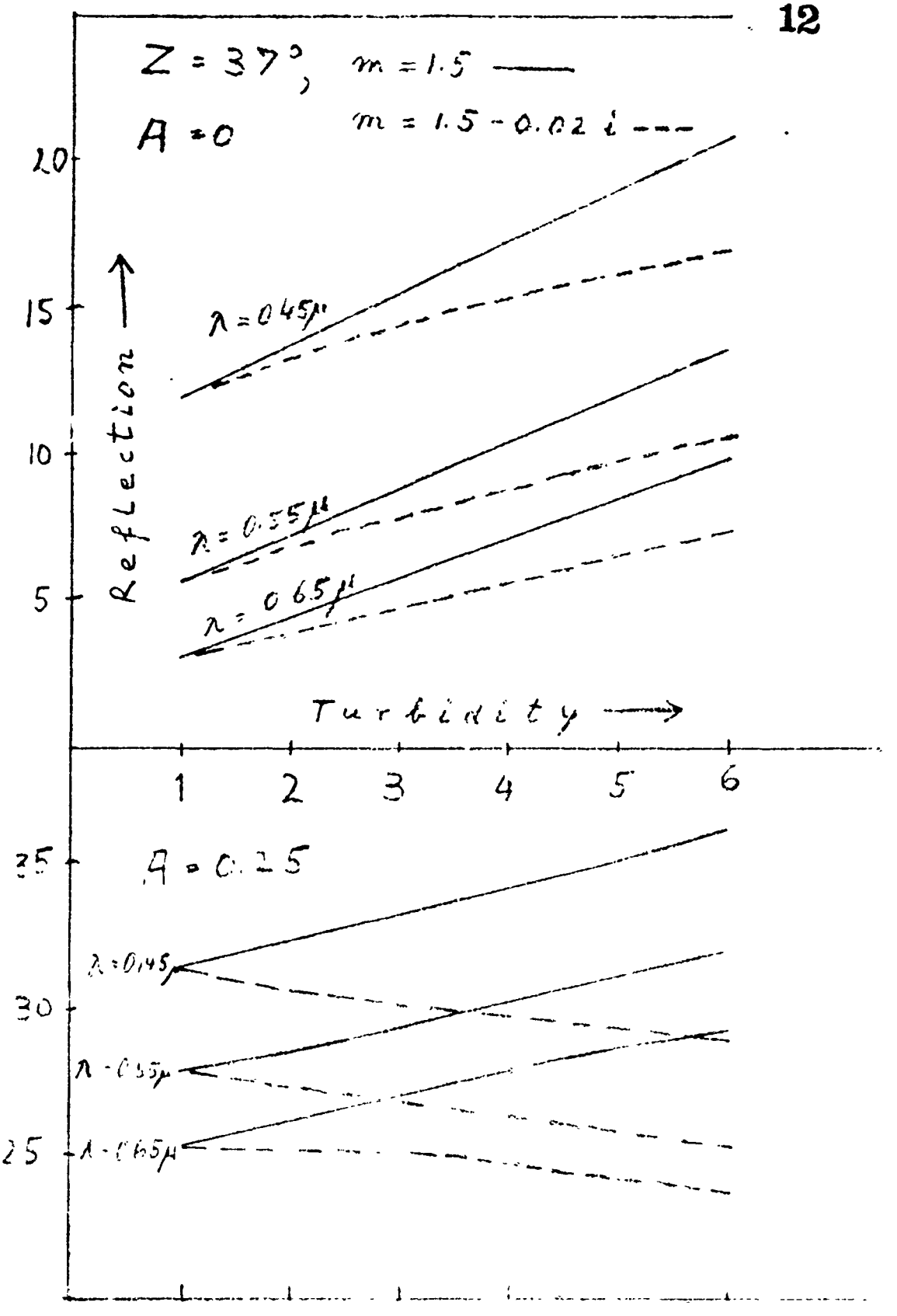
Z = 37°, m = 1.5 ——
A = 0
m = 1.5 - 0.02 i ---
20
15
10
5
Reflection
λ = 0.45μ
λ = 0.55μ
λ = 0.65μ
Turbidity
1
2
3
4
5
6
35
A = 0.25
λ = 0.145
30
λ = 0.55μ
25
λ = 0.65μ

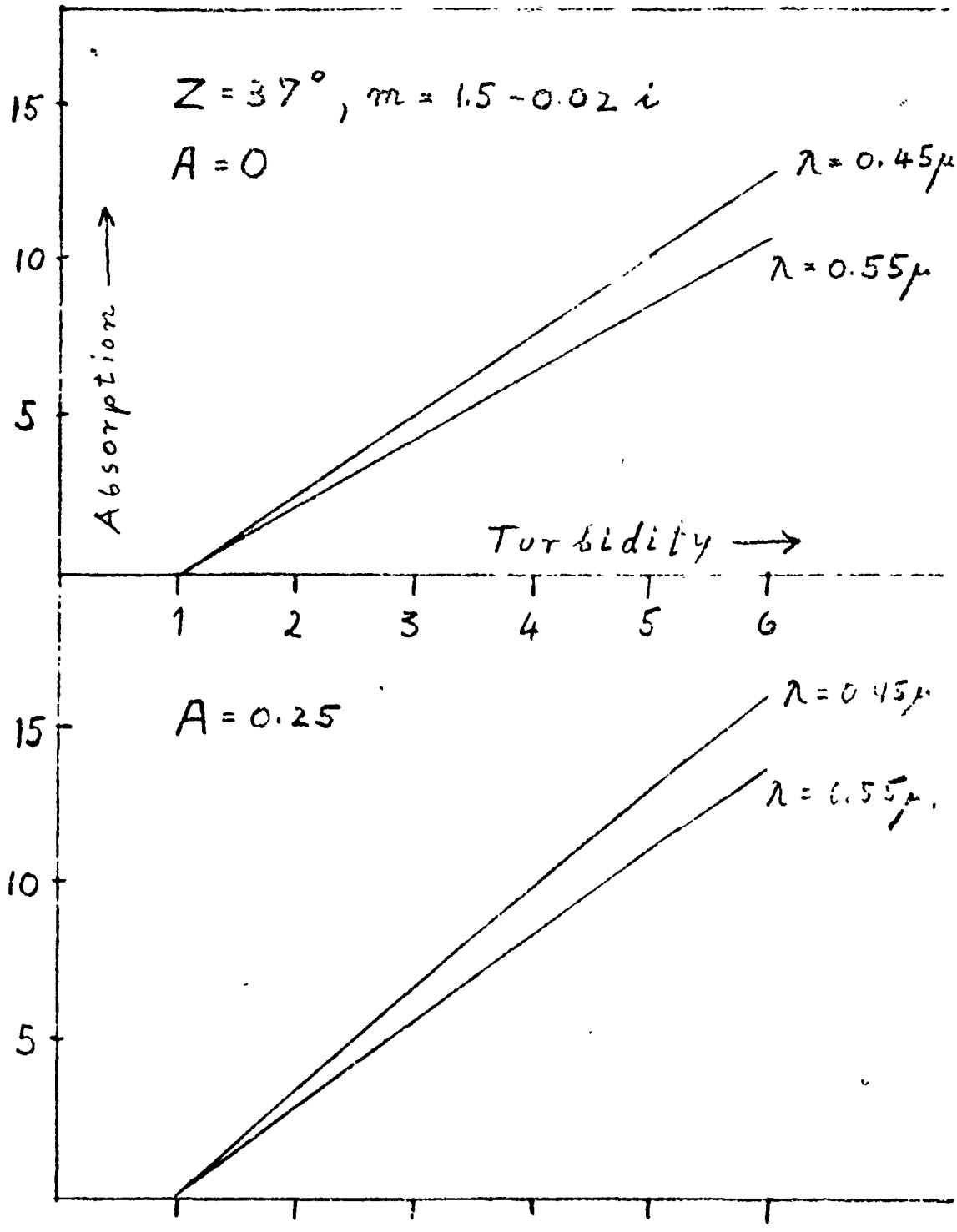
Z = 37°, m = 1.5 - 0.02 i
A = 0
λ = 0.45μ
λ = 0.55μ
Absorption →
Turbidity →
15
10
5
1
2
3
4
5
6
A = 0.25
λ = 0.45μ
λ = 0.55μ
15
10
5

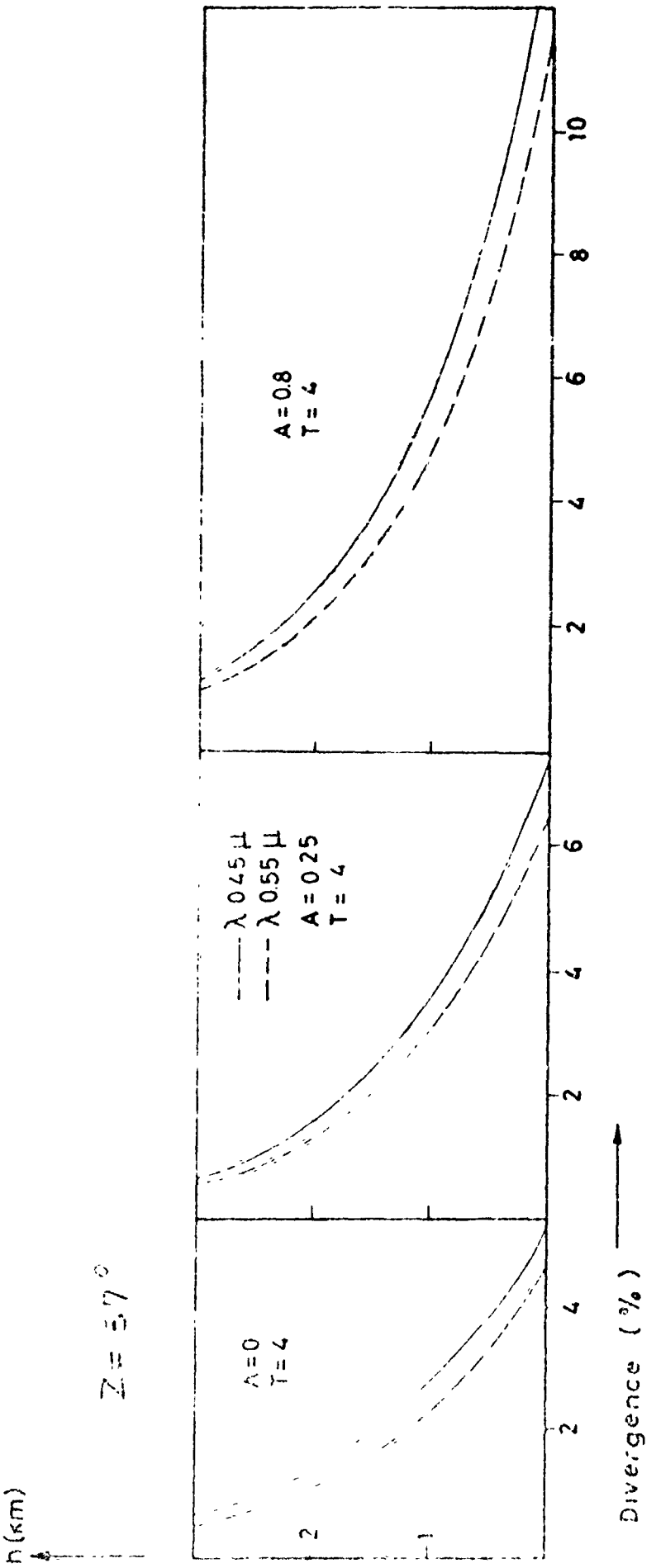
h (km)
Z = 37°
A=0
T=4
λ 0.45 μ
λ 0.55 μ
A=0.25
T=4
A=0.8
T=4
Divergence (%)

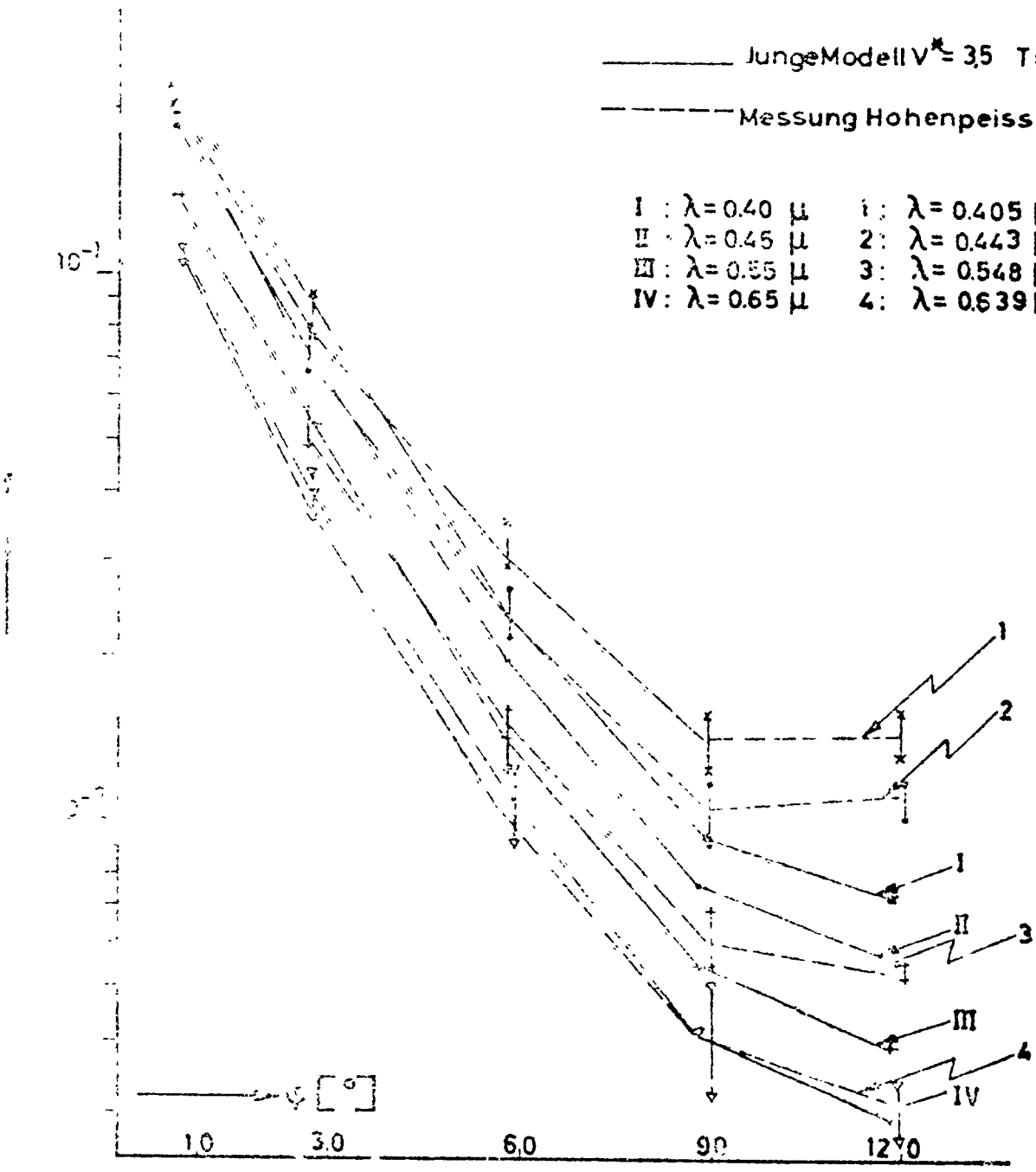
Junge Modell V* = 3,5 T = 3.9 (I-IV)
Messung Hohenpeissenberg Juni 1971 (1-4) T = 3.9
I : λ = 0.40 μ
II : λ = 0.45 μ
III : λ = 0.55 μ
IV : λ = 0.65 μ
1 : λ = 0.405 μ
2 : λ = 0.443 μ
3 : λ = 0.548 μ
4 : λ = 0.639 μ
10^-1
1.0
3.0
6.0
9.0
12.0

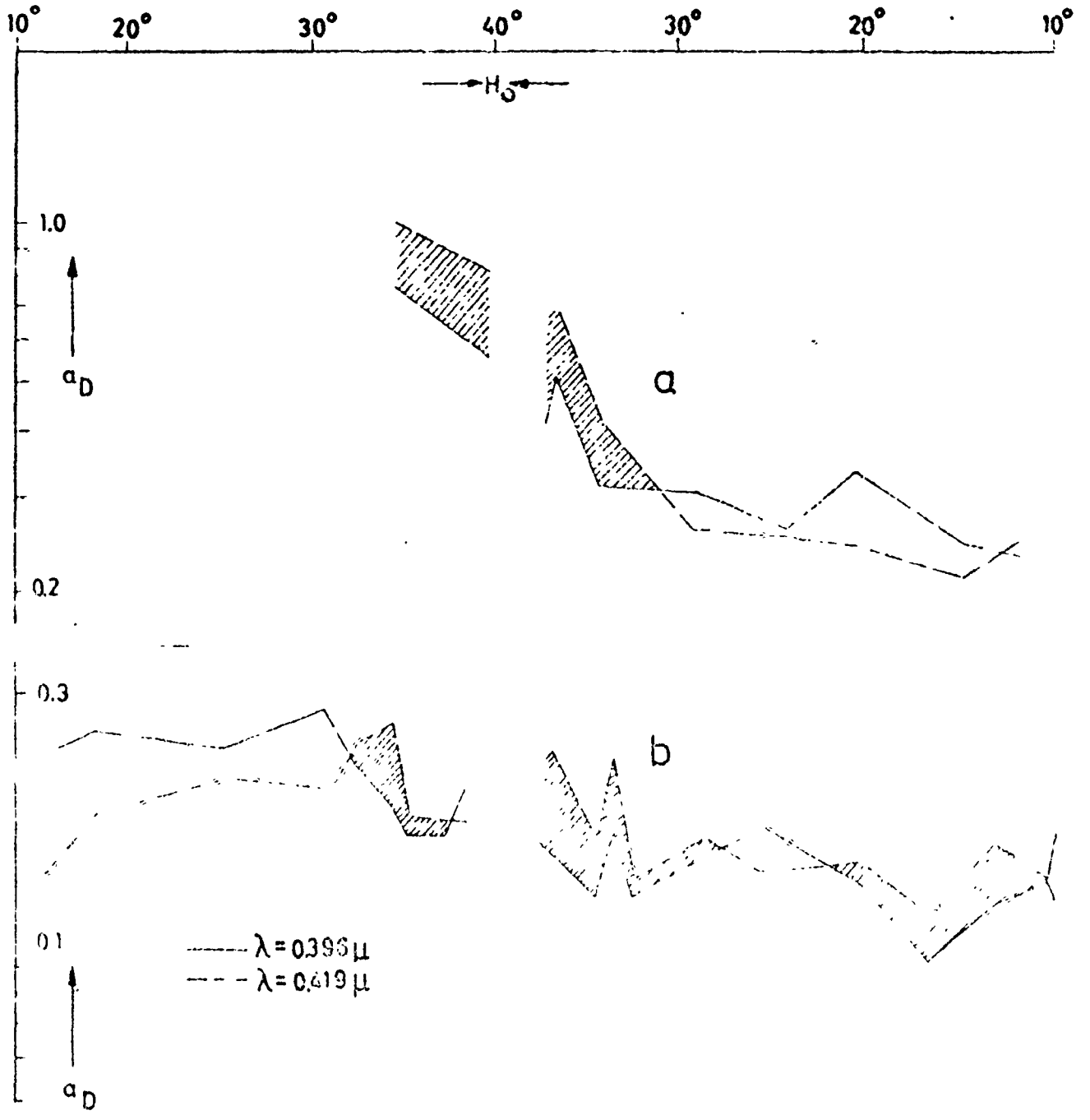
10°
20°
30°
40°
30°
20°
10°
H_S
1.0
a_D
0.2
a
0.3
b
0.1
a_D
λ = 0.396 μ
λ = 0.419 μ

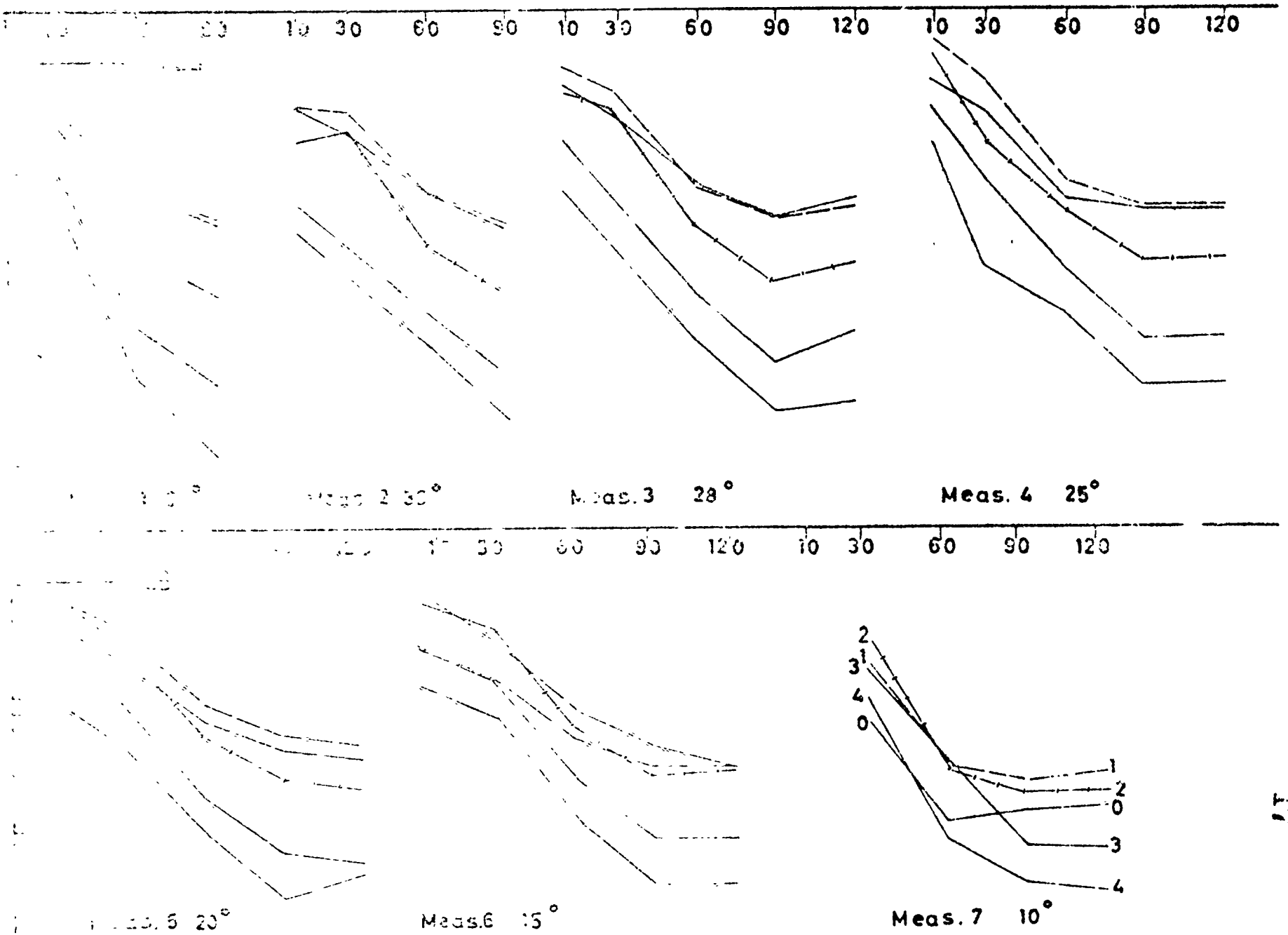
10 30 60 90 10 30 60 90 120 10 30 60 90 120
Meas. 3 28°
Meas. 4 25°
10 30 60 90 120 10 30 60 90 120
Meas.6 15°
2
3
4
0
1
2
0
3
4
Meas. 7 10°

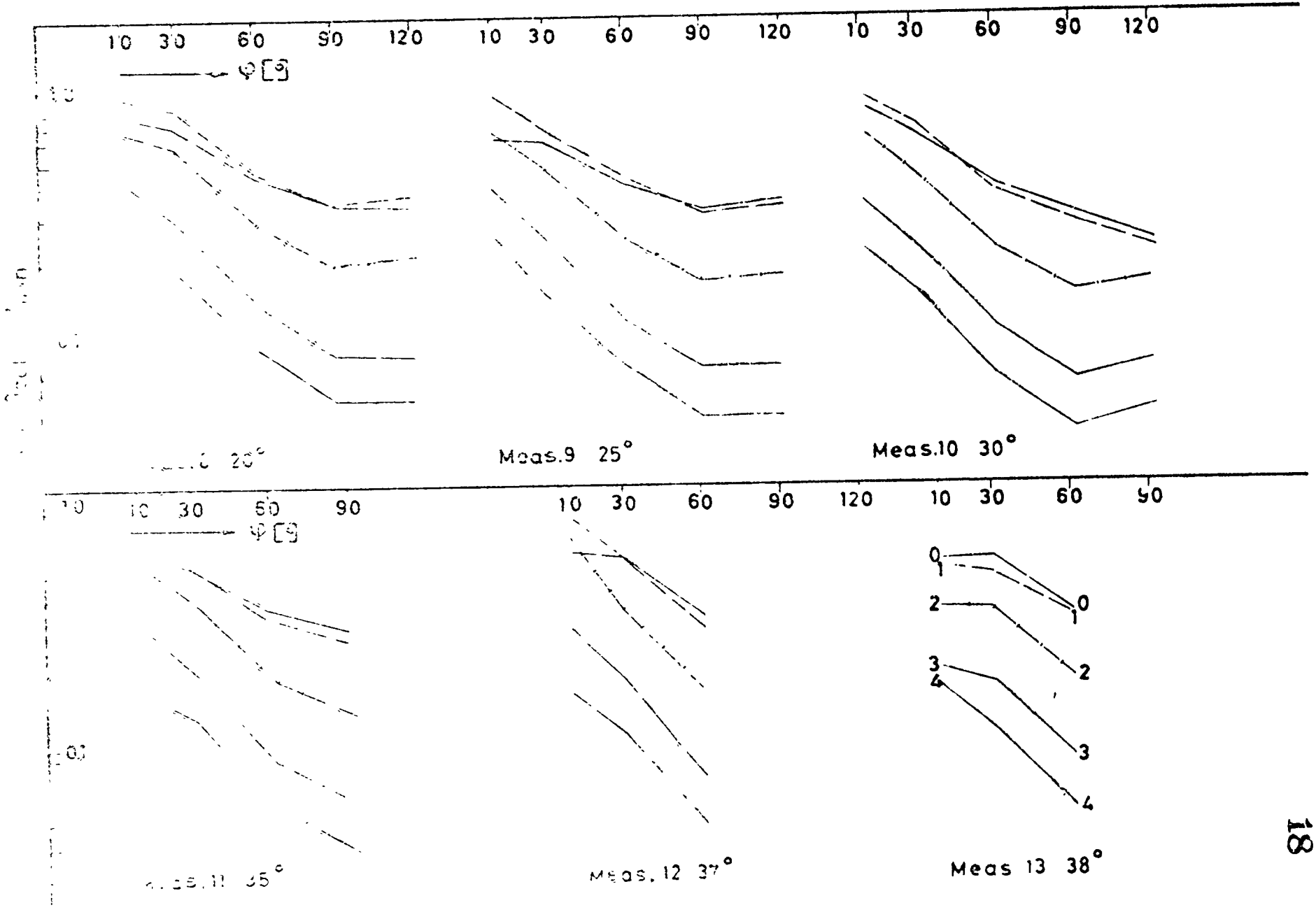
10 30 60 90 120 10 30 60 90 120 10 30 60 90 120
φ [°]
Meas.9 25°
Meas.10 30°
10 30 60 90 10 30 60 90 120 10 30 60 90
φ [°]
Meas.12 37°
Meas 13 38°
0
1
2
3
4

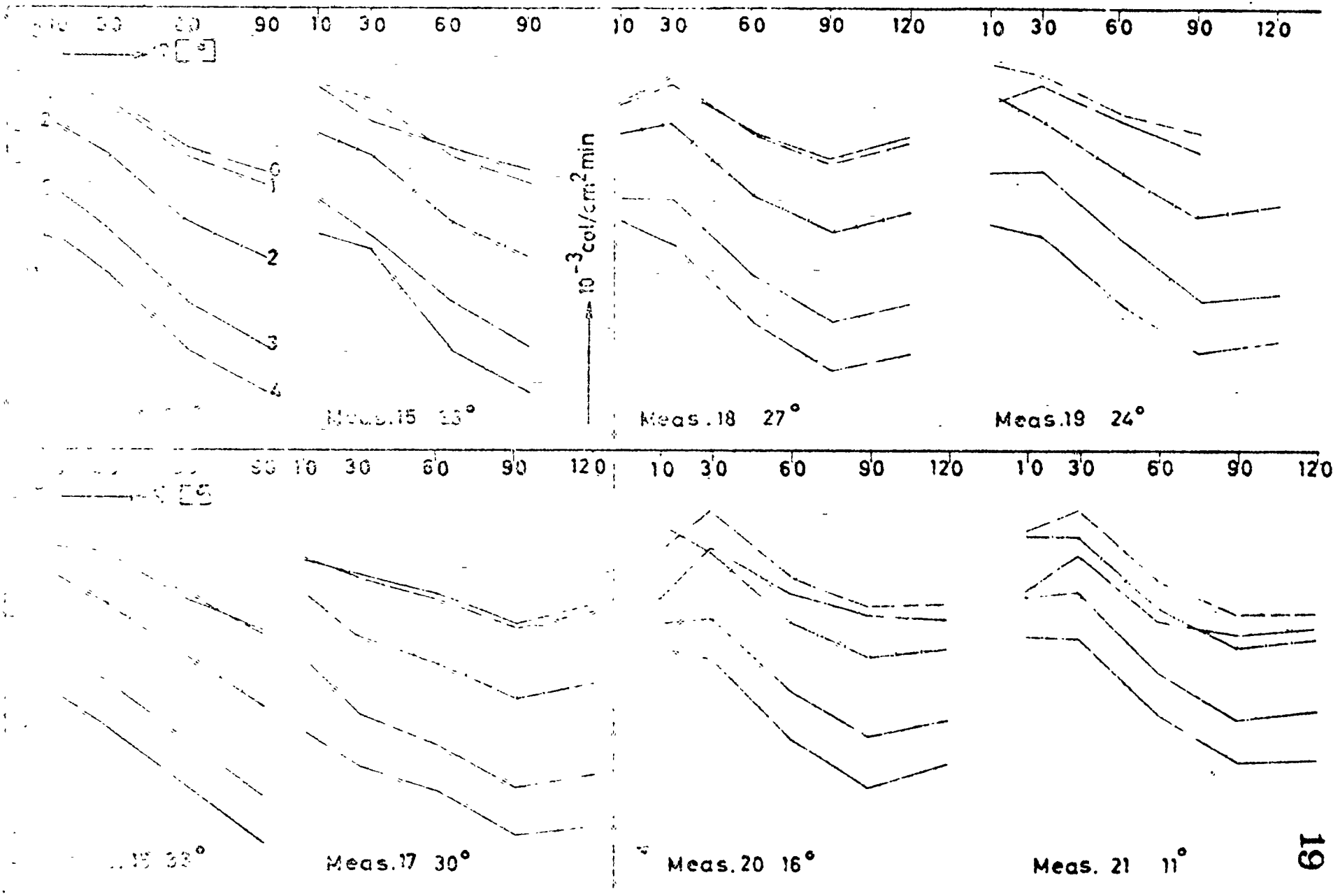
10 30 60 90 120
0
1
2
3
4
10^{-3}cal/cm^{2}min
Meas.18 27°
Meas.19 24°
Meas.17 30°
Meas.20 16°
Meas. 21 11°

Summer 1966, Mainz

20a

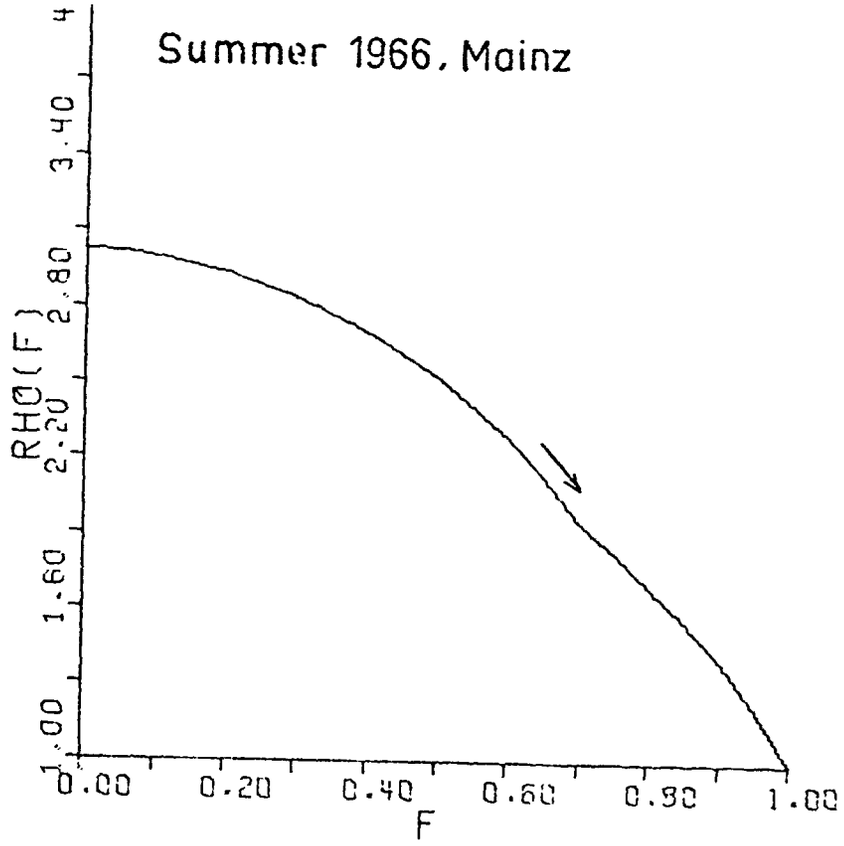

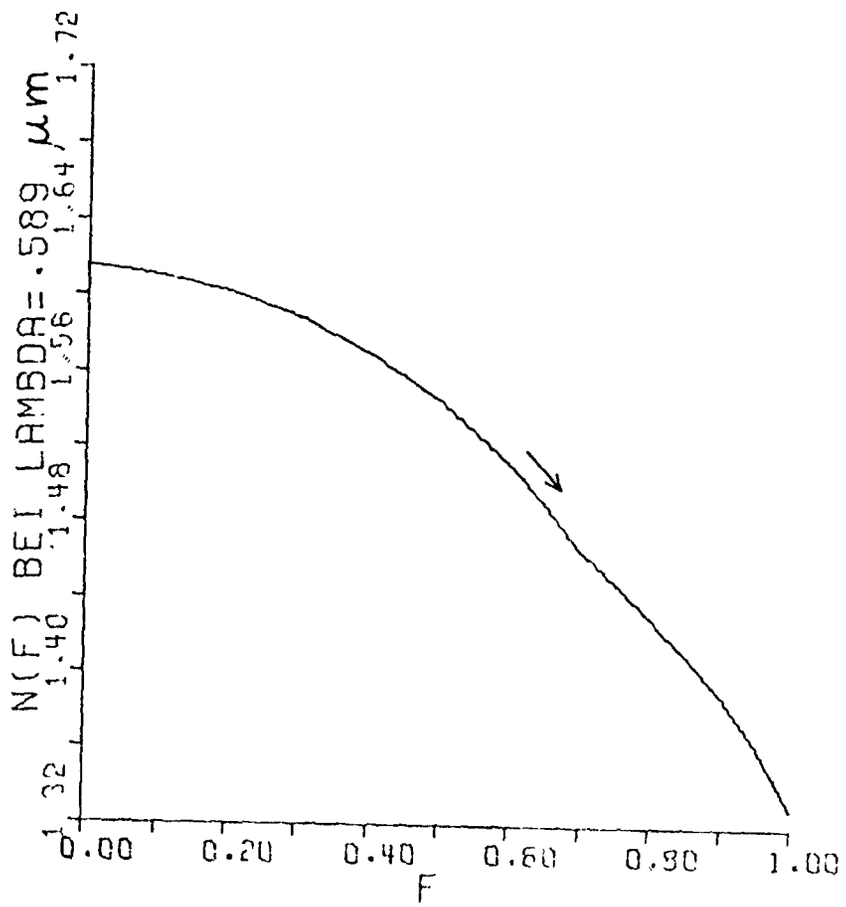

Summer 1966, Mainz

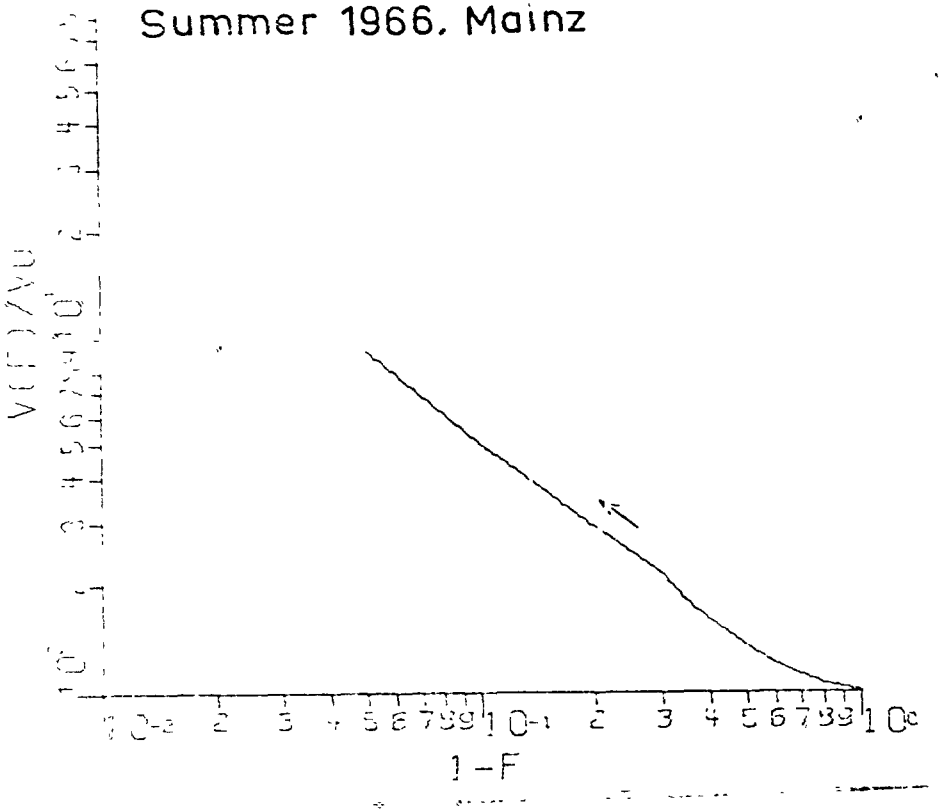

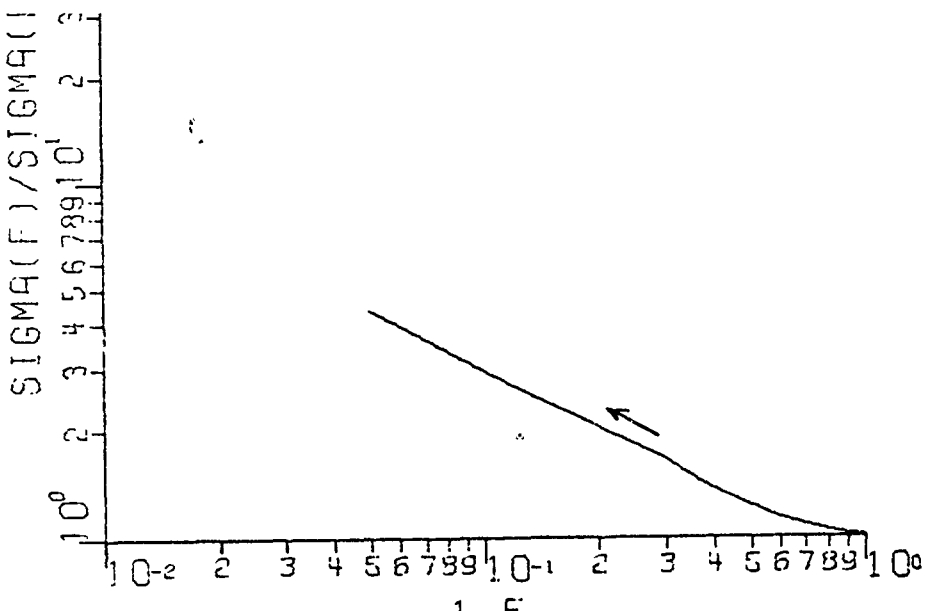

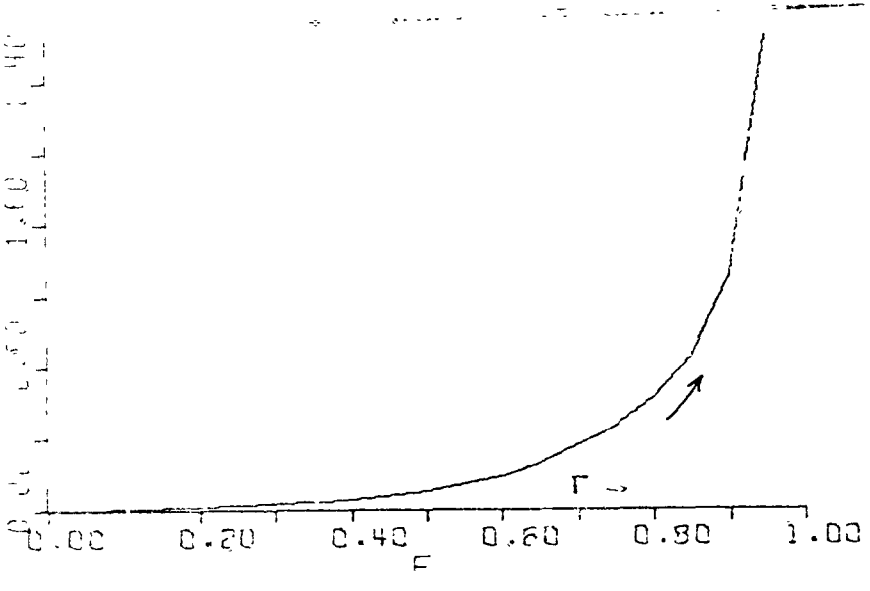

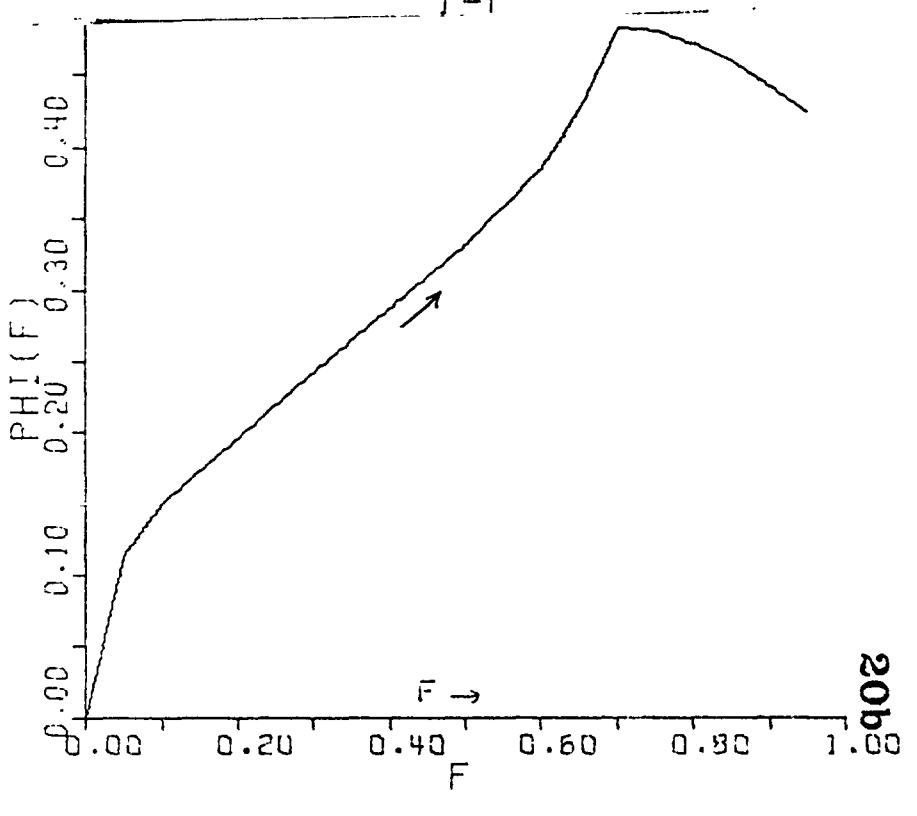

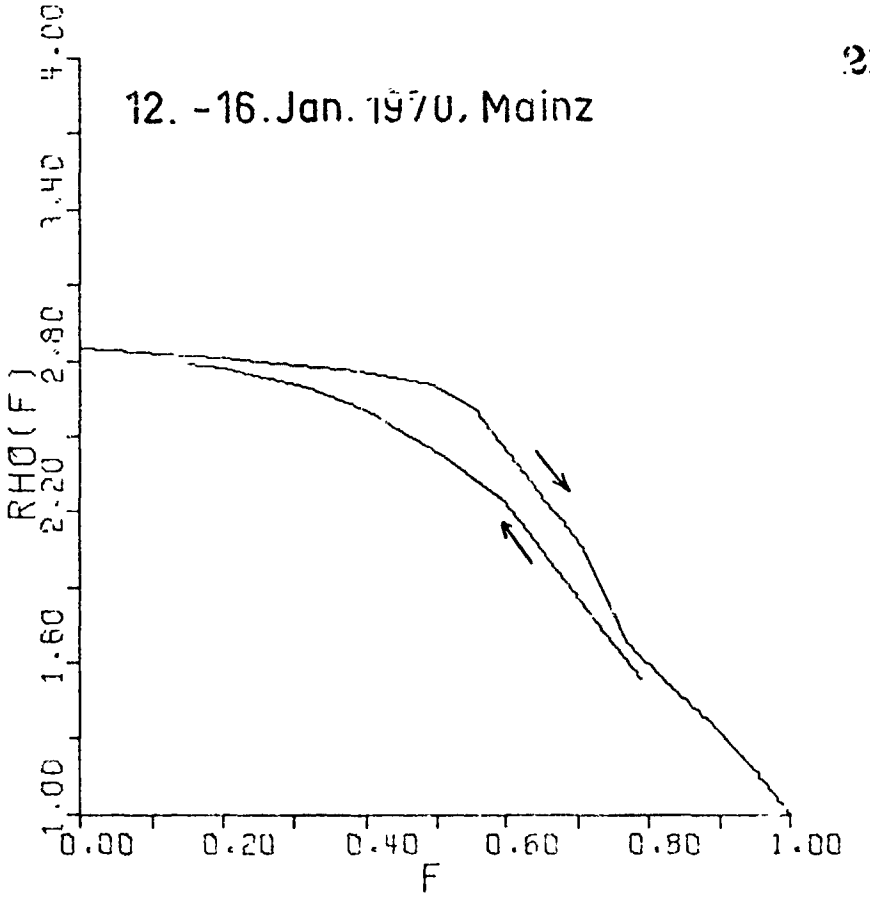
12. -16. Jan. 1970, Mainz
RHO(F)
4.00
3.40
2.80
2.20
1.60
1.00
0.00
0.20
0.40
0.60
0.80
1.00
F

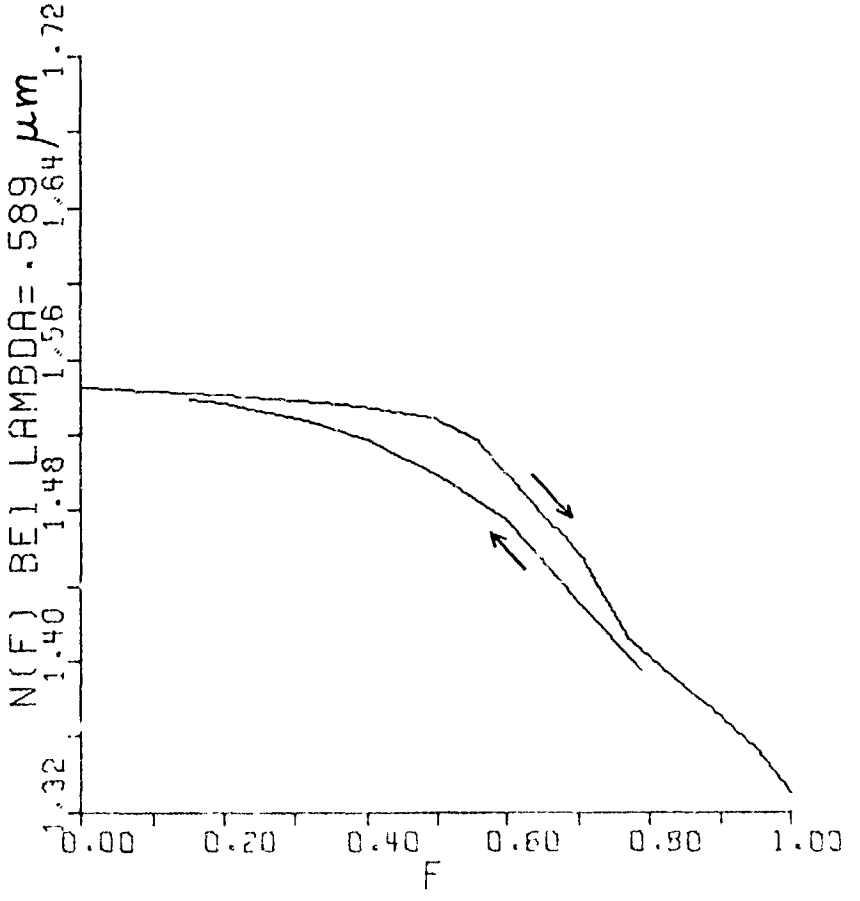
N(F) BEI LAMBDA=.589 µm
1.72
1.64
1.56
1.48
1.40
1.32
0.00
0.20
0.40
0.60
0.80
1.00
F

12. -16. Jan. 1970, Mainz

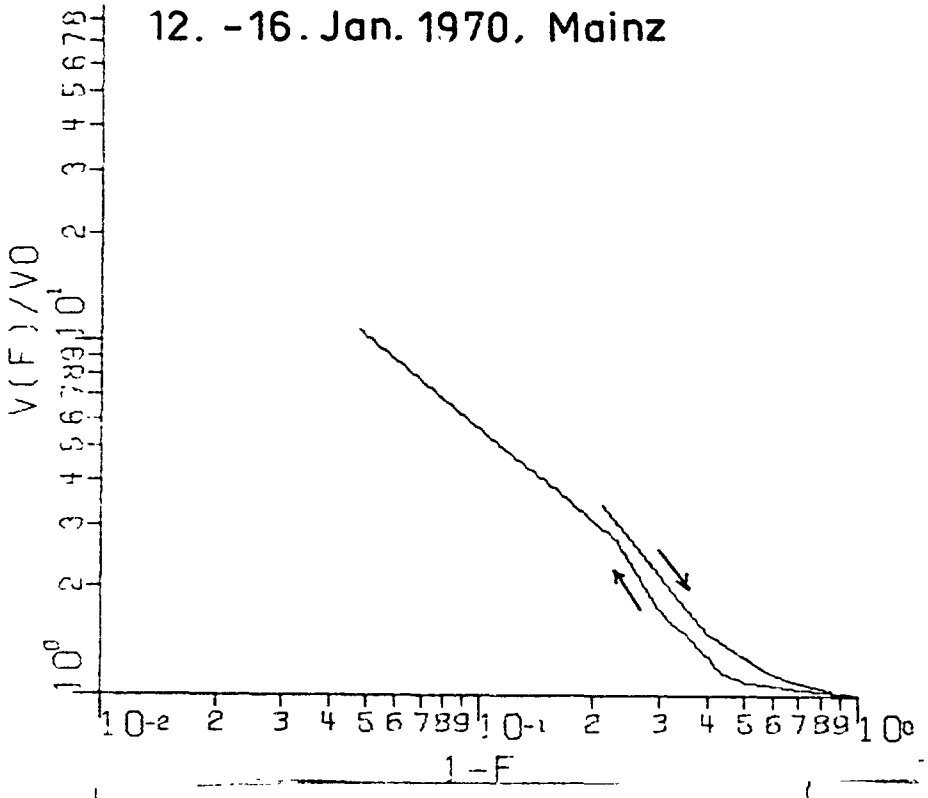

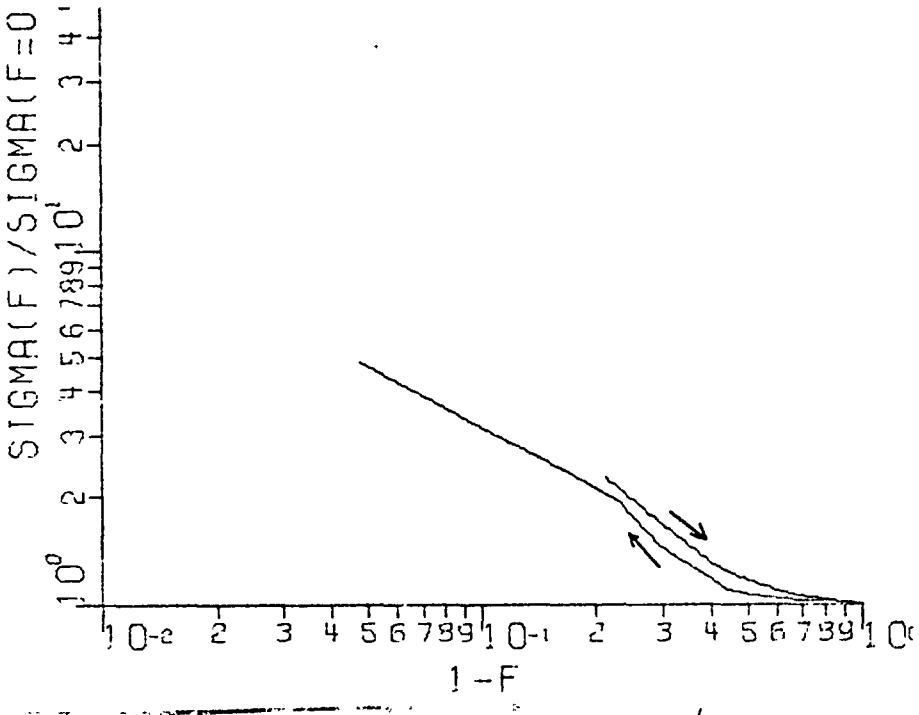

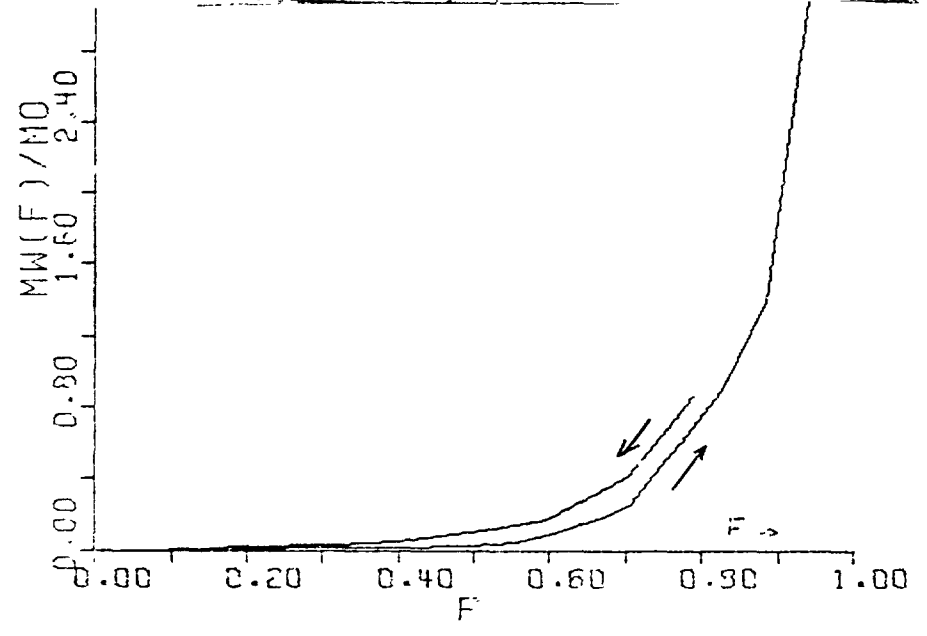

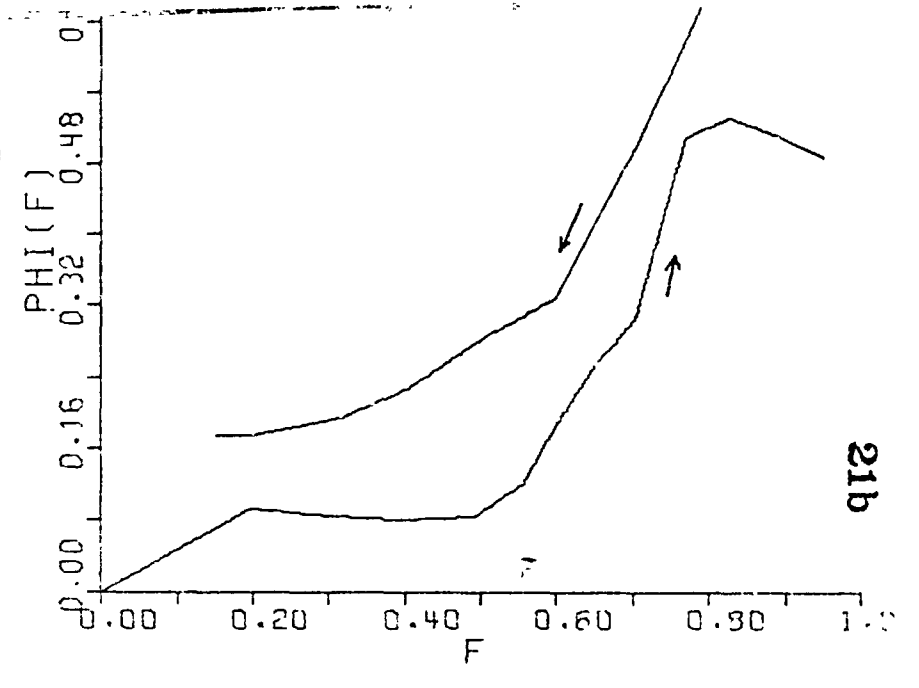

21b

18.6. - 26.8.1970
Hohenpeißenberg

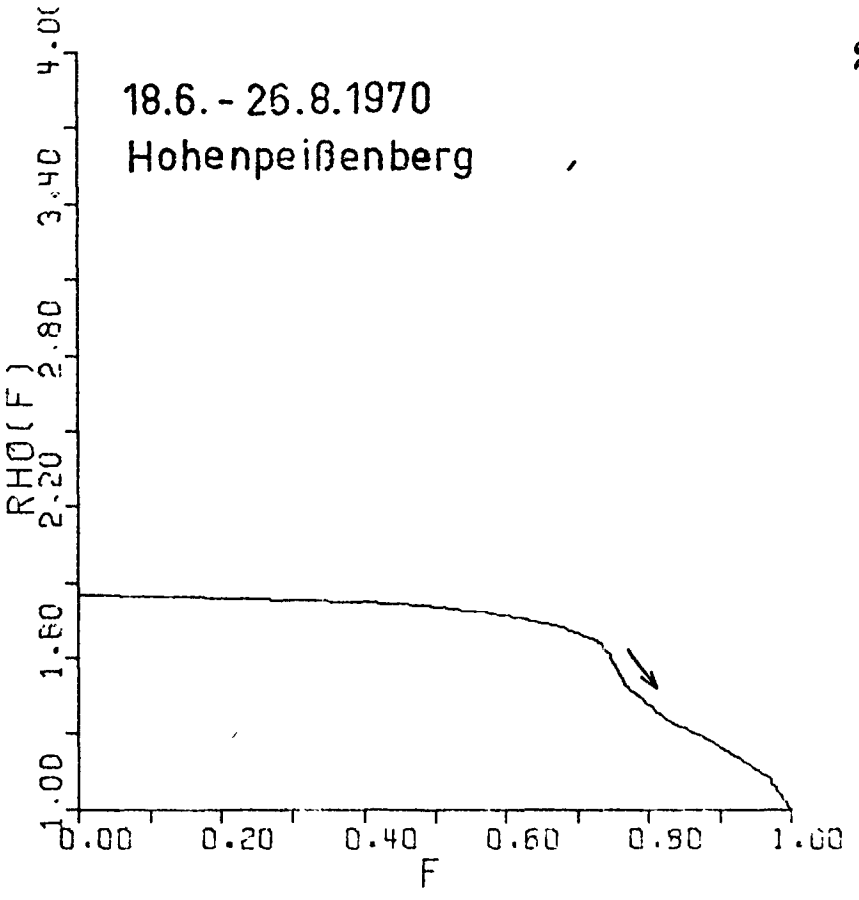

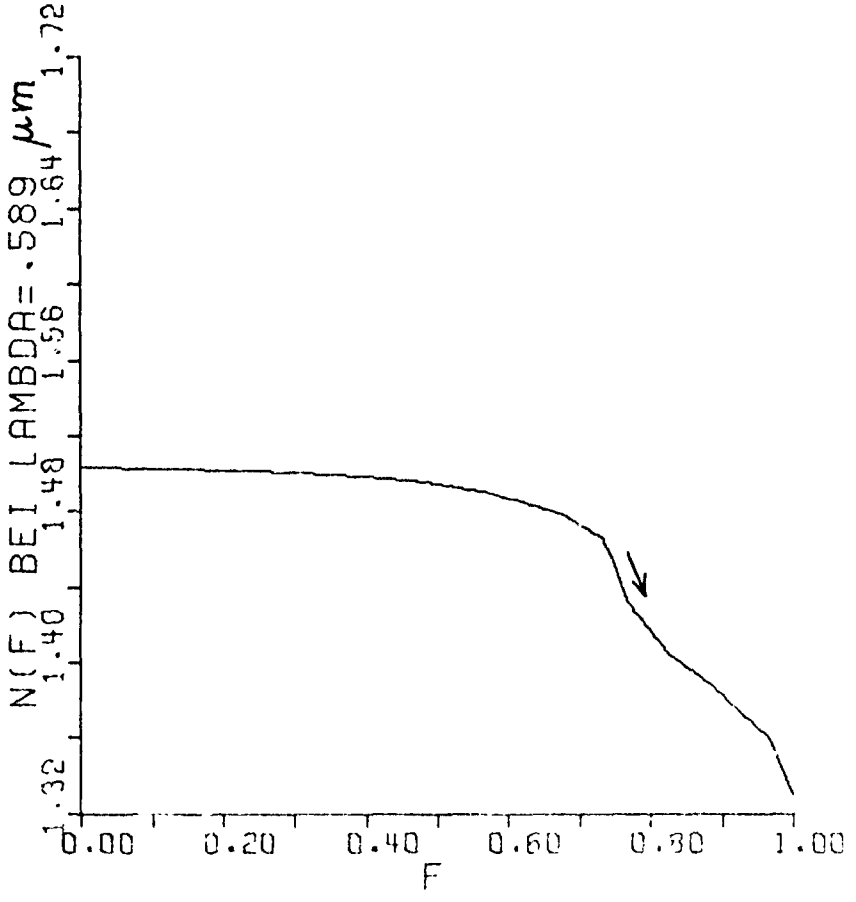

Sea - Spray

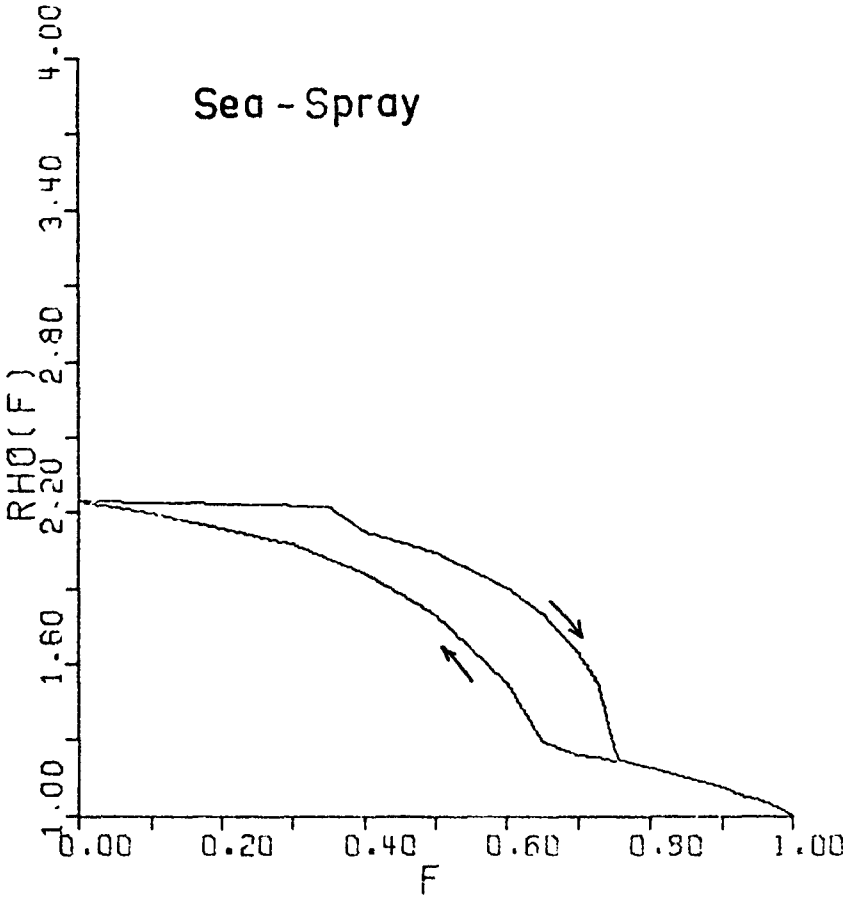
RHO(F)
4.00
3.40
2.80
2.20
1.60
1.00
0.00
0.20
0.40
0.60
0.80
1.00
F

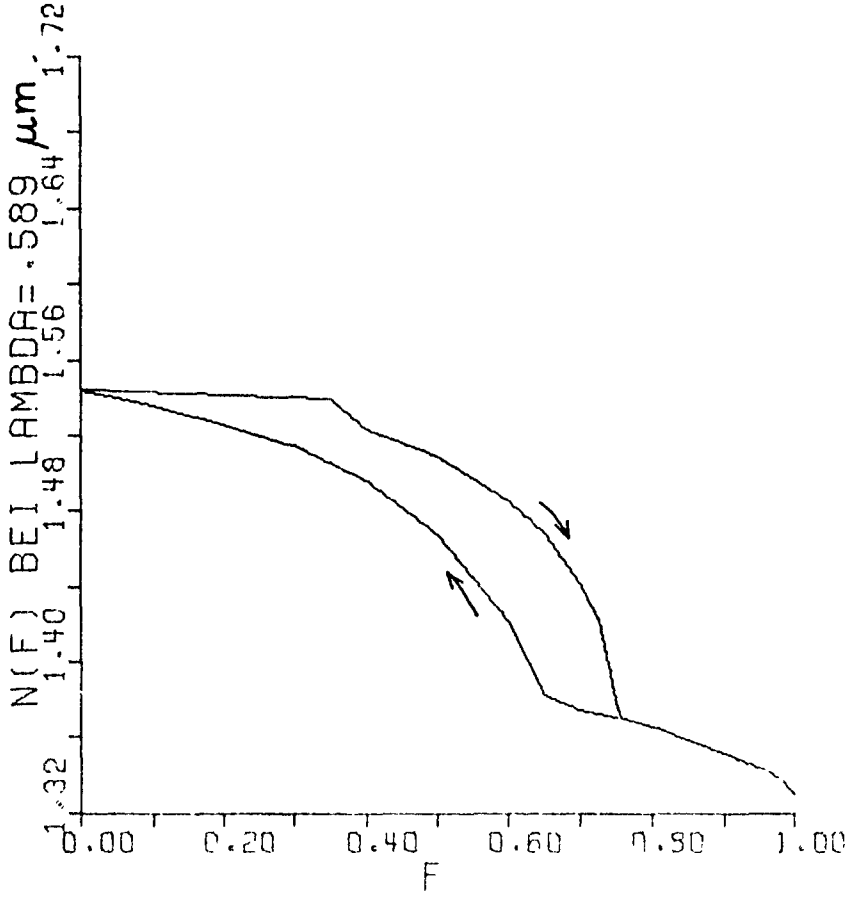
N(F) BEI LAMBDA=.589 μm
1.72
1.64
1.56
1.48
1.40
1.32
0.00
0.20
0.40
0.60
0.80
1.00
F

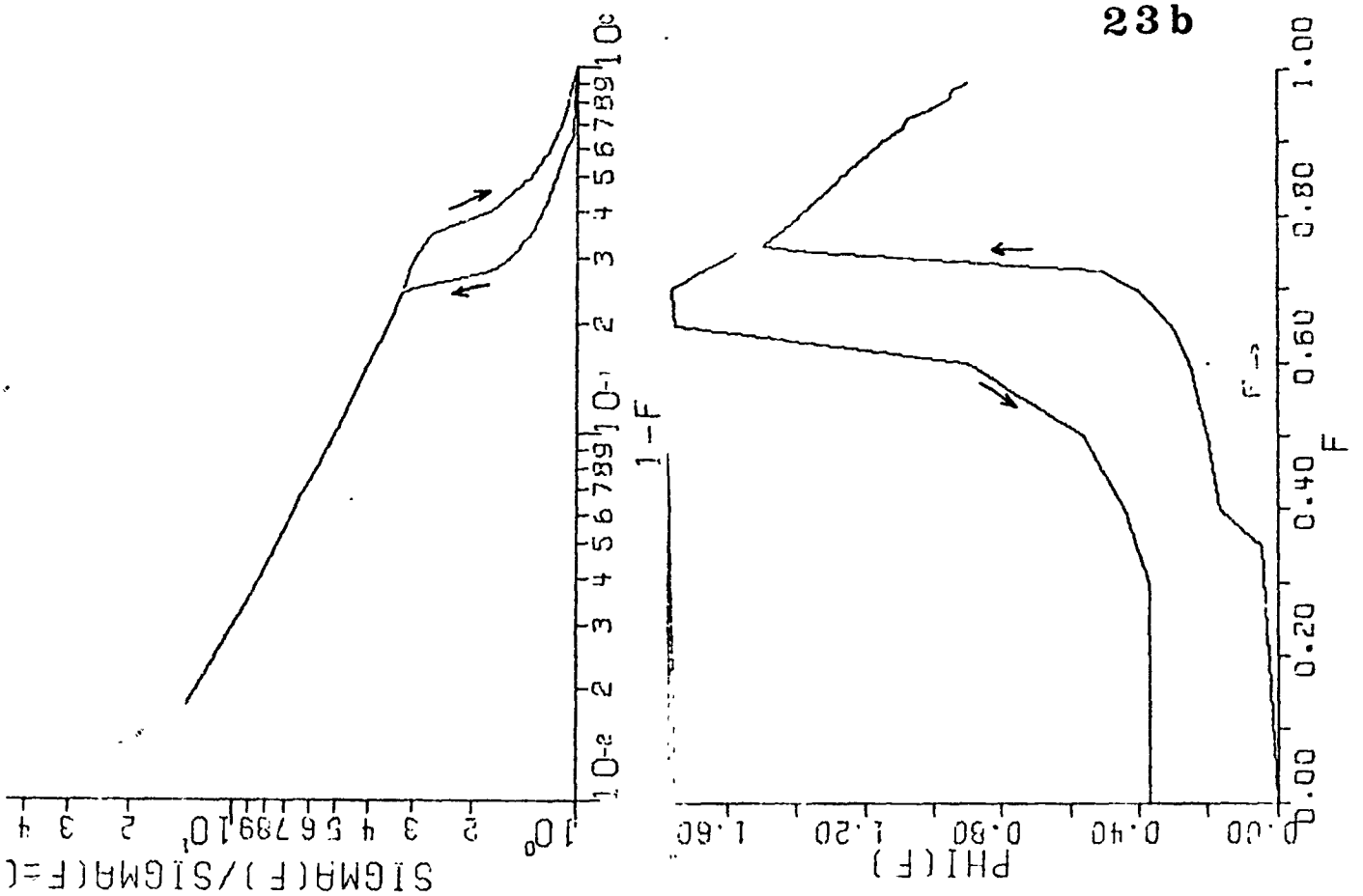
SIGMA(F)/SIGMA(F=0)
1-F
PHI(F)
F
0.00
0.20
0.40
0.60
0.80
1.00
0.40
0.80
1.20
1.60

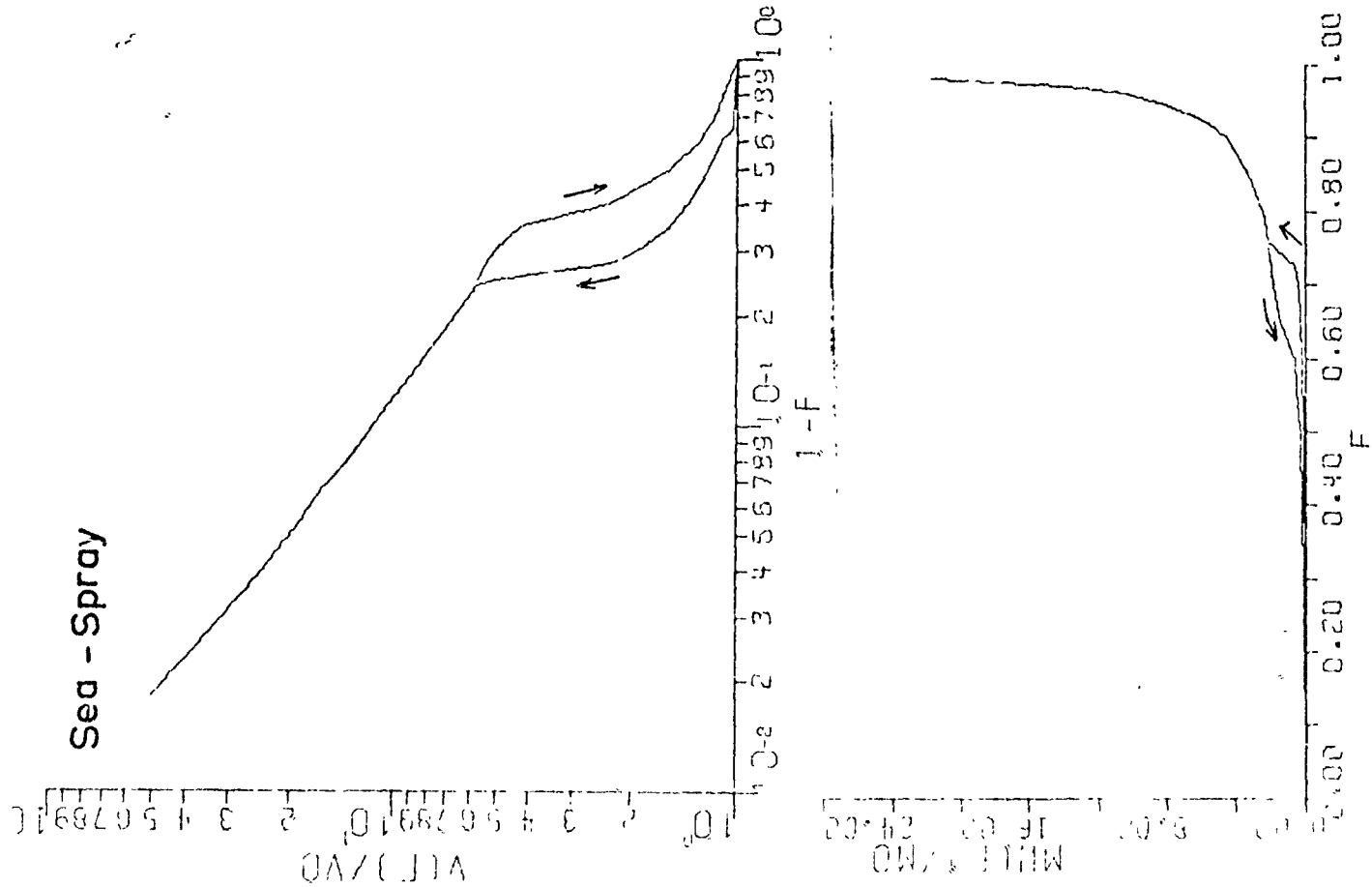
Sea - Spray
V(F)/V0
1-F
F
0.00
0.20
0.40
0.60
0.80
1.00

13.-16. April 1969, „Meteor"

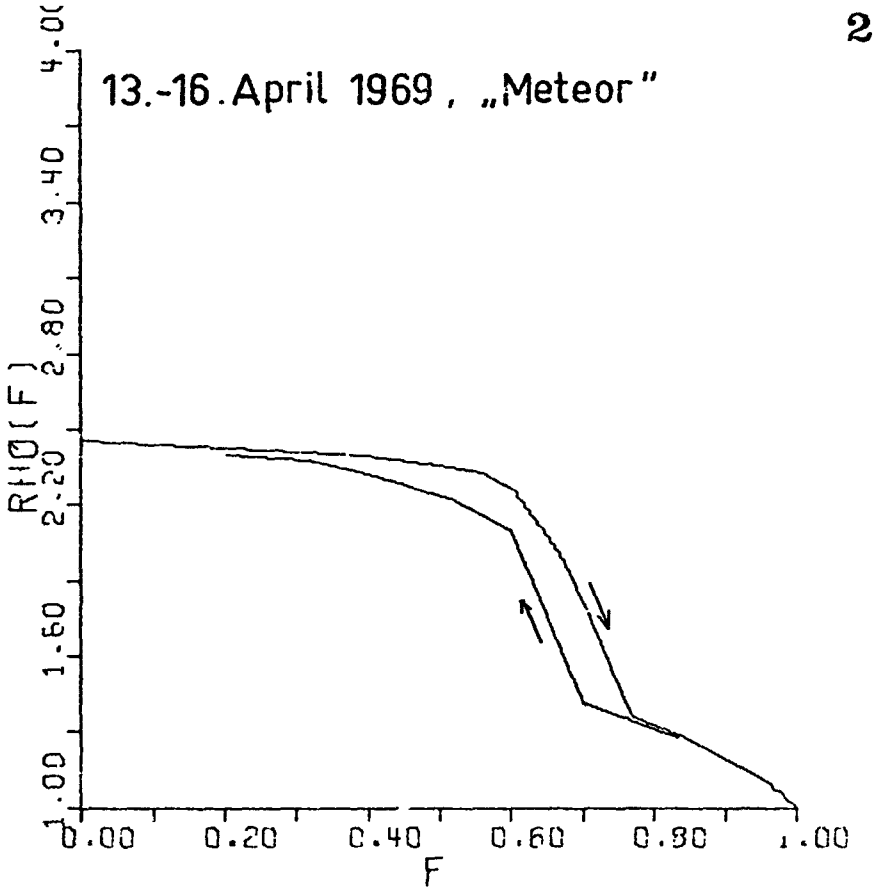

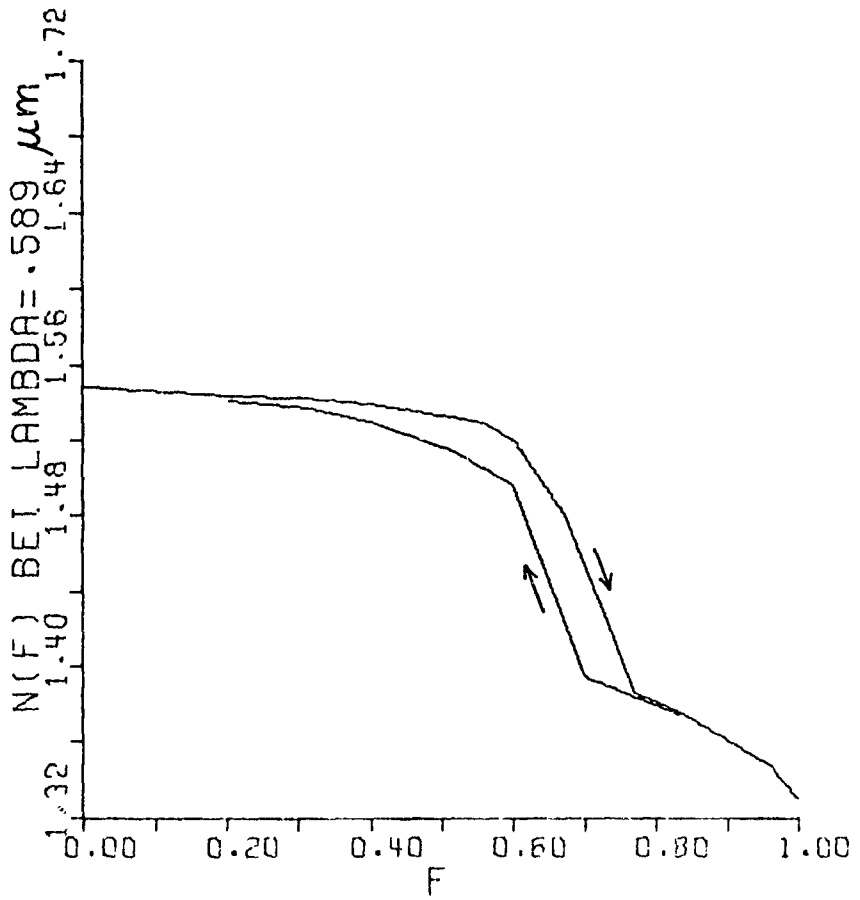

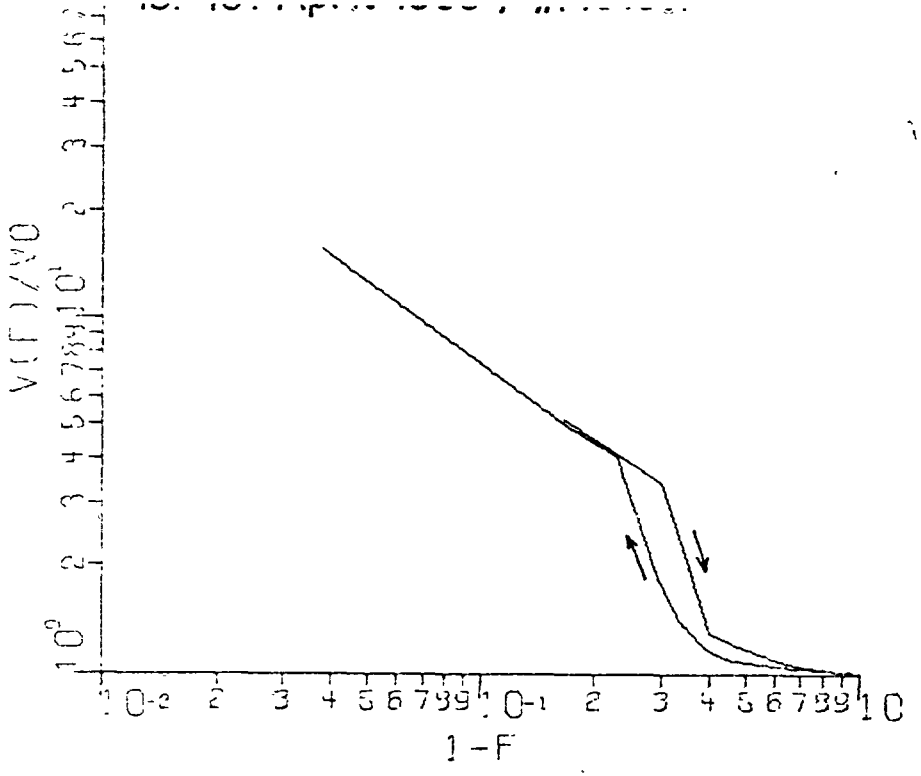

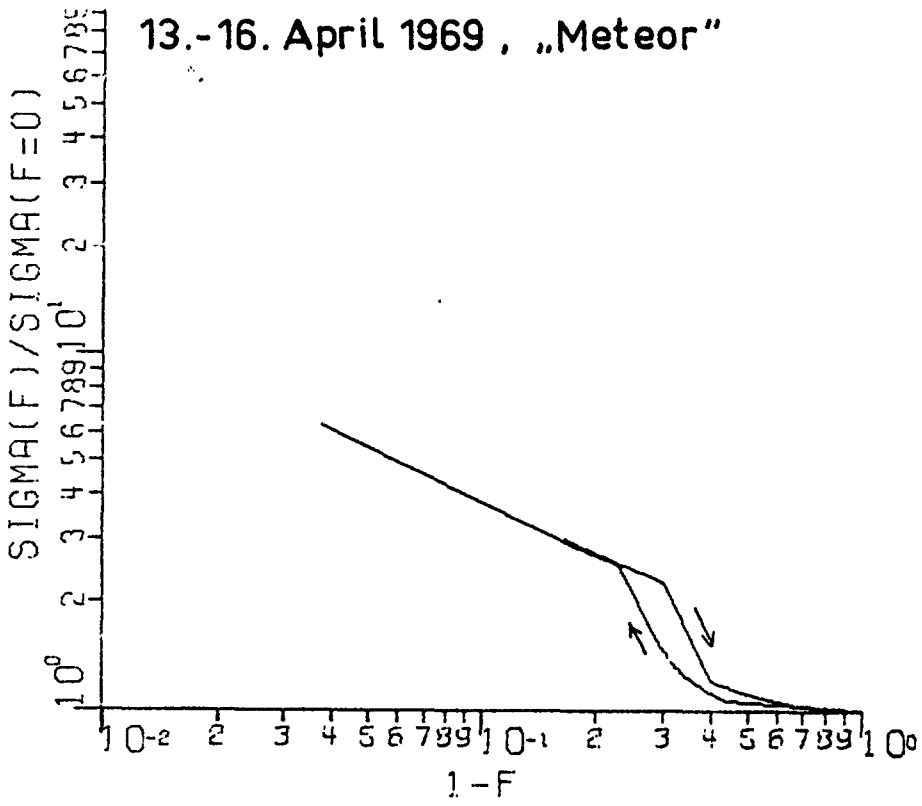

13.-16. April 1969 , „Meteor"

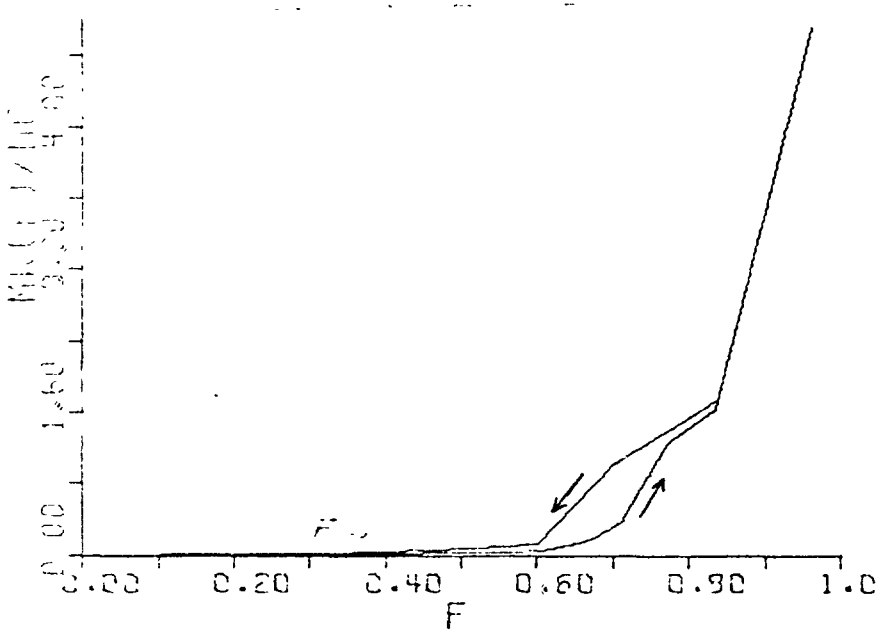

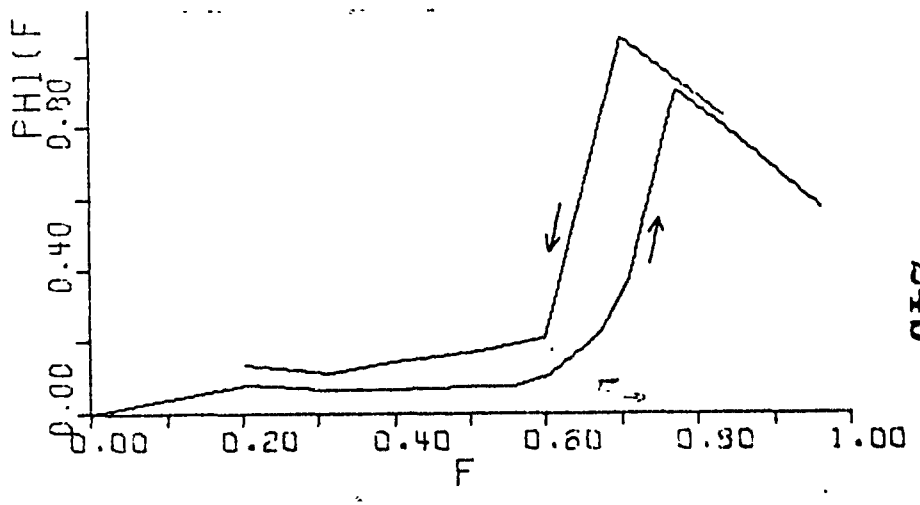

24b

16. -25. April 1969, „Meteor"

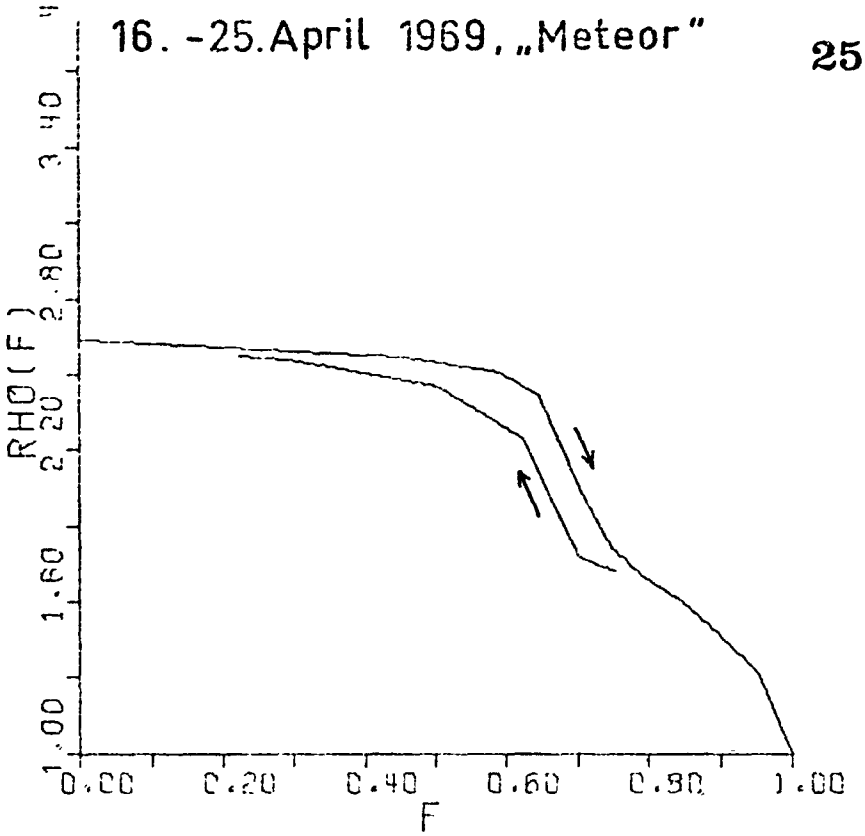

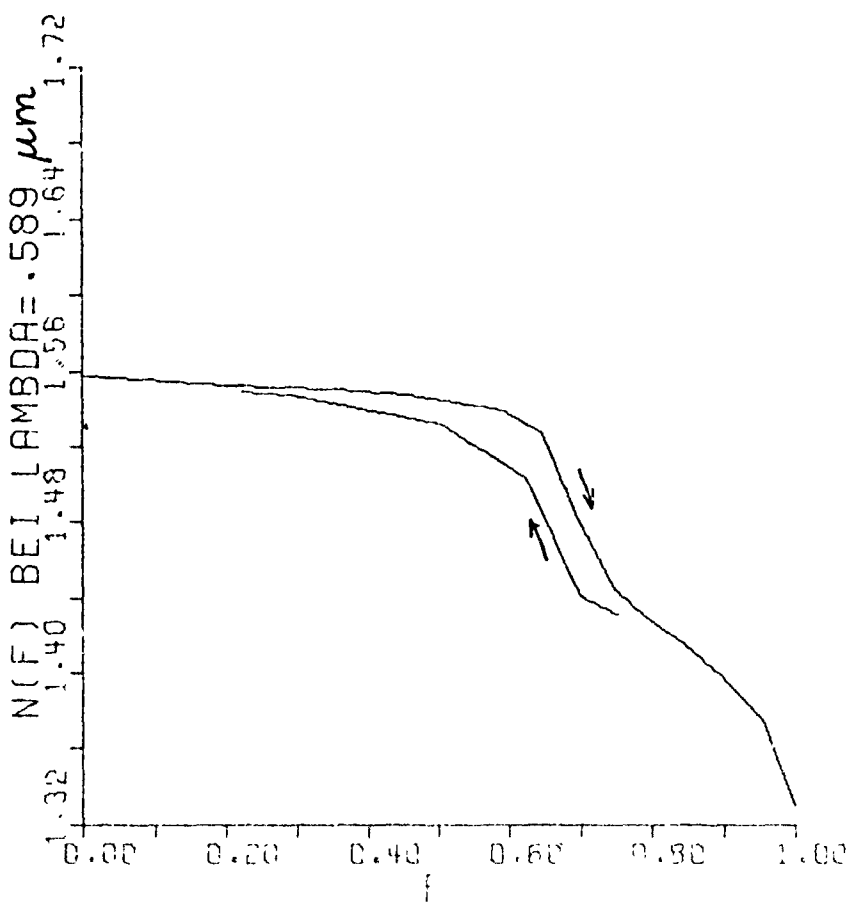

16. - 25. April 1969, „Meteor

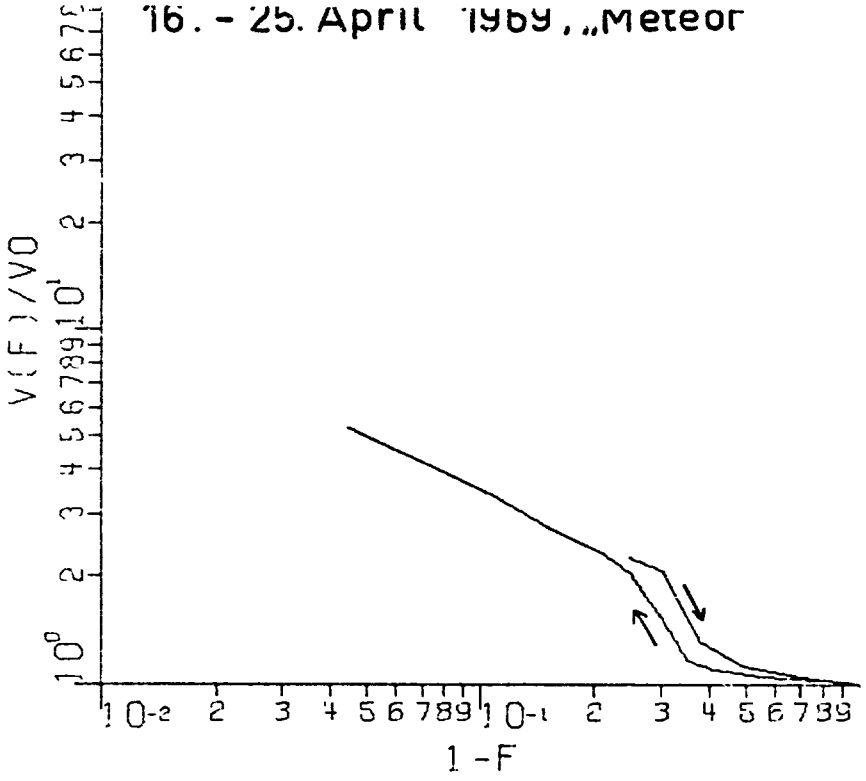

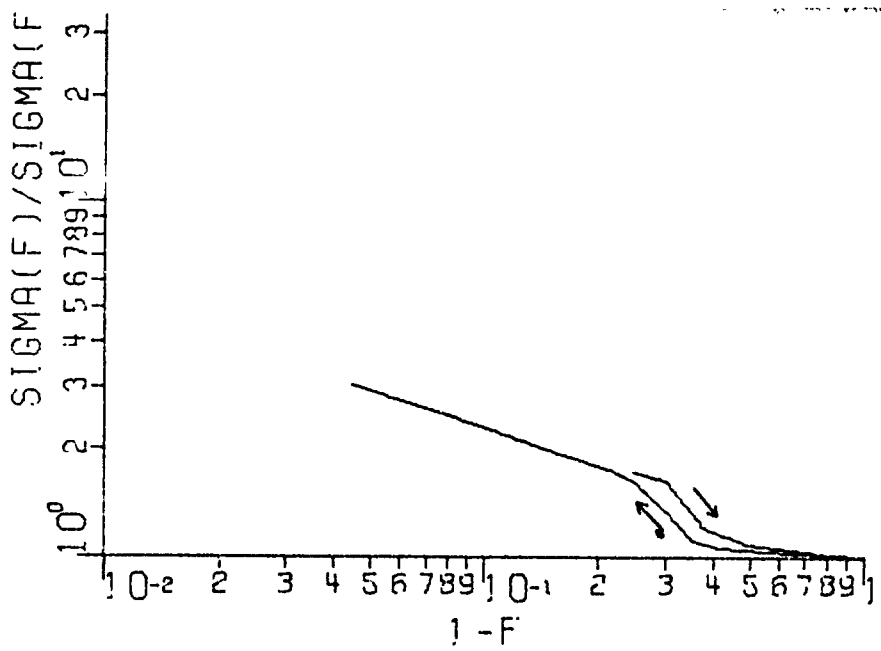

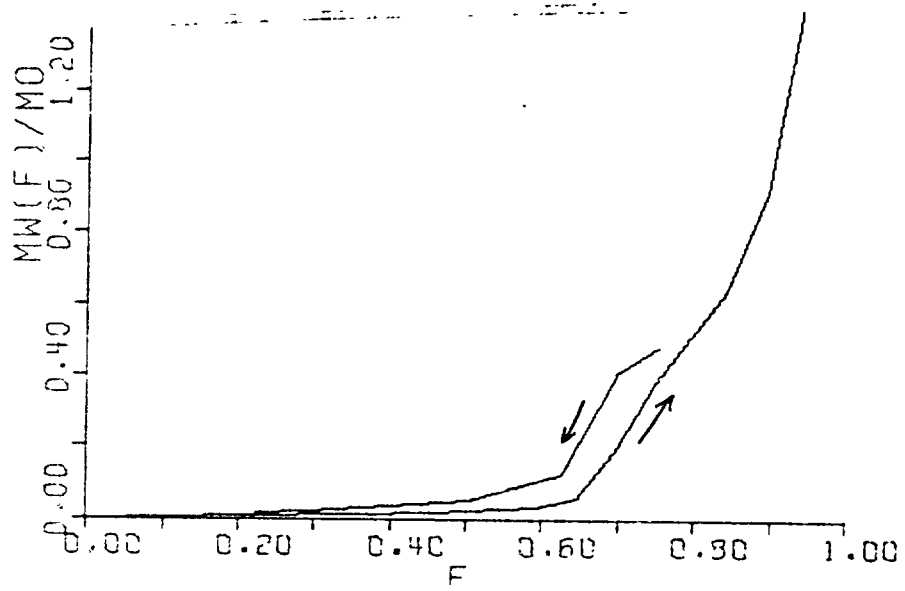

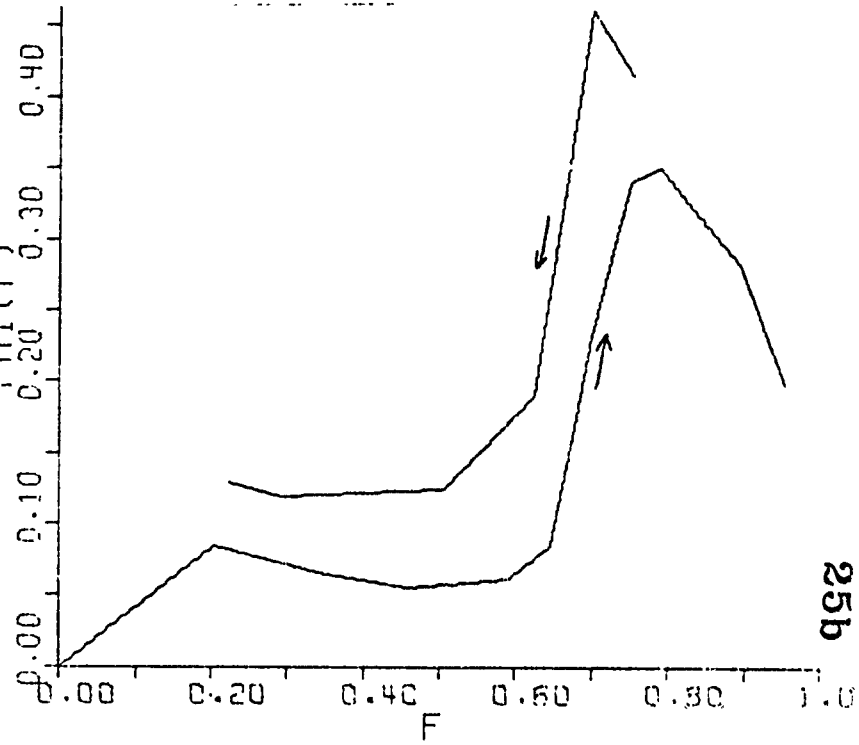

25b